

MODULATION OF SYNAPTIC AMPLIFICATION IN SYMPATHETIC GANGLIA

by

Mitchell George Springer

University of Wisconsin – Eau Claire, Bachelor of Science, 2007

Submitted to the Graduate Faculty of
Medicine in partial fulfillment
of the requirements for the degree of
Doctor of Philosophy

University of Pittsburgh

2013

UNIVERSITY OF PITTSBURGH

SCHOOL OF MEDICINE

This dissertation was presented

by

Mitchell George Springer

It was defended on

July 12, 2013

and approved by

Committee Chair: Elias Aizenman, Professor, Neurobiology

Kathryn M. Albers, Professor, Medicine

Bruce A. Freeman, Professor, Pharmacology & Chemical Biology

Edwin S. Levitan, Professor, Pharmacology & Chemical Biology

Dissertation Advisor: John P. Horn, Professor, Neurobiology

Copyright © by Mitchell G. Springer

2013

MODULATION OF SYNAPTIC AMPLIFICATION IN SYMPATHATIC GANGLIA

Mitchell G. Springer, PhD

University of Pittsburgh, 2013

The purpose of this dissertation was to assess synaptic integration in neurons from the rat superior cervical ganglion (SCG) using complex temporal patterns of virtual synaptic activity that mimic *in vivo* conditions. The SCG is a paravertebral ganglion that innervates different targets in the head. One of its important roles is to regulate vascular tone. Previous reports have concluded that SCG neurons behave as simple relays between preganglionic synaptic activity from the spinal cord and postganglionic control of end organs. We have tested the hypotheses that (1) postganglionic convergence of strong and weak nicotinic synapses produces variable synaptic amplification in SCG neurons; (2) entrainment of preganglionic activity to the cardiac cycle through arterial baroreceptors increases synaptic gain; (3) the contribution of weak nicotinic synapses to postganglionic integration has been underestimated *in vivo* due to membrane damage caused by sharp microelectrodes; and (4) angiotensin II (AngII) acts postsynaptically to increase ganglionic synaptic amplification.

The approach to creating virtual synapses relied on dynamic clamp. Using whole-cell recordings of SCG neurons in short-term cultures, we found evidence for activity dependent synaptic gain and for the enhancement of gain by cardiac entrainment. Based on this approach, a computational model was developed to simulate human data – this showed that the statistics of human firing patterns could be accounted for by a model that includes secondary synapses and synaptic amplification. Cellular damage was simulated with dynamic clamp by implementing a non-depolarizing shunt conductance. This revealed that damage introduced by microelectrode

recordings transformed the intrinsic firing properties of sympathetic neurons and obscured the contribution of weak nicotinic synapses to synaptic gain. Finally, G-protein coupled receptors for AngII increased postganglionic excitability, which facilitated the integration of weak synaptic activity and enhanced synaptic gain.

These results have implications for understanding human blood pressure regulation during exercise and hypertension. Until now, the SCG had been discounted as a regulator of blood pressure. Data in this thesis supports an integrative role for synaptic convergence in sympathetic ganglia and the modulation of gain by AngII. These results suggest that future efforts to control blood pressure and treat hypertension could target ganglionic mechanisms.

TABLE OF CONTENTS

PREFACE.....	XIII
1.0 INTRODUCTION.....	1
1.1 STATEMENT OF PURPOSE	1
1.2 SYNAPTIC ORGANIZATION OF SYMPATHETIC GANGLIA	2
1.2.1 Phenotypic Specialization of Postsynaptic Neurons	9
1.3 SYNAPTIC GAIN THEORY	11
1.4 DYNAMIC CLAMP.....	16
1.5 <i>IN VIVO</i> PATTERNS OF SYNAPTIC ACTIVITY.....	18
1.6 HYPERTENSION	21
1.6.1 Renocentric View of Essential Hypertension	23
1.6.2 Neurocentric View of Essential Hypertension	24
1.6.3 Therapies and Treatments for Essential Hypertension	25
2.0 CARDIAC RHYTHMS ENHANCE SYNAPTIC GAIN IN SYMPATHETIC NEURONS.....	28
2.1 INTRODUCTION	28
2.2 METHODS.....	30
2.2.1 SCG Primary Cell Culture	30
2.2.2 Whole-cell Current Clamp Recording.....	32

2.2.3	Dynamic Clamp Templates.....	33
2.2.4	Simulation of Human Data	35
2.2.5	Dynamic Clamp	36
2.2.6	Analysis and Statistics.....	37
2.3	RESULTS	38
2.3.1	Mammalian Dynamic Clamp Recordings	38
2.3.2	A Periodic Model of Stimulation	40
2.3.3	Periodic Versus Continuous Synaptic Activity	43
2.3.4	Presynaptic Activity at < 1.0 Hz is Sufficient to Generate Synaptic Gain	47
2.3.5	Modeling Human Activity at Rest and During Disease	49
2.4	DISCUSSION.....	57
3.0	MEMBRANE SHUNTS DEGRADE SYNAPTIC INTEGRATION	62
3.1	INTRODUCTION	62
3.2	METHODS.....	64
3.2.1	Preparation of Intact Ganglia	64
3.2.2	Microelectrode Recordings.....	65
3.2.3	SCG Primary Cell Culture	65
3.2.4	Whole-Cell Recordings.....	66
3.2.5	Classification of Neuronal Excitability Following Hodgkin's Criteria	67
3.2.6	Dynamic Clamp Recordings.....	68
3.2.7	Analysis and Statistics.....	69
3.3	RESULTS	70
3.3.1	Tonic Firing is not a Tissue Culture Artifact.....	70

3.3.2	SCG Neurons Display Three Classes of Excitability	72
3.3.3	SCG Neurons are Integrators.....	77
3.3.4	A Shunt Conductance Modulates Firing Dynamics	80
3.3.5	Anti-leak Conductances can Compensate for Leaky Membranes	84
3.3.6	Leak Conductances Reduce Synaptic Gain.....	87
3.4	DISCUSSION.....	89
3.4.1	Future Experiments.....	95
4.0	ANGIOTENSIN II ENHANCES SYNAPTIC GAIN	97
4.1	INTRODUCTION	97
4.2	METHODS.....	102
4.2.1	mRNA Extraction and RT-PCR	102
4.2.2	SCG Primary Cell Culture	103
4.2.3	Whole-cell Current Clamp Recording.....	104
4.2.4	Dynamic Clamp	104
4.3	RESULTS	104
4.3.1	SCG Neurons Contain a Subset of RAS Elements	104
4.3.2	AngII Increased Excitability and Synaptic Gain.....	106
4.4	DISCUSSION.....	110
5.0	CONCLUSION.....	113
	LIST OF ABBREVIATIONS.....	116
	BIBLIOGRAPHY	118

LIST OF TABLES

Table 1 – GPCRs and the channels they modulate in sympathetic neurons	8
Table 2 – Spiking frequency of postganglionic activity induced by periodic stimulation	43
Table 3 – Spike count comparison of postsynaptic activity from noisy and periodic stimulation	46
Table 4 – Spike per interval distribution and cumulative ISI exponential analysis.....	53
Table 5 – Primer pairs for RT-PCR analysis	103

LIST OF FIGURES

Figure 1 – A schematic of preganglionic divergence and postganglionic convergence in paravertebral sympathetic ganglia.	6
Figure 2 – The coincidence detection model of synaptic activity.	13
Figure 3 – Forms of integration that arise from different innervation patterns.	14
Figure 4 – Dynamic clamp feedback loop.	16
Figure 5 – Regulatory mechanisms that control blood pressure.	22
Figure 6 – Schematic of the periodic dynamic clamp template.	34
Figure 7 – Measurement of thresh- g_{syn} using a binary search routine.	37
Figure 8 – Synaptic gain during continuous random stimulation by virtual nicotinic synapses. .	39
Figure 9 – Exponential distribution of intervals between synaptic events.	40
Figure 10 – SCG voltage response to periodic stimulation.	42
Figure 11 – Periodic entrainment increased spike output.	45
Figure 12 – Periodic entrainment significantly increased gain.	46
Figure 13 – Synaptic gain can increase at lower presynaptic frequencies.	48
Figure 14 – Gain decreased at higher frequencies because spike afterhyperpolarization inhibited subthreshold EPSP summation.	49
Figure 15 – Simulated postganglionic activity driven by a single primary synapse.	51

Figure 16 – Entrained primary simulations have a different exponential ISI distribution.	52
Figure 17 – Simulated postganglionic activity driven by 1 primary and 6 secondary synapses. .	55
Figure 18 – Simulations incorporating secondary synapses can model sympathetic activity from human vasoconstrictor neurons.....	56
Figure 19 – The effect of a 2 nS leak on the model cell.	69
Figure 20 – A whole-cell recording from a dissociated SCG neuron displayed tonic firing dynamics.	71
Figure 21 – Tonic firing is not an artifact of tissue culturing.	71
Figure 22 – SCG neurons exhibit three classes of firing dynamics.....	73
Figure 23 – Frequency-current relationships are different between class 1 and class 2 neurons.	74
Figure 24 – Threshold synaptic conductance is higher in class 3 neurons.	75
Figure 25 – Ramp currents confirm neuronal excitability classification.....	76
Figure 26 – ZAP currents show SCG neurons are integrator neurons.....	78
Figure 27 - Paired pulse stimulation demonstrates integration.....	79
Figure 28 – Leak conductances reduced neuronal excitability, linearized IV relationships and decreased τ	82
Figure 29 – A leak conductance significantly decreased input resistance.	83
Figure 30 – Neurons from microelectrode recordings were significantly depolarized.	84
Figure 31 – Anti-leak conductances can compensate for leaky cells.	85
Figure 32 – Some class 3 neurons do not fire repetitively with large anti-leak conductances.	86
Figure 33 – A leak conductance reduced the efficacy of EPSPs.	88
Figure 34 – Leak conductances occluded weak nicotinic synapses.	89
Figure 35 - The renin-angiotensin pathway.	98

Figure 36 – RT-PCR of RAS elements in SCG neurons.	105
Figure 37 – AngII increased action potential output.	107
Figure 38 – AngII decreased thresh- g_{syn} and depolarized V_{rest}	107
Figure 39 – AngII increased sympathetic output and synaptic gain.	109
Figure 40 – AngII effects on electrophysiological properties.	109

PREFACE

This thesis represents the culmination of work that has taken place in the Department of Neurobiology at the University of Pittsburgh from May 2008 to July 2013. All experiments and analyses presented herein are original work performed by myself unless explicitly stated.

My time at the University of Pittsburgh has truly been a rewarding time. I cannot speak highly enough about the Graduate Program and specifically the Molecular Pharmacology Program. It takes a lot of dedication from many people to see that we graduate students become successful scientists. I could not get to this point without the help and support of several people.

First, I would like to thank my advisor John P. Horn for giving me the opportunity to work in his lab. He knew that I had a very limited background in neurobiology, but he took a chance with me and gave me the confidence to learn and progress in the field of neurobiology. He has given me numerous opportunities to present my work at conferences in the form of posters and presentations, something that is beyond rewarding. He has always pushed me so that I can become a better scientist, writer, and speaker. I also want to thank the past and current members of the lab who have taught me techniques, helped troubleshoot experiments, or at least lend an ear to talk about ideas.

I would like to thank my committee members Elias Aizenman, Kathy Albers, Ed Levitan, and Bruce Freeman for giving me their time and input to make my project a success. Their

insightfulness, critiques, and suggestions have been an incredible resource for helping me to develop into a successful scientist.

Special thanks are necessary for the faculty and staff of the graduate program. They have set forth an incredible program with classes and a structure that has been useful for my entire time in the program. The leadership of Bruce Freeman, Patrick Pagano, and Guillermo Romero has provided a rigorous and rewarding environment and it was a privilege to be a part of it. Thanks are also in order for Pat Smith and, the now retired, Cindy Duffy for always being willing to answer any questions that I had and help me in any way that they could.

Finally, I would like to thank my parents, Dan and Mary Springer, for their constant support in my life. Thank you to Marcel and Geta Cuperman for their support and giving me a home away from home. To my fiancé, Tzvia Cuperman, thank you for your unconditional love and encouragement throughout my graduate work. You provided me the motivation to always work my hardest to make you proud.

1.0 INTRODUCTION

1.1 STATEMENT OF PURPOSE

Hypertension presents a major threat to worldwide health. In the United States, high blood pressure affects 1 in 3 adults and leads to heart disease, which is the number one cause of death (Georgiopolou, Kalogeropoulos et al. 2012). Identifying the major causes of hypertension has been difficult. Emerging evidence suggests that increased activity in the sympathetic nervous system plays a major role in driving the development of hypertension. The working hypothesis of this thesis is that a significant component of sympathetic hyperactivity may originate from the amplification of preganglionic activity in sympathetic ganglia. According to this concept, 50 – 98% of all sympathetic activity in postganglionic sympathetic neurons arises as a consequence of preganglionic divergence, postganglionic convergence, and synaptic gain. Previous work to define ganglionic gain has relied, in part, on studies of bullfrog sympathetic neurons. Here, we examine the concept of sympathetic amplification in mammalian sympathetic neurons using the rat superior cervical ganglion (SCG) as an experimental model and using dynamic clamp to simulate physiological patterns of synaptic activity. The results suggest that new therapies to control hypertension may become feasible by targeting postganglionic neurons to reduce the amplification of preganglionic activity.

1.2 SYNAPTIC ORGANIZATION OF SYMPATHETIC GANGLIA

The sympathetic motor system regulates bodily homeostasis by controlling the activity of targets made of cardiac muscle, smooth muscle, and gland cells. Sympathetic motor activity originates in a central autonomic network. This network includes the hypothalamus, areas in the brain stem such as the ventral medulla and nucleus tractus solitarius, and spinal preganglionic neurons located in the intermediolateral cell column and central autonomic area (Horn and Swanson 2013). The central autonomic network integrates sensory information to generate activity that drives preganglionic neurons in the spinal cord. Preganglionic axons exit the spinal cord to form synapses in ganglia, where activity can be relayed, distributed, and integrated before being conveyed to peripheral end organ targets (Baluk 1995; Gibbins 1995; Elenkov, Wilder et al. 2000; Dorval and White 2006; Fargali, Sadahiro et al. 2012).

The sympathetic motor system contains two types of ganglia. Paravertebral ganglia are organized as bilateral segmental chains that lie on each side of the vertebral column (Baluk 1995; Gibbins 1995; Horn and Swanson 2013). Every neuron in paravertebral ganglia is innervated by axons from a subset of spinal segments and each cell is dominated by input from one spinal segment (Nja and Purves 1977; Lichtman, Purves et al. 1979; Baluk 1995; Gibbins 1995). Unlike paravertebral sympathetic chain ganglia, prevertebral sympathetic ganglia are located anterior to the vertebral column and are important for abdominal visceral control (Baluk 1995; Gibbins 1995; Janig 2006). The celiac, superior mesenteric and inferior mesenteric ganglia are more complex than paravertebral ganglia because they integrate sensory feedback from both the peripheral organs they control and from the enteric nervous system (Baluk 1995; Gibbins 1995; Gibbins, Teo et al. 2003; Horn and Swanson 2013). Paravertebral sympathetic neurons lack sensory feedback, and are therefore simpler to analyze.

Within paravertebral ganglia, preganglionic axons undergo extensive divergence. In addition, several preganglionic axons converge to form synapses on each postganglionic neuron. Generally, one preganglionic axon forms a very strong cholinergic nicotinic synapse, while the others form weak nicotinic synapses (Skok and Ivanov 1983; Dodd and Horn 1983b; Hirst and McLachlan 1986; Janig and McLachlan 1992; Karila and Horn 2000; Rimmer and Horn 2010). Karila and Horn (2000) classified strong and weak inputs as primary and secondary nicotinic synapses. Excitatory postsynaptic potentials (EPSPs) generated at primary synapses are suprathreshold in strength and will always fire a postganglionic action potential. Secondary synapses generate subthreshold EPSPs that do not trigger postganglionic action potentials (Karila and Horn 2000). In the 1980s, Vladimir Skok and colleagues initially identified primary and secondary synapses in rabbit SCG neurons, but referred to them as dominant and accessory inputs (Skok and Ivanov 1983). They determined that dominant EPSPs always evoked spikes while accessory EPSPs evoked spikes through summation (Skok and Ivanov 1983). However, body size of the species correlates with synaptic convergence and the numbers of secondary synapses varies from one experimental animal model to another (Purves, Rubin et al. 1986). For example, mouse SCG neurons receive an average of 4.5 inputs while rat SCG neurons receive 8.7 inputs (Purves, Rubin et al. 1986). Karila and Horn (2000) defined this as the $n + 1$ pattern of ganglionic convergence, where n refers to the number of secondary synapses and 1 refers to the solitary primary synapse.

In this thesis, we focus on the rat superior cervical ganglion. The SCG has long been important for studying fundamental mechanisms of synaptic transmission. By applying nicotine, John Langley and colleagues were able to determine, in the late 1800s, that ganglion cells act as a link between central efferents and peripheral end organs (Langley and Dickinson 1890;

Langley 1921; Davenport 1991). Langley concluded that nicotine acts directly upon cells in the ganglia by combining with a “receptive substance”, now known as receptors, to transmit the signal and cause contraction (Langley 1921; Davenport 1991). Subsequent experiments, in the 1930s, to explain synaptic transmission in the SCG became highly controversial. The debate centered on whether transmission was purely chemical or electrical in nature. In the one camp, Wilhelm Feldberg, working in Henry Dale’s laboratory, showed that acetylcholine (ACh) is released during synaptic transmission (Feldberg and Gaddum 1934; Davenport 1991). By collecting arterial perfusate, Feldberg showed ACh was present after stimulating the cervical sympathetic trunk (Feldberg and Gaddum 1934). In the other camp, John Eccles and his colleagues were electrophysiologists who argued that transmission was exclusively electrical in nature (Eccles 1935a; Eccles 1935b; Eccles 1964; Davenport 1991). Eccles insisted that transmission was too fast to be chemical in nature and therefore must occur electrically. Bernard Katz and his colleagues settled the debate, in the 1950s, with intracellular recordings at the frog neuromuscular junction (Fatt and Katz 1951; Del Castillo and Katz 1954; Katz 1966). They showed that ACh increased postsynaptic conductance by making the membrane permeable to ions (Fatt and Katz 1951). They also showed that ACh is released in packets, known as synaptic vesicles, and that the quantal content of transmitter release is independent of the postsynaptic driving force (Fatt and Katz 1951; Del Castillo and Katz 1954; Katz 2003). Takeuchi and Takeuchi (1960) uncovered the ions responsible for the ACh induced conductance change at the end-plate by showing that the reversal potential for the synaptic current shifts with changes in sodium and potassium concentration, but not chloride concentration. Rosmond Eccles was the first to record intracellular potentials from sympathetic neurons, using the rabbit SCG (Eccles 1955). Subsequent work demonstrated that the mechanism of ACh action on frog sympathetic

neurons was similar to that seen at the neuromuscular junction (Nishi and Koketsu 1960; Blackman, Ginsborg et al. 1963). In a subsequent paper, Eccles and Libet (1961) provided the first evidence of non-nicotinic slow synaptic potentials using the rabbit SCG. This set the stage for future experiments to analyze metabotropic signaling in sympathetic neurons (see [Chapter 4](#)).

Over time, the SCG has been extensively studied for several reasons. It is large and easily accessible due to its location in the neck and is situated adjacent to the carotid artery at the point where it bifurcates into the internal and external carotid branches. By virtue of being at the rostral end of the paravertebral chain, preganglionic inputs are separate from the postganglionic outputs (e.g. Li and Horn 2006). In the acutely isolated intact SCG, one can therefore stimulate the presynaptic cervical sympathetic trunk and record postsynaptic activity from the internal and external carotid nerves. Estimates of ganglionic divergence are based on pre- and postganglionic cell counts. Retrograde tracing studies determined that 1600 preganglionic neurons innervate the SCG, which contains about 25000 – 45000 neurons (Rando, Bowers et al. 1981; Gibbins 1995; Wang, Holst et al. 1995). Hence there is an approximate 1:20 divergence between pre and postganglionic neurons in the SCG and in other ganglia that have been analyzed (Figure 1) (Purves and Hume 1981; Wang, Holst et al. 1995).

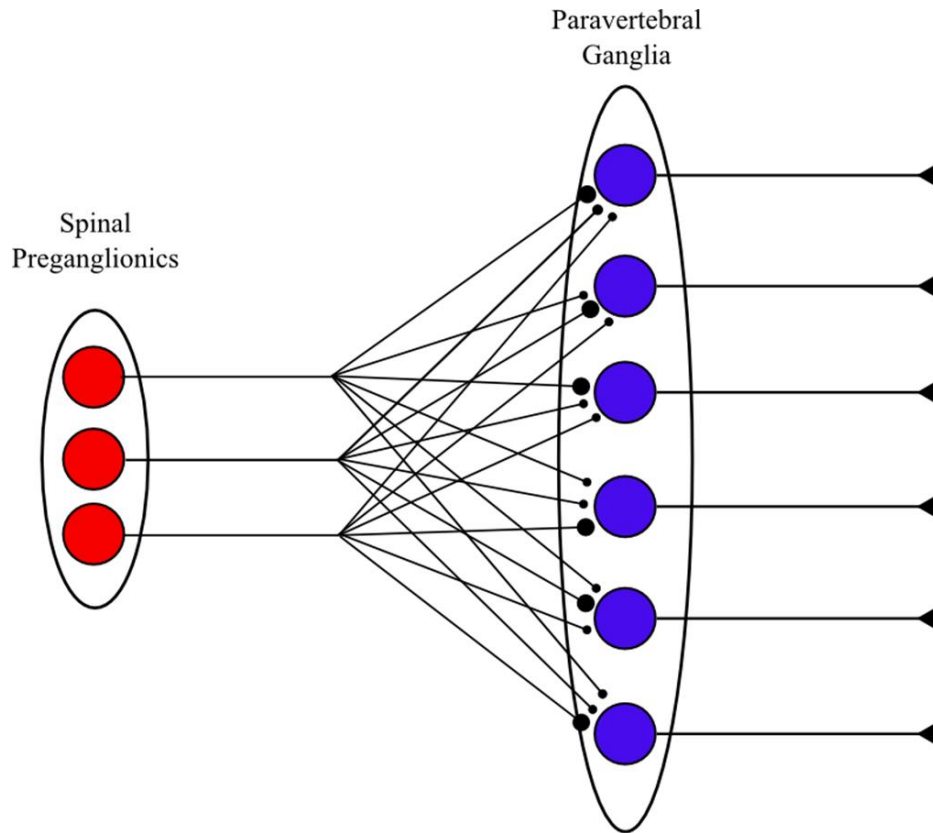


Figure 1 – A schematic of preganglionic divergence and postganglionic convergence in paravertebral sympathetic ganglia. In this simplified drawing, three spinal preganglionic neurons extend axons that diverge to form synapses on six postganglionic neurons. This indicates 1:2 divergence between pre and postganglionic neurons. However, divergence in the rat SCG is about 1:20 (Purves and Hume 1981). The diagram also depicts postganglionic convergence of 1 primary and 2 secondary synapses on each cell. Rat SCG neurons normally receive 1 primary and an average of 8.7 secondary synapses (Purves, Rubin et al. 1986). Because postganglionic neurons exhibit no lateral connections, the properties of a neuron are representative of all postganglionic neurons. Modeled neurons can therefore be extrapolated to understand how the entire population behaves. Figure adapted from Horn and Kullmann (2007).

Although nicotinic EPSPs in sympathetic ganglia and the neuromuscular junction are pharmacologically and functionally similar, they are not identical. The receptors expressed by muscle and neurons differ in their subunit expression, but all belong to the superfamily of ligand-gated ion channels (McGehee and Role 1995; Liu, Zhang et al. 2007). Muscle receptors are heteromeric pentamers composed of α_1 , β_1 , δ , γ , and ϵ subunits. Neuronal nicotinic acetylcholine receptors (nAChR) that mediate fast EPSPs are homomeric pentamers of α_7 or α_9 subunits or heteromeric pentamers of α - and β -subunits (α_2 - α_{10} and β_2 - β_4) (Schoepfer, Conroy et al. 1990; Role 1992; Sargent 1993; Gotti and Clementi 2004). In the SCG, the predominant subunits expressed are α_3 and β_4 , with lesser expression of α_5 and β_2 subunits (Papke, Boulter et al. 1989; Rust, Burgunder et al. 1994; Mao, Yasuda et al. 2006).

In addition to nicotinic receptors, sympathetic neurons express G-protein coupled receptors (GPCRs) that alter cellular excitability (Table 1). Muscarinic receptors were the first GPCR studied when it was discovered they elicit slow EPSPs and slow inhibitory postsynaptic potentials (Libet, Chichibu et al. 1968; Kuba and Koketsu 1976a; Kuba and Koketsu 1976b; Dodd and Horn 1983b; Hille 2001; Brown and Passmore 2009). Subsequent experiments showed SCG neurons express receptors for norepinephrine, angiotensin II, bradykinin, pituitary adenylate cyclase-activating protein, and substance P (Table 1). Although, the signaling mechanisms for these receptors have been extensively analyzed (Alexander, Mathie et al. 2011), their physiological significance for autonomic behavior is not well understood. [Chapter 4](#) examines the role of angiotensin II in changing the gain of synaptic amplification.

Table 1 – GPCRs and the channels they modulate in sympathetic neurons

<u>Transmitter/hormone</u>	<u>Receptor (gene)</u>	<u>Channel (gene)</u>	<u>Reference</u>
norepinephrine	α_2 (<i>ADRA</i>)	gCa _N (Ca _v 2.2)	(Horn and McAfee 1979; Kafka, Horn et al. 1980; Galvan and Adams 1982; Gold, Dastmalchi et al. 1997)
acetylcholine	M ₁ (<i>CHRM1</i>) M ₂ (<i>CHRM2</i>), M ₄ (<i>CHRM4</i>)	gK _M (K _v 7.2, K _v 7.3) gCa _N (Ca _v 2.2) gK _{ir} (GIRK/Kir3) gCa _N (Ca _v 2.2)	(Fernandez-Fernandez, Abogadie et al. 2001; Brown and Passmore 2009)
angiotensin II	AT _{1A} (<i>AGTR1A</i>) AT _{1B} (<i>AGTR1B</i>) AT ₂ (<i>AGTR2</i>)	gK _M (K _v 7.2, K _v 7.3) gCa _N (Ca _v 2.2) gK (K _v 4.2, K _v 11.3)	(Kang, Sumners et al. 1993; Shapiro, Wollmuth et al. 1994; Gao and Zucker 2011)
bradykinin	B ₂ (<i>B2BKR</i>)	gK _M (K _v 7.2, K _v 7.3)	(Jones, Brown et al. 1995; Edelbauer, Lechner et al. 2005; Hernandez, Zaika et al. 2008)
pituitary adenylate cyclase-activating peptide	PAC ₁ (<i>ADCYAP1R1</i>)	h-type g _{cation} (HCN1-4)	(Beaudet, Parsons et al. 2000; May, Beaudet et al. 2000; Tompkins, Lawrence et al. 2009)
substance P	NK-1R (<i>TACR1</i>)	gK _M (K _v 7.2, K _v 7.3)	(Womack, Morris et al. 2007)
adenosine	adenosine A1 receptor (<i>ADORA1</i>)	gCa _N (Ca _v 2.2)	(Henon and McAfee 1983; Zhu and Ikeda 1993)
ATP	P2Y (<i>P2RY1</i>)	gK _M (K _v 7.2, K _v 7.3)	(Hernandez, Zaika et al. 2008)

Sympathetic neurons express a repertoire of GPCRs that activate various ion channels and regulate neuronal excitability and synaptic activity.

1.2.1 Phenotypic Specialization of Postsynaptic Neurons

Sympathetic neurons are phenotypically diverse. Subsets of neurons that innervate different targets also differ in the transmitters, neuropeptides, receptors, and ion channels that they express. This principle is illustrated by bullfrog sympathetic ganglia 9 and 10, which contain large secretomotor B neurons and small vasomotor C neurons (Nishi, Soeda et al. 1965; Honma 1970; Dodd and Horn 1983a). These neurons can be distinguished by their axonal conduction velocities. B neurons conduct at 2.0 m/sec while C neurons conduct action potentials at 0.3 m/sec (Dodd and Horn 1983a). Immunoreactivity also distinguishes the cell groups. Luteinizing hormone releasing hormone (LHRH) is a peptidergic co-transmitter (together with ACh) that is responsible for the late slow EPSP (Jan, Jan et al. 1979; Jan, Jan et al. 1980; Jan and Jan 1982). Co-immunostaining reveals that preganglionic nerve terminals containing LHRH innervate neurons that contain neuropeptide Y (NPY), a 36 amino acid neuropeptide that acts as a co-transmitter in the sympathetic nervous system and a marker for C neurons (Horn and Stofer 1988; Wahlestedt, Hakanson et al. 1990). Additionally, calcitonin gene-related peptide immunoreactive fibers make contact with NPY negative B neurons (Horn and Stofer 1989). Finally, C neurons are more excitable than B neurons (Kullmann and Horn 2010b). Phenotypic specialization can identify groups of neurons in bullfrog ganglia, but are these functional specializations conserved in mammals?

The phenotypic organization of the SCG is more difficult to analyze than bullfrog ganglia for two main reasons. First, the SCG innervates more targets in the head, which requires greater cell type diversity than in amphibian ganglia 9 and 10, which innervate the hind limbs. Second, axonal conductance velocities in the rat sympathetic system all fall within the C fiber range making them more difficult to distinguish than B and C axons (Li and Horn 2006). Nonetheless,

three cell groups account for 85% of SCG neurons (Gibbins 1991; Gibbins 1995; Li and Horn 2006; Li and Horn 2008). Vasomotor neurons comprise 50 – 70% of the SCG and are noradrenergic neurons that project to both large and small arteries to elicit vasoconstrictor action (Gibbins 1995). Vasomotor neurons are chemically distinguished by NPY expression (Li and Horn 2006). Vasomotor neurons are also significantly smaller than secretomotor and pilomotor neurons and have slower postsynaptic conduction velocities (Gibbins 1995; Li and Horn 2006). In addition, vasomotor neurons are high threshold neurons meaning vasomotor nicotinic synapses require a larger presynaptic stimulus to trigger a postsynaptic action potential. Pilomotor neurons are NPY negative, high threshold neurons that constitute 15 – 25% of SCG neurons and project to the skin to control piloerection (Gibbins 1995; Li and Horn 2006; Li and Horn 2008). These neurons are significantly larger and have faster action potential conduction velocities than vasomotor neurons (Gibbins 1995; Li and Horn 2006). Secretomotor neurons are NPY negative, low threshold neurons that comprise about 15% of the neuronal population and project to salivary and lacrimal glands (Gibbins 1995; Li and Horn 2006; Li and Horn 2008). These neurons are the largest in the SCG and have a significantly faster postsynaptic conduction velocity (Li and Horn 2006). Therefore, the major SCG cell types can be distinguished on the criteria of their size, conduction velocity, NPY reactivity and presynaptic threshold excitability (Li and Horn 2006; Li and Horn 2008). While there are additional cell types in the SCG that innervate the iris, pineal gland, and thyroid gland, each of these phenotypes account for <5% of the neuronal population (Gibbins 1991; Li and Horn 2008).

In [Chapter 3](#), we investigate distinctions in the firing properties of rat SCG neurons using Hodgkin's criteria for classifying excitability (Hodgkin 1948) and examine the consequences for synaptic gain in these cell groups.

1.3 SYNAPTIC GAIN THEORY

Karila and Horn (2000) hypothesized that $n + 1$ convergence could lead to synaptic amplification. Their theory relies on observations of synaptic strength in isolated bullfrog ganglia and natural activity in living animals. Early studies of B neurons in isolated bullfrog ganglia concluded that cells were singly innervated by one primary synapse (Blackman, Ginsborg et al. 1963; Nishi, Soeda et al. 1965; Weitsen and Weight 1977). However, when Ivanoff and Smith studied bullfrog sympathetic ganglia *in vivo*, their intracellular recordings of natural activity demonstrated that 53% of B neurons had at least one secondary synapse in addition to the primary synapse (Ivanoff and Smith 1995). Karila and Horn (2000) then re-examined B neurons in isolated ganglia. Using graded presynaptic stimulation and intracellular recording, they found that 93% of B neurons have at least one secondary nicotinic synapse (Karila and Horn 2000).

The simplicity of convergence in B cells allowed Karila and Horn to study single secondary synapses in isolation. They showed that summation between pairs of subthreshold secondary EPSPs was sufficient to drive action potentials in many cases (Karila and Horn 2000). This raised a question as to whether secondary synapses contribute to postganglionic output in a meaningful way.

To answer this question, Karila and Horn developed a probabilistic model of coincidence detection that incorporates information about the timing of natural *in vivo* sympathetic activity. Their model assumed that all preganglionic neurons form both primary and secondary synapses on postganglionic neurons. They also argued that because of a lack of lateral connections between ganglion cells (Figure 1), one can infer from a single cell how the entire population behaves (Karila and Horn 2000).

The goal of the coincidence detection model is to determine how secondary EPSPs modulate ganglionic amplification. Since pairs of subthreshold EPSPs are sufficient to drive action potentials, a window of summation was defined. Two subthreshold EPSPs that fall within this window will generate a postganglionic action potential. Therefore, ganglionic amplification can be determined by calculating the probability of secondary EPSPs occurring within the window. The calculation assumes that the generation of EPSPs is a random process, which is supported by evidence from mammalian sympathetic neurons (McLachlan, Habler et al. 1998). Neuronal activity is described as the average firing rate of random activity. For randomly timed synaptic events that occur at an average rate, the intervals between events are exponentially distributed and synaptic events follow a random, Poisson process (McLachlan, Habler et al. 1998). Therefore, the model can predict the probability that two random subthreshold EPSPs will fall within a given window. This probability relies on the size of the summation window, presynaptic frequency (f_{pre}), and number of secondary synapses (Karila and Horn 2000). Increasing any of those factors will increase the probability of secondary synaptic summation. The firing rate of each postganglionic neuron (f_{post}) will be the sum of the primary and secondary postsynaptic firing rates. Dividing the output frequency by the input frequency will calculate synaptic gain ($g = f_{post}/f_{pre}$). A $g > 1$ suggests that subthreshold coincidences drove postganglionic action potentials, making the postsynaptic output faster than the presynaptic input (Figure 2).

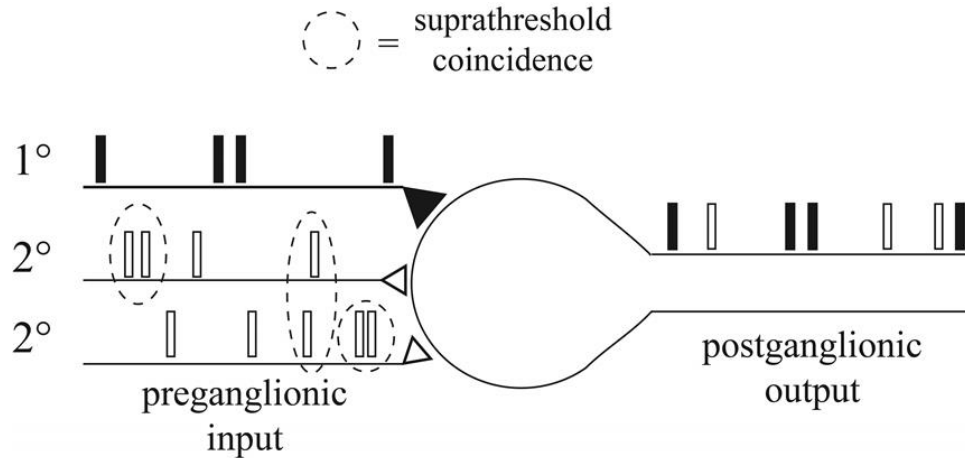


Figure 2 – The coincidence detection model of synaptic activity. Coincidences between subthreshold secondary nicotinic EPSPs can produce synaptic amplification by eliciting a postganglionic action potential in addition to those triggered by the primary synapse. Bars of the preganglionic input represent the EPSPs that the presynaptic synapses would evoke. The bars in the postganglionic output represent action potentials triggered by primary synapses (black bars) and coincidences of secondary EPSPs (white bars). Synaptic gain = $f_{post}/f_{pre} = 7/4 = 1.75$. Figure adapted from Horn and Kullmann (2007).

Lower and upper boundaries of postsynaptic activity were defined to predict the limits of physiological activity. If one assumes that the average f_{pre} is so low that coincidences never occur between secondary EPSPs, then the primary synapse becomes the sole determinant of postganglionic activity (Figure 3A). At this lower limit, the system behaves as a simple relay where $f_{post} = f_{pre}$. This means the lower limit for gain is 1.0. On the other hand, one can argue that at an arbitrarily large value for f_{pre} , all secondary EPSPs will become suprathreshold coincidences and drive spikes (Figure 3B) (Karila and Horn 2000).

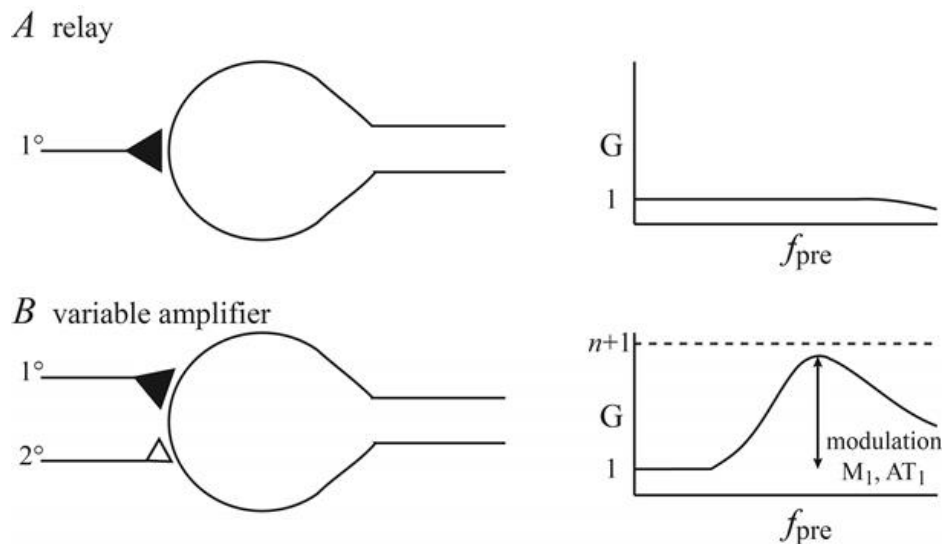


Figure 3 – Forms of integration that arise from different innervation patterns. (A) Innervation by a unitary primary synapse enables the neuron to act as a relay of activity where presynaptic activity is faithfully transmitted to the postsynaptic axon. Primary synaptic innervation produces a baseline synaptic gain, which does not change with presynaptic frequency. (B) $n + 1$ convergence produces a variable amplifier where summation of subthreshold EPSPs will influence postganglionic firing. Secondary synapses elevate synaptic gain, which can be modulated by changes in the number and strength of secondary synapses and by GPCRs that modulate excitability. The theoretical limit of gain is the sum of all primary and secondary synaptic events. Figure adapted from Wheeler, Kullmann, *et al.* (2004).

Although coincidence detection theory provides a simple model to understand how ganglionic convergence can produce synaptic gain, it lacks biophysical details, and is therefore difficult to test with experiments. To solve this problem, a conductance-based model was

developed to simulate ganglionic integration (Schobesberger, Wheeler et al. 2000; Wheeler, Kullmann et al. 2004).

The conductance-based model is a Hodgkin-Huxley style model that implements ionic conductances for voltage gated sodium and potassium channels, leak channels, and M-type potassium channels to mimic B neurons. Solving the equations by numerical integration simulates a resting membrane potential and action potential spiking behavior. Stimulating with synaptic conductance allows one to determine how the model integrates synaptic activity. As in the coincidence detection model, the timing of synaptic events was assumed to follow a Poisson process. However, a window of summation was not included because the ionic conductances determine whether pairs of subthreshold EPSPs are sufficient to drive action potentials (Wheeler, Kullmann et al. 2004).

By simulating ganglionic integration with the conductance-based model, Wheeler *et al.* (2004) showed $n + 1$ convergence could generate synaptic gain that varies with f_{pre} . They also showed that the magnitude of synaptic gain is determined by the number, strength, and frequency of secondary synapses (Wheeler, Kullmann et al. 2004). Neurons innervated by a single primary synapse will act as relays of preganglionic activity (Figure 3A). The $n + 1$ convergence pattern produces a variable amplifier where the activity of secondary synapses determines synaptic gain and gain can be modulated by GPCRs that affect neuronal excitability (Figure 3B).

An advantage of the conductance-based model is that the templates of synaptic activity used for simulations can also be used to stimulate living neurons using a technique known as dynamic clamp. By taking this approach, one can devise experimental tests of computational predictions.

1.4 DYNAMIC CLAMP

Dynamic clamp provides a method for creating virtual ionic conductances in living cells. With this approach, one can analyze, in a reproducible manner, the consequences of synaptic convergence in living neurons. Dynamic clamp is a modified form of current clamp that uses real-time feedback (Dorval, Christini et al. 2001; Kullmann, Wheeler et al. 2004; Horn and Kullmann 2007; Piwkowska, Destexhe et al. 2009). The feedback loop measures the membrane potential, calculates the magnitude of the virtual conductance, uses Ohm's law to calculate the amount of current that should be flowing through the virtual conductance and sends an appropriate command signal to the current clamp amplifier (Figure 4) (Dorval, Christini et al. 2001; Kullmann, Wheeler et al. 2004; Horn and Kullmann 2007).

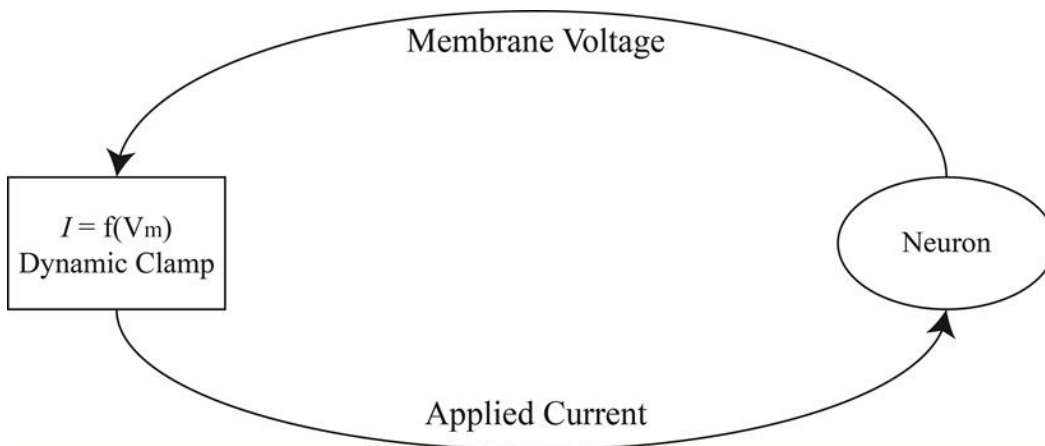


Figure 4 – Dynamic clamp feedback loop. This simple schematic illustrates the dynamic clamp feedback loop. A conductance command is input into the computer, which will use the membrane voltage to calculate the size of the current injection. As membrane voltage changes, the dynamic clamp will rapidly recalculate the amplitude of the current injection. This feedback loop relies on accurate measures of membrane voltage and very rapid calculations of current strength to model ion channels.

However, there is a caveat to using dynamic clamp in that the loop must operate at a cycle time faster than the gating of all ion conductances in the system. All ion channels follow Ohm's law [$I = g * (V_m - E_{rev})$]. In order to create the virtual conductance, one needs information about conductance (g) as a function of time, a measurement of the membrane voltage (V_m) and the reversal potential (E_{rev}) of the modeled ion channel or synapse (Kullmann, Wheeler et al. 2004). The nicotinic synapse mediates a fast EPSP whose conductance waveform can be defined as the sum of two exponentials; one for the activation time constant and one for the decay time constant (Schobesberger, Wheeler et al. 2000). The synapse cannot be modeled with simple current injections because V_m will change as current is injected, which will also change the driving force ($V_m - E_{rev}$). Therefore, fast real-time measurements of V_m are required to properly adjust the size of the current injection to model a defined level of g at a specific time point. Dynamic clamp can be used to determine the precise role of a specific ion channel in the regulation of membrane voltage and to understand how the complex interactions of various ion channels regulate synaptic output (Piwkowska, Destexhe et al. 2009).

Dynamic clamp allows preganglionic activity to be controlled in ways that are impossible using nerve stimulation or observations of *in vivo* activity. In an isolated ganglion preparation, it is impossible to independently stimulate all the presynaptic axons. In addition, changing synaptic strength, modifying postganglionic convergence, and altering the frequency of presynaptic activity cannot be accomplished in a controllable way. Dynamic clamp makes it possible to normalize these parameters to allow comparison between cells (Horn and Kullmann 2007).

In this thesis, dynamic clamp was used to measure ganglionic amplification in rat SCG neurons and to determine how different patterns of presynaptic activity and angiotensin II modulate synaptic gain. Additionally, dynamic clamp was used to model a damaged cell to investigate how intracellular recordings with microelectrodes affect postganglionic activity.

1.5 *IN VIVO* PATTERNS OF SYNAPTIC ACTIVITY

In the probability based model (Karila and Horn 2000) and the conductance based model (Wheeler, Kullmann et al. 2004), it was assumed that noisy preganglionic activity could be described as a Poisson process. This assumption was drawn from intracellular recordings showing that intervals between synaptic events in sympathetic neurons are exponentially distributed. (McLachlan, Habler et al. 1998). However, it has also been known for some time that the timing of synaptic events exhibits another prominent feature in a subset of sympathetic neurons.

Sympathetic activity in neurons that control blood pressure is rhythmic and linked to the cardiac cycle. Edgar Adrian and colleagues, in the early 1930s, made pioneering extracellular recordings of discharges from mammalian renal sympathetic nerves (Adrian, Bronk et al. 1932; McAllen and Malpas 1997). They found that postganglionic sympathetic activity fluctuated in response to the rise and fall of arterial blood pressure during the cardiac cycle (Adrian, Bronk et al. 1932). Subsequent work demonstrated similar behavior in muscle vasoconstrictor neurons (Janig 1988). Cardiac rhythmicity of firing by these cell groups depends upon the pulsatile activation of arterial baroreceptors. In experimental animals, rhythmic synchronization is lost after baro-denervation (Malpas 2010). Interestingly, a similar pattern of rhythmic sympathetic

activity is found in awake humans (Macefield, Wallin et al. 1994; Macefield and Wallin 1996; Macefield, Rundqvist et al. 1999).

By inserting tungsten microelectrodes through the dermis into fascicles of peripheral nerves supplying the skin and striated muscles, one can record multi-unit postganglionic sympathetic activity from human subjects (Janig and Habler 2003). Isolated bundles of vasoconstrictor motor axons that supply skeletal muscle vascular beds revealed that barosensitive vasomotor neurons exhibited cardiac rhythmicity (Macefield, Wallin et al. 1994). Subsequent experiments using high impedance electrodes permitted the isolation of single postganglionic axons and confirmed that muscle vasoconstrictors are under baroreflex control (Janig and Habler 2003; Macefield and Elam 2003; Macefield 2009; Macefield 2011). These studies revealed that sympathetic activity occurs in bursts, an increase in sympathetic activity results in more cardiac cycles containing bursts, and single-unit recordings revealed that the increase in bursting is a result of the recruitment of additional neurons to become active (Macefield, Elam et al. 2002; Ichinose, Saito et al. 2008). Increases in blood pressure, associated with exercise and hypertension, manifest as increases in total sympathetic activity, burst frequency, and burst strength (Janig and Habler 2003; Ichinose, Saito et al. 2008). This raises two questions; (1) is there any physiological significance to this coordinated activity and (2) is this activity a reflection of activity from the CNS or is activity modified by sympathetic ganglia?

A potential consequence of coordinated activity is that synchronized discharges facilitate cardiovascular control by increasing the gain of the system. The general consensus is that the brain and brainstem are the primary sites of integration and that activity from preganglionic neurons is sent in a direct fashion to postganglionic vasoconstrictor neurons, where activity is directly relayed to the effector organ (Janig 1988; McAllen and Malpas 1997; Guyenet 2006). In

this hypothesis, all gain is generated in the brain and spinal cord with no additional gain being generated at the level of the ganglia. This sparks a debate as to the nature of postganglionic nicotinic synapses and whether or not the SCG uses secondary synapses to drive postganglionic action potentials.

Intracellular recordings from anesthetized rats have been interpreted to indicate that the natural discharge of SCG neurons is primarily driven by suprathreshold preganglionic inputs (McLachlan, Davies et al. 1997; McLachlan, Habler et al. 1998; McLachlan 2003). However, intracellular recordings from the L3 lumbar sympathetic ganglia suggest that activity from subthreshold synapses was sufficient to drive about half of the total postganglionic activity (Bratton, Davies et al. 2010). This provides the first evidence that subthreshold inputs may contribute significantly to postganglionic activity in mammalian sympathetic ganglia. While the L3 is a completely different ganglion than the SCG, direct nerve stimulation in the SCG revealed innervation by multiple secondary synapses and that pairs of subthreshold EPSPs are sufficient to drive action potentials (Rimmer and Horn 2010). What can account for these opposing ideas concerning the function of secondary synaptic innervation in the SCG? One possibility is that in the initial microelectrode studies, impaled cells were hyperpolarized by steady state current injection (McLachlan, Davies et al. 1997; McLachlan, Habler et al. 1998). Hyperpolarization did not block action potentials from suprathreshold EPSPs (McLachlan, Habler et al. 1998), but may have minimized the role of other subthreshold synaptic inputs.

In [Chapter 3](#), we use dynamic clamp to test an additional hypothesis that may account for the underrepresentation of secondary synaptic activity *in vivo*. Additionally, [Chapter 2](#) examines the importance of rhythmic activity in regulating synaptic gain.

1.6 HYPERTENSION

Might sympathetic ganglia play a role in human hypertension? High blood pressure is the leading cause of cardiovascular disease. It is an epidemic - at least 65 million, or about 33%, of US adults are diagnosed with hypertension (Georgiopolou, Kalogeropoulos et al. 2012). The lifetime risk of developing hypertension in middle-aged and older adults is about 90% (Georgiopolou, Kalogeropoulos et al. 2012). Hypertension is known as a “stealth disease” and “silent killer” because there are no obvious symptoms, yet it is a major risk factor for stroke and heart disease, the number one cause of death. Essential hypertension is a syndrome where arterial pressure is chronically elevated above 140/90 mmHg with no known etiology (Wesson 2001; Georgiopolou, Kalogeropoulos et al. 2012). Blood pressure and flow are regulated by intrinsic, and extrinsic factors that act on the heart and vascular system and are important for normal cardiovascular function. Intrinsic factors include vascular resistance, cardiac output, stroke volume, heart rate, venous filling pressure, end diastolic volume, and vascular compliance. Hormones such as aldosterone, angiotensin II, and norepinephrine also regulate blood pressure (Figure 5) (Wesson 2001; Hall 2011b; Boulpaep 2012). There appear to be two main factors that drive development of essential hypertension: (1) dysregulation of salt secretion and blood volume by the kidney (Berne 1986; Wesson 2001; Hall 2011b; Stolarz-Skrzypek, Bednarski et al. 2013), and (2) hyperactivity of the sympathetic nervous system (Joyner, Charkoudian et al. 2008; Joyner, Charkoudian et al. 2010; Malpas 2010; Parati and Esler 2012).

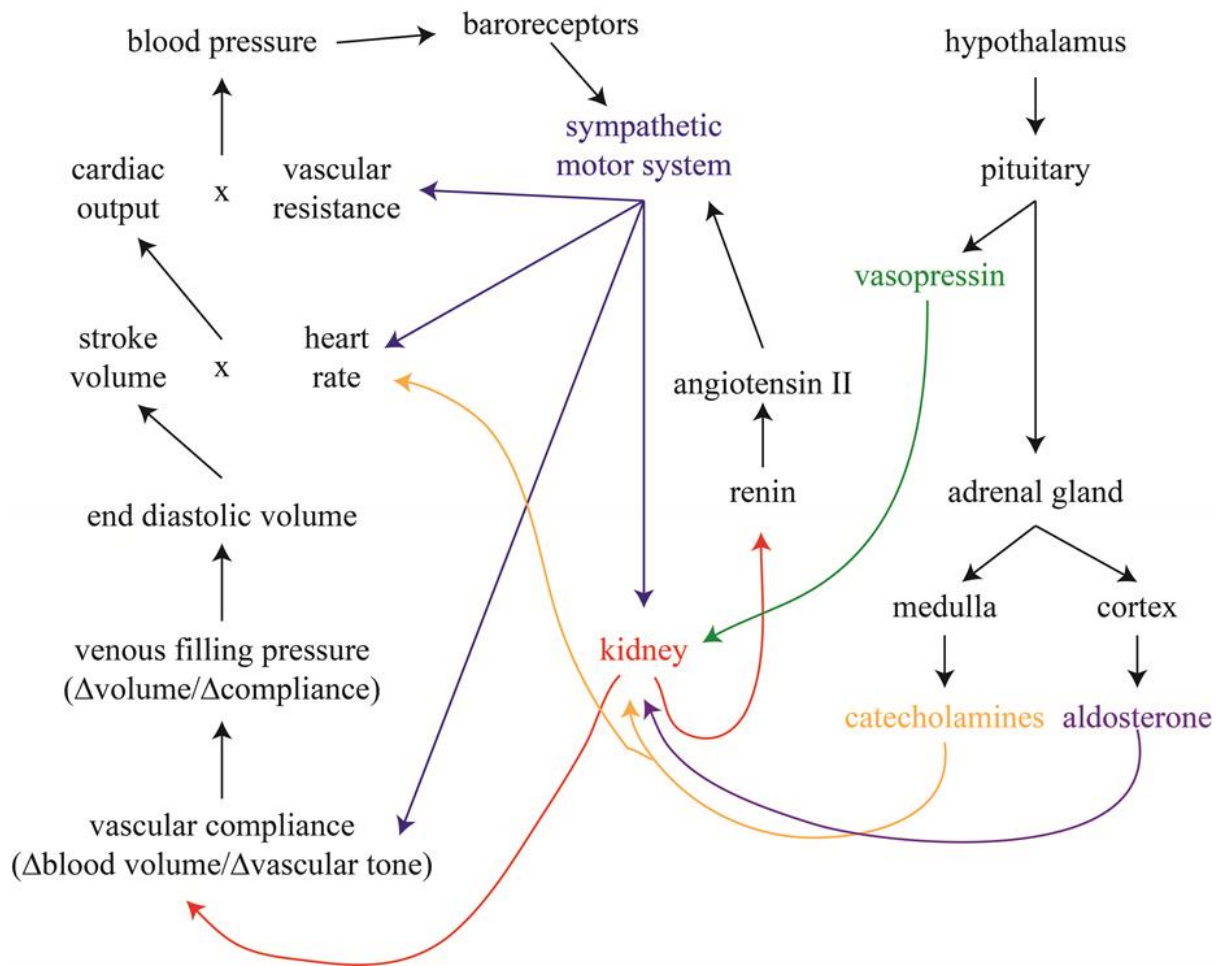


Figure 5 – Regulatory mechanisms that control blood pressure. This schematic view of blood pressure control illustrates the complexity and redundancy of blood pressure regulation. These control mechanisms can originate from the sympathetic motor system, the kidney, or the brain. The balance between these regulatory mechanisms will control blood pressure.

1.6.1 Renocentric View of Essential Hypertension

Essential hypertension can occur through defects in renal sodium regulation. Sodium balance is critical in regulating blood volume, arterial pressure and organ perfusion (Stolarz-Skrzypek, Bednarski et al. 2013). Pressure natriuresis is the sodium excretion response to high arterial pressure. It is responsible for the long term control of blood pressure by regulating body fluid balance and plasma volume (Anderson, Evans et al. 1995). Under normal conditions, a decrease in sodium intake will result in a decrease in blood volume and pressure. To counteract this effect, short term factors such as the vasoactive hormones renin, which produces angiotensin II, and vasopressin are released to mediate vasoconstriction, limit fluid loss from the kidneys, and restore blood pressure (Stolarz-Skrzypek, Bednarski et al. 2013). Additionally, aldosterone is released from adrenal glands to prevent sodium excretion. These three hormones work in harmony to counteract the reduction in blood volume by retaining fluid and restoring blood pressure. Dysregulation of these homeostatic mechanisms can result in essential hypertension.

Several lines of evidence support the renocentric view of essential hypertension. A high salt diet expands the extracellular fluid volume thereby increasing renal vascular resistance. A blunted renal salt excretion is unable to compensate for the increased extracellular fluid and leads to chronic blood pressure elevation (Wesson 2001; Stolarz-Skrzypek, Bednarski et al. 2013). There is also evidence to suggest a genetic component to renal factors that mediate essential hypertension. When kidneys from genetically predisposed hypertensive rats are implanted into rats that do not develop hypertension and vice versa, the normotensive rats with the hypertensive kidneys develop hypertension while the genetically hypertensive rats with normal kidneys are protected from essential hypertension (Wesson 2001; Joyner, Charkoudian et al. 2008).

Additional evidence for the renocentric view includes the dysregulation of renin in response to excess salt. Renin is a renal enzyme that cleaves the hormone angiotensinogen to form angiotensin I. A second enzymatic cleavage by angiotensin converting enzyme produces the vasoconstrictor angiotensin II. Normotensive animals that undergo salt loading will suppress renin release to prevent angiotensin II induced vasoconstriction. Exogenous application of modest amounts of renin in the presence of high salt significantly raises blood pressure, suggesting that unsuppressed renal renin release, in response to high salt, will lead to hypertension (Joyner, Charkoudian et al. 2008).

1.6.2 Neurocentric View of Essential Hypertension

Some normotensive rats that are fed a high salt diet do not develop essential hypertension. However, a baro-denervated normotensive animal, whose baroreflex has been disrupted, will develop hypertension in response to a high salt diet, providing evidence that the sympathetic nervous system also plays a role in essential hypertension (Joyner, Charkoudian et al. 2008).

In the last three decades, the sympathetic motor system has moved towards center stage in the field of cardiovascular physiology, due to emerging evidence that sympathetic motor system hyperactivity drives hypertension and other downstream cardiovascular disorders (Joyner, Charkoudian et al. 2008; Joyner, Charkoudian et al. 2010; Malpas 2010; Parati and Esler 2012). Part of the neural control of circulation involves barosensitive sympathetic efferents that are controlled by arterial baroreflexes (Guyenet 2006). These efferents act as a negative feedback loop to regulate blood pressure and are important for the rapid, short-term regulation of blood pressure. Postural mediated changes in blood pressure and exercise adaptation require barosensitive efferents to regulate heart rate and vascular tone. They are sensitive to blood

pressure changes so that under normal conditions a rise in arterial pressure will inhibit nerve activity (Guyenet 2006).

Evidence for long-term sympathetic mediated blood pressure regulation is found in hypertensive human data. Norepinephrine spillover measurements are used to monitor sympathetic activity around the heart and kidney. About half of the increased norepinephrine spillover during hypertension can be accounted for by increased sympathetic nerve activity (Malpas 2010; Parati and Esler 2012). Microneurographic recordings, used to monitor skeletal muscle vasculature sympathetic nerve activity, showed a two to three fold increase in sympathetic activity of hypertensive individuals (Parati and Esler 2012).

Obesity related hypertension has also become a major health problem with 1 in 10 adults worldwide diagnosed as obese (Ruster and Wolf 2013) and up to 70% of newly diagnosed hypertensive cases being attributed to obesity (Malpas 2010). The accumulation of body fat is closely linked to a two to three fold increase in sympathetic nerve activity of the kidneys and skeletal muscle vasculature (Lim, Burke et al. 2013). A prolonged high fat diet significantly raised arterial pressure, heart rate, and renal sympathetic nerve activity (Lim, Burke et al. 2013). This was also demonstrated by overfeeding studies in animals, which showed that suppressing sympathetic activity was sufficient to lower blood pressure (Joyner, Charkoudian et al. 2010). Obesity is also related to increased vascular stiffness and reduced endothelial function which will limit the effectiveness of the baroreflex response (Joyner, Charkoudian et al. 2010).

1.6.3 Therapies and Treatments for Essential Hypertension

Fortunately, controlling blood pressure can greatly reduce the risk of hypertension related cardiovascular diseases. There are several therapeutic approaches to reducing and controlling

blood pressure. The most effective treatment is a healthy lifestyle involving exercise, proper diet, and caloric restriction (Malpas 2010; Georgiopolou, Kalogeropoulos et al. 2012; Parati and Esler 2012; Stolarz-Skrzypek, Bednarski et al. 2013). Not only is weight loss associated with blood pressure reduction, but a 5% loss in body weight can lead to a clinically meaningful suppression of sympathetic activity (Parati and Esler 2012; Ruster and Wolf 2013). Individuals that exercise on a regular basis have a 30 – 50% reduced risk of developing hypertension (Georgiopolou, Kalogeropoulos et al. 2012). Limiting sodium intake will also significantly lower blood pressure and reduce the risk of developing hypertension by 20% (Georgiopolou, Kalogeropoulos et al. 2012; Stolarz-Skrzypek, Bednarski et al. 2013). However, lifestyle changes are usually not well received in a real world setting. Therefore, drug therapies such as diuretics, angiotensin II receptor blockers, vasodilators, and angiotensin converting enzyme inhibitors are used to control blood pressure. Diuretics are usually the first line drug treatment and have shown to have the best blood pressure reducing effect for at least the first year of use (Georgiopolou, Kalogeropoulos et al. 2012).

In some cases, individuals acquire treatment-resistant hypertension. This is a hypertensive state where three or more drugs are no longer capable of reducing blood pressure to a safe target level. To address this problem, other measures can be taken such as catheter-based renal denervation (Esler, Krum et al. 2010; Gewirtz and Bisognano 2011) or surgically implanted electrical devices that stimulate the baroreflex and reduce sympathetic nerve activity (Parati and Esler 2012). While these types of treatments have been shown to significantly reduce blood pressure and morbidity (Esler, Krum et al. 2010; Gewirtz and Bisognano 2011), these invasive treatments are reserved for the most intractable cases of hypertension and are not feasible for the treatment of millions of individuals. Instead, new therapies need to be developed and

hypertensive patients may require personalized treatments using a combination of drugs to lower blood pressure and reduce sympathetic nerve activity.

Ganglionic integration can account for 50 – 98% of postganglionic activity. As a result of ganglionic divergence, an action potential from one preganglionic neuron can generate action potentials in 20 postganglionic neurons. As a result of ganglionic convergence, ganglionic amplification can double preganglionic input and one preganglionic spike can therefore generate action potentials in 40 postganglionic neurons. Consequently, 39 of the 40 (98%) postganglionic spikes arise from the combination of preganglionic divergence and postganglionic convergence. These mechanisms may therefore play a very significant role in sympathetic hyperactivity. Essential hypertension is a progressive disease that worsens over time and drug treatments will eventually fail. As the population becomes more obese and sympathetic activity in those individuals increases, humans will enter an era of sympathetically driven hypertension (Joyner, Charkoudian et al. 2010). Elucidating the mechanism of sympathetic amplification could potentially lead to the development of new treatments and therapies for hypertension.

The work presented herein will evaluate synaptic integration in rat SCG neurons by using dynamic clamp to create virtual nicotinic synapses to stimulate neurons with temporal patterns of synaptic activity that mimic *in vivo* conditions. It will demonstrate synaptic amplification in SCG neurons and explore how cardiac entrainment modifies amplification. Furthermore, it will assess discrepancies between *in vivo* and *in vitro* studies to show that the contribution of secondary synapses has been devalued *in vivo*. Finally, angiotensin II will be used to show how metabotropic factors can alter neuronal excitability and synaptic amplification.

2.0 CARDIAC RHYTHMS ENHANCE SYNAPTIC GAIN IN SYMPATHETIC NEURONS

2.1 INTRODUCTION

Extracellular recordings from postganglionic sympathetic nerve fibers that regulate blood pressure in animals and humans are typically characterized by low frequency activity in a periodic bursting pattern. Multi-unit recordings from muscle vasoconstrictor sympathetic fibers in the limbs of awake humans reveal that postganglionic bursts are locked to the cardiac cycle. Arterial baroreceptors drive this entrainment during falls in diastolic blood pressure (Macefield, Wallin et al. 1994; Macefield and Elam 2003; Malpas 2010). Single unit recordings from resting subjects reveal that individual neurons tend to fire only one spike per burst and that bursts with repetitive action potentials are rare (Macefield and Elam 2003; Macefield 2009; Macefield 2011). Multi-unit bursts of action potentials occur during 30 – 40% of cardiac cycles (Macefield, Wallin et al. 1994; Macefield and Wallin 1996; Macefield, Rundqvist et al. 1999; Macefield and Elam 2003). Repetitive firing of single units during bursts does not seem to account for changes in burst strength or frequency during exercise and hypertension. Instead, the increase in spiking results from more neurons spiking in a larger percentage of the heartbeats (Macefield, Elam et al. 2002; Ichinose, Saito et al. 2008). Are these changes a direct measure of the central nervous system or do they reflect the integrative action of secondary nicotinic synapses in ganglia?

The physiological significance of secondary synapses in sympathetic neurons has remained enigmatic. Previous work in animal models suggest that secondary synapses have little to no role in ganglionic transmission (McLachlan, Davies et al. 1997; McLachlan, Habler et al. 1998; McLachlan 2003). Consequently, human microneurographic studies have assumed that convergent inputs are suprathreshold in strength. Sympathetic ganglia are thought to behave as passive relays for preganglionic activity and transmission rarely occurs as a result of subthreshold EPSP summation (Macefield, Wallin et al. 1994; McLachlan, Habler et al. 1998; Macefield, Elam et al. 2002; McLachlan 2003). However, this thought is open for interpretation.

Direct nerve stimulation of mammalian SCG neurons suggests innervation by multiple secondary synapses and that pairs of subthreshold EPSPs are sufficient to drive postganglionic action potentials (Rimmer and Horn 2010). Further evidence from mammalian lumbar sympathetic ganglia also suggests that secondary synaptic innervation drives about 50% of postganglionic activity (Bratton, Davies et al. 2010). Studies in bullfrog sympathetic neurons reveal the number and strength of secondary synapses and demonstrate that synaptic gain occurs in a range of conditions (Kullmann and Horn 2006; Horn and Kullmann 2007; Kullmann and Horn 2010b). In this chapter, we use dynamic clamp to determine if mammalian SCG neurons generate gain by applying synaptic templates similar to those used with bullfrog sympathetic neurons. We are also interested in studying the firing patterns of vasomotor neurons for their role in blood pressure regulation. Therefore, we will test how periodic stimulation serves to regulate synaptic gain. Finally, we will use these experimental results to develop a model that can account for human microneurographic recordings. **We hypothesize that (1) noisy stimulation of SCG neurons will generate synaptic gain, (2) that cardiac entrainment of preganglionic activity will increase subthreshold EPSP summation and enhance synaptic gain, and (3) that**

simulations of preganglionic activity that incorporate $n + 1$ convergence, can model human sympathetic activity at rest and disease.

2.2 METHODS

2.2.1 SCG Primary Cell Culture

All procedures for animal use were approved by the Institutional Animal Care and Use Committee at the University of Pittsburgh. Litters of P12 - P15 Sprague Dawley rat pups (Charles River, Wilmington, MA) were anaesthetized in an isoflurane (Piramal Critical Care, Bethlehem, PA) filled chamber until the pups lacked a withdrawal response to a paw pinch. Prior to dissection, surgical instruments were sterilized in 70% ethanol and placed under the UV hood for 30 min. Pups were pinned to the dissection table through outstretched paws under a dissecting microscope in a sterile laminar flow hood. The abdomen was opened to the liver and micro dissection scissors were used to enter the diaphragm and cut the heart at least 3 times to assure death. The head was pinned down to keep tension on the neck region to facilitate SCG extraction.

An incision was made through the skin just above the rib cage, blunt dissection was used to separate the skin from the underlying connective tissue, and a patch of skin covering the throat was removed. Connective tissue was removed around the lymph nodes and other superficial glands and retracted to reveal the trachea. A vertical incision was made along the trachea from the top of the rib cage to the larynx and tissue was further retracted to reveal the underlying carotid artery and cervical sympathetic trunk. The SCGs were opaque, white, fusiform bodies

that lied on either side of the trachea, at the bifurcation of the internal and external carotid arteries. The cervical sympathetic trunk runs along the carotid artery, and was used as a guide to remove the SCG. Once removed, the SCG were transferred to a sylgard-coated petri dish that contained ice-cold L-15 media (Invitrogen, Grand Island, NY). This procedure was repeated for the entire litter, a process that generally took 20 – 30 minutes. The tissue was placed under a dissecting microscope where the SCG was gently separated from surrounding tissue and placed in a new petri dish with ice cold L-15. Once all ganglia were isolated, they were desheathed, projecting nerves are removed, and the SCG was chopped into 5 – 7 pieces to increase the surface area for enzyme contact.

SCG fragments were transferred to 1 mg/ml of pre-warmed collagenase IV (Worthington Biomedical Corp, Lakewood, NJ) in L-15 and incubated at 37°C for 30 min. Every 10 – 15 min, a Pasteur pipette was used to blow air into the liquid to agitate tissue fragments. SCG fragments were transferred from the collagenase to 3 ml of pre-warmed 0.25% trypsin (Invitrogen, Grand Island, NY) and placed in the shaking water bath at 37°C for 30 min with agitation every 10-15 min.

After trypsin digestion, tissue was transferred to a Falcon tube containing 1 ml Minimum Essential Media (MEM, Invitrogen, Grand Island, NY). The tissue was triturated with a large diameter flame polished Pasteur pipette, making sure not to force tissue into the pipette, but only using torsional and shearing forces to remove individual cells from the tissue. The tissue settled and was transferred to a new MEM containing tube. The cells remaining in the previous tube were transferred to the original trypsin containing tube. Trituration continued using smaller diameter flame polished pipettes as the tissue broke down. Once the tissue broke down, all

fractions were collected in the trypsin containing tube and cells were centrifuged at 4000 rpm for 5 min.

During centrifugation, three PCR epi-tubes were prepared with 100 μ l of pre-incubated tissue culture media (10% fetal bovine serum (Atlanta Biologicals, Norcross, GA), 1% penicillin-streptomycin (Atlanta Biologicals, Norcross, GA), 50 ng/ml nerve growth factor (Harlan Bioproducts, Indianapolis, IN), 1.0 μ M cytosine arabinoside hydrochloride (Sigma-Aldrich, St. Louis, MO), in MEM and vacuum filtered). Media was gently decanted, so as to not disrupt the pellet, and 400 μ l of pre-incubated culture media was added to the pellet. With a p-20 pipette, the pellet was placed in the first PCR tube and resuspend 2-3 times. The remaining pellet was transferred to the next PCR tube, resuspended again, and the process was repeated for the final PCR tube. The cell fractions were collected back to the 15 ml Falcon tube, being careful not to introduce air. The cells were plated onto 12 mm round Poly-D-Lysine/Laminin coated coverslips (BD Biosciences, San Jose, CA) in a 24 well plate. Since neurons only adhere to the coverslip, it was critical to not break surface tension on the coverslips. The plate was placed in the 37°C incubator with 5% CO₂ to allow neurons to settle and attach to the coverslips. After 1 hour, 2 ml of pre-incubated tissue culture media were added to each well. Neurons were fed with incubated tissue culture media on a daily basis to keep non-neuronal cell growth to a minimum.

2.2.2 Whole-cell Current Clamp Recording

Whole cell current clamp recordings were conducted with 2-4 M Ω glass patch electrodes (Glass 8250, 1.65 mm OD, 1.20 mm ID, A-M Systems Inc, Sequim, WA). The extracellular solution contained (in mM): 146 NaCl, 7.8 glucose, 20 HEPES, 4.7 KCl, 0.6 MgSO₄, 1.6 NaHCO₃, 0.13 NaH₂PO₄, 2.5 CaCl₂; pH 7.3, bubbled with 100% O₂. The electrode solution contained (in mM):

94 K⁺-gluconate, 30 KCl, 10 Phosphocreatine di(tris) salt, 10 HEPES, 0.2 EGTA, 4 Mg₂ATP, 0.3 Na₂GTP; pH 7.3. A coverslip of cells was placed in the recording chamber on a Zeiss IM35 microscope and extracellular solution was bath applied using a Minipuls 3 peristaltic pump (Gilson Inc, Middleton, WI, USA) with a total superfusion rate of about 1 ml min⁻¹. Recordings were performed with an Axoclamp 2B amplifier with filtering set to 20 kHz and G-clamp 2.2 software (Kullmann, Wheeler et al. 2004). Stable recordings had the following criteria: $V_{rest} \leq -64$ mV, $R_{input} \geq 300$ M Ω , and thresh- g_{syn} was constantly monitored for drift, a sign of deteriorating cell quality. A typical recording was stable for about 60 min.

2.2.3 Dynamic Clamp Templates

To model physiological activity, we assumed a 5 Hz heart rate (McLachlan, Habler et al. 1998) and an average f_{pre} of 1 Hz for each synapse (Ivanov and Purves 1989; Ivanov 1991). A simple scheme was employed where preganglionic activity cycled between on and off (Figure 6). For each 200 ms cardiac cycle, we assumed a 20% duty cycle with an overall average f_{pre} of 1 Hz, which provided a 40 ms window where activity could occur. Preganglionic activity was set to 5 Hz within the active window and 0 Hz during the off window.

Timing of synaptic events followed a Poisson distribution (Wheeler, Kullmann et al. 2004). For each 50 μ s step, a random number (0-1) was drawn. This number was compared to P_{syn} , the probability of a synaptic event occurring. For a Poisson process, $P_{syn} = 1 - \exp(-nf_{pre}t_{win})$, where n is the number of synapses, f_{pre} is the presynaptic firing rate and t_{win} is the temporal resolution of the amplifier. If the random number was greater than or equal to P_{syn} , a synaptic event was placed at that time point. With a temporal resolution of 0.05 ms, there were 800 time points per duty cycle where this comparison was performed. This approach was used to construct

40-second templates that encoded for 1 primary synapse and either 4, 6, or 8 secondary synapses. The same procedure was employed to construct templates with an average f_{pre} of 0.5 Hz and 0.75 Hz.

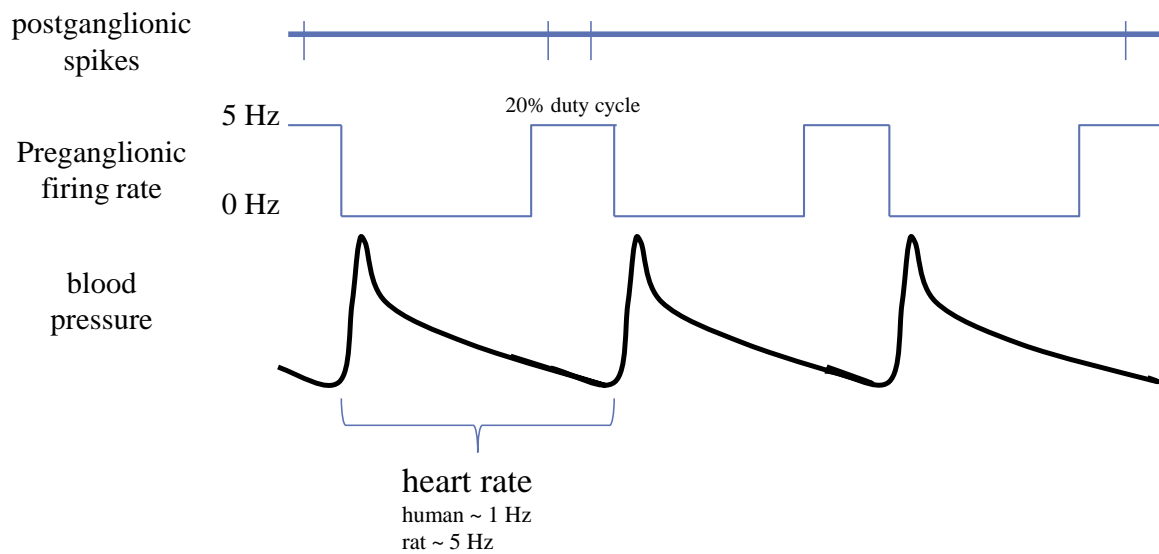


Figure 6 – Schematic of the periodic dynamic clamp template. To make a periodic dynamic clamp template, activity was confined to a 40 ms duty cycle window. To give an average preganglionic firing rate of 1 Hz, noisy activity within the duty cycle was 5 Hz, while activity outside the window was quiescent. This scheme was employed to produce the primary and secondary dynamic synaptic events in the dynamic clamp templates.

2.2.4 Simulation of Human Data

For human simulations, activity was also based on a Poisson distribution. Initially, we considered a single primary synapse whose activity was modeled either continuous or entrained to the cardiac cycle. For continuous simulations, synaptic activity could occur at any time point. With a temporal resolution of 0.05 ms, each second had 20,000 time points (1000 ms/0.05 ms) and activity was simulated for 200-second epochs for a total of 4 million time points (20,000*200) where a random number was compared to P_{syn} . Five 200-second simulations were then concatenated to generate 1000 seconds of activity. When activity was entrained, we assumed a 200 ms duty cycle, which contained 4000 points (200 ms/0.05 ms) where a synaptic event could occur. This template was also generated 200 seconds at a time for a total of 1000 seconds of simulated activity. These simulations were conducted with a f_{pre} of 0.25 Hz, 0.4 Hz, 0.5 Hz, and 0.8 Hz. Since this modeled only primary synapses, all events were assumed to generate postganglionic action potentials. The number of spikes per cycle were counted and tabulated. A chi-squared two-sample test was used to determine if spikes per cycle of the simulated activity shared a common distribution with human activity.

A similar approach was used when simulating entrained activity with secondary synapses. For these simulations, six secondary synapses were included in the calculation of P_{syn} . After the timing of preganglionic events was simulated, postganglionic action potentials were assumed to occur when pairs of secondary events were less than 82.5 ms apart, a window of summation based on recordings from rat sympathetic neurons (n = 7; data not shown). The timing of each postganglionic action potential was set as the average of the two preganglionic secondary EPSPs. The simulated action potentials from secondary synapses were combined with primary events of the same f_{pre} to generate a final 1000-second postganglionic spike output.

Activity was simulated to generate a postganglionic frequency of 0.4 Hz and 0.8 Hz. The number of spikes per cycle was counted and a chi-squared two-sample test was used to compare the spike distribution with human activity.

To construct cumulative interspike interval (ISI) histograms, intervals between spikes were measured. The ISIs were then sorted in ascending order and plotted with the number of bins equal to the number of intervals. Activity was fit with the exponential equation, $y_0 + A^{(-\frac{1}{\tau} * x)}$, and chi-squared goodness of fit values were calculated with Minitab v16.2.3 (State College, PA). These values were used to calculate a P-value to determine if the ISI histograms fit an exponential distribution.

2.2.5 Dynamic Clamp

Virtual nicotinic synapses were implemented according to $I_{syn}(t) = k \times g_{syn}(t) \times (V_M - E_{rev})$. Synaptic conductance $g_{syn}(t)$ was modeled as the sum of two exponentials, with time constants of 1 ms for the activation phase and 7 ms of the decay phase (Sacchi, Rossi et al. 2006). The synaptic reversal potential E_{rev} was set to 0 mV (Derkach, Selyanko et al. 1983). Synaptic strength was adjusted to a peak amplitude of 1 by setting the dimensionless factor $k = -1.614$. Threshold- g_{syn} , the minimal conductance required to trigger an action potential, was determined with an automated binary search routine that delivered virtual EPSPs at a rate of 0.5 Hz. Systematically adjusting the strength of a virtual EPSP found thresh- g_{syn} within 10 trials (Figure 7) (Kullmann, Wheeler et al. 2004). Scaling of the conductance templates was based on a mean of at least three similar, consecutive threshold- g_{syn} measurements. Recordings were performed with an Axoclamp 2B amplifier (Molecular Devices, Sunnyvale, CA) with filtering at 20 kHz and G-clamp 2.2 software (Wheeler, Kullmann et al. 2004). Postsynaptic activity was collected

with G-clamp and was further analyzed with Igor v6 (WaveMetrics, Lake Oswego, OR) and Excel 2010 (Microsoft, Redmond, WA) software.

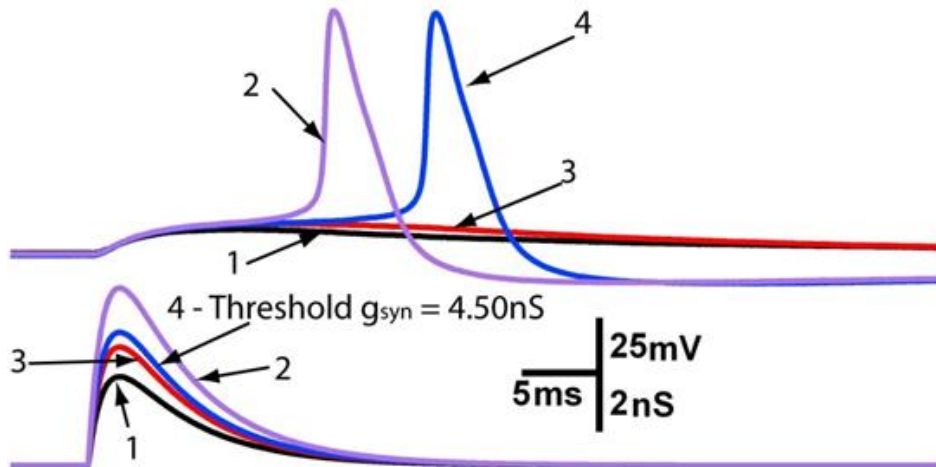


Figure 7 – Measurement of $thresh-g_{syn}$ using a binary search routine. $Thresh-g_{syn}$ was determined by systematically adjusting the strength of the virtual EPSP until the search determines the minimal conductance to cause an action potential.

2.2.6 Analysis and Statistics

Synaptic gain was calculated by dividing the frequency of postsynaptic action potentials by the frequency of presynaptic activity per synapse. Action potentials were counted and each action potential was compared to the template to determine if it was initiated by a suprathreshold EPSP

or summation of subthreshold EPSPs. Statistics were prepared with GraphPad InStat 3 (La Jolla, CA) using an ANOVA and Tukey post-hoc test, setting $P < 0.05$ as criterion for significance. All grouped data is expressed as mean \pm S.E.M.

2.3 RESULTS

2.3.1 Mammalian Dynamic Clamp Recordings

Initial dynamic clamp studies were designed to determine whether synaptic gain in mammalian SCG neurons resembled that previously seen in bullfrog B neurons (Kullmann, Wheeler et al. 2004; Kullmann and Horn 2006; Kullmann and Horn 2010b). The original bullfrog template sought to maximize the number of events available in order to obtain a statistically meaningful number of events while also operating at a physiologically plausible firing rate. However, memory in the G-clamp system limits the size of the synaptic template to 40 seconds at a 20 kHz sampling rate. Using this approach, setting f_{pre} of the template to 5 Hz resulted in a synaptic gain of about 2.0 (Kullmann and Horn 2006). As a starting point for this project, we wanted to replicate these bullfrog findings in mammalian neurons and explore comparisons with *in vivo* recordings. Pilot studies revealed that 5 Hz templates were too intense for rat SCG neurons – they depolarized and stopped firing. Therefore, we modified the synaptic template by lowering f_{pre} to 3 Hz. As in bullfrog templates, 9 secondary synapses were set to 90% thresh- g_{syn} . In 30 neurons, synaptic gain was 2.25 ± 0.09 ($V_{rest} = -62.2 \pm 1.2$ mV, $R_{input} = 394.0 \pm 14.8$ M Ω) indicating that postganglionic neurons more than doubled the presynaptic firing rate (Figure 8). A histogram of intervals between synaptic events fit an exponential distribution as would be

expected based on the methods used to build the template (Figure 9). Plotting the interval data as a cumulative histogram (Figure 9 inset), provides a better method for assessing the distribution of synaptic intervals because it makes no assumption about binning the data.

These initial results support the hypothesis that mammalian sympathetic neurons can detect synaptic coincidences between secondary EPSPs to amplify presynaptic activity.

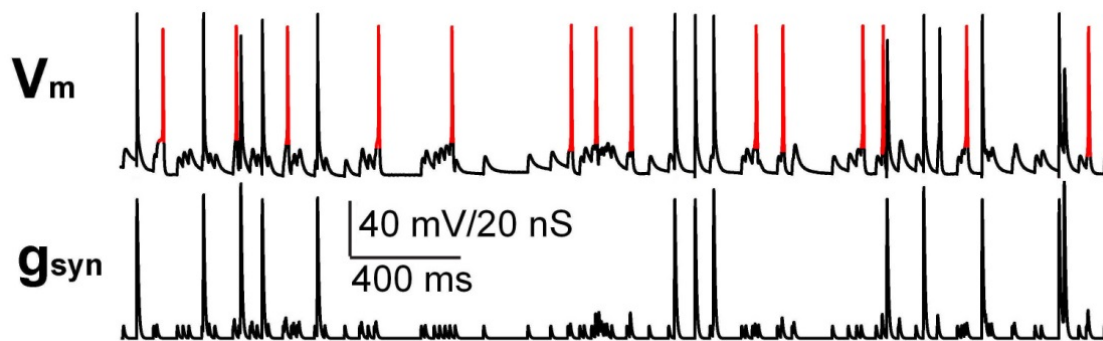


Figure 8 – Synaptic gain during continuous random stimulation by vitrual nicotinic synpases. A 3 Hz dynamic clamp template (g_{syn}) encoding for 1 primary and 9 secondary nicotinic synapses was used to stimulate a rat sympathetic neuron. This displays a 4 sec window out of a 40 sec experiment. The membrane response (V_m) demonstrates that SCG neurons can integrate subthreshold EPSPs and initiate action potentials (red spikes).

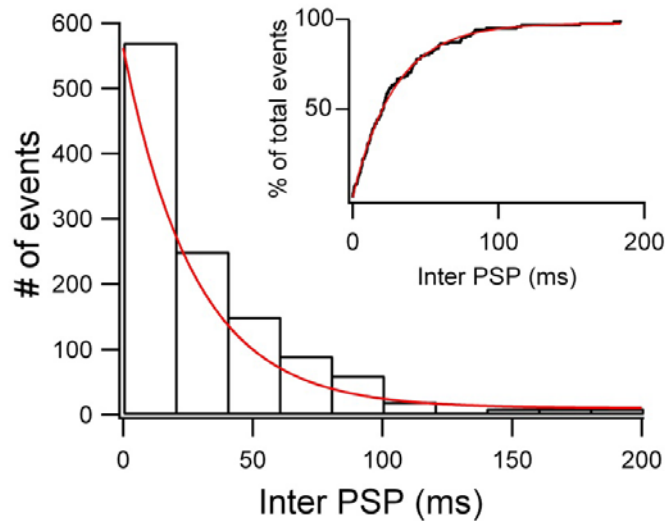


Figure 9 – Exponential distribution of intervals between synaptic events. The time intervals between presynaptic events in the original template were fit to an exponential curve indicating that the template consists of noisy random activity. The inset shows the cumulative histogram of the 1160 presynaptic events that comprised the 3 Hz dynamic clamp template. Consistent with a Poisson process, the cumulative histogram fit an exponential distribution.

2.3.2 A Periodic Model of Stimulation

Despite lowering f_{pre} to 3 Hz, postsynaptic activity still did not reproduce mammalian *in vivo* activity of vasomotor neurons, whose firing was entrained by the cardiac cycle and was more sparse than our 3 Hz template. To model the cardiac entrainment of preganglionic activity in vasomotor neurons, we employed a non-stationary stochastic process. Since the exact time course of baroreceptor modulation is unknown, we assumed a simple model in which preganglionic neurons alternated between quiescent and active states during the cardiac cycle

and that the duration of the active state was 20% of the cardiac cycle (Figure 6). F_{pre} was further reduced from 3 Hz used during continuous stimulation, to 1 Hz during periodic stimulation and the strength of primary synapses was reduced from $10x \text{ thresh-}g_{syn}$ to $3x \text{ thresh-}g_{syn}$. This resulted in bursts of sympathetic activity that drove spikes in some, but not all, cardiac cycles. Figure 10 illustrates a neuron stimulated with the 1 Hz periodic template that modeled 1 primary synapse, at $3x \text{ thresh-}g_{syn}$, and 8 secondary synapses, at $90\% \text{ thresh-}g_{syn}$. In a 40 second trial, the template elicited 41 action potentials that were driven by primary synapses and 57 action potentials driven by secondary synapses, which equates to a synaptic gain of 2.30 (Figure 10). In 16 neurons, the average synaptic gain was 2.21 ± 0.06 ($V_{rest} = -66.4 \pm 0.8 \text{ mV}$, $R_{input} = 430.0 \pm 22.0 \text{ M}\Omega$). This showed that reducing the overall level of activity to 1 Hz, but delivering it in bursts, produced gain similar to that elicited by continuous 3 Hz stimulation (2.21 vs. 2.25). The results also resembled human single unit data where bursts of activity only occur in some cardiac cycles. Additionally, the incidence of multi-spiking was rare within a given cardiac cycle.

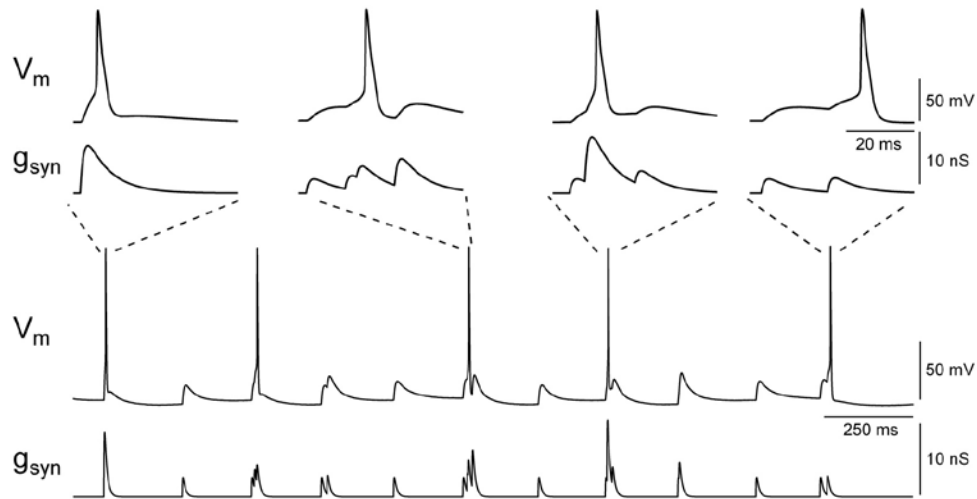


Figure 10 – SCG voltage response to periodic stimulation. Cultured SCG neurons were stimulated with a 1 Hz periodic dynamic clamp template. Templates encoded for 1 primary ($3 \times \text{thresh-}g_{\text{syn}}$) and 8 secondary ($90\% \text{ thresh-}g_{\text{syn}}$) synapses. Select voltage responses are highlighted to demonstrate action potentials generated by a unitary primary synapse and summation of subthreshold EPSPs.

To assess the importance of secondary synapses for generating gain using periodic stimulation, the numbers of secondary synapses was varied between 4 and 8. As expected for the gain theory, a higher number of secondary synapses increased the percentage of cardiac cycles that contained action potentials thereby increasing synaptic gain (Table 2). Similar to human microneurographic data (Macefield, Wallin et al. 1994; Macefield and Elam 2004), 34 – 43% of cardiac cycles contained a burst of activity that generated an action potential, while repetitive firing within a cardiac cycle was rare.

Table 2 – Spiking frequency of postganglionic activity induced by periodic stimulation

Number of secondary synapses and average firing frequency	# of cardiac cycles with spikes	# of cardiac cycles with > 1 spike	Synaptic gain ($\sum 1^\circ + 2^\circ$ spikes/ #1 $^\circ$ spikes)
4 @ 1 Hz (n=6) $R_{input} = 300.0 \pm 22.2$, $V_{rest} = -66.4 \pm 1.2$ mV	68.0 ± 2.2 34%	1.0 0.5%	1.73 ± 0.05
6 @ 1 Hz (n=15) $R_{input} = 323.3 \pm 14.1$, $V_{rest} = -68.7 \pm 1.3$ mV	75.2 ± 2.0 37.5%	3.4 ± 0.4 1.7%	2.06 ± 0.05
8 @ 1 Hz (n=11) $R_{input} = 310.1 \pm 26.7$, $V_{rest} = -68.7 \pm 1.5$ mV	87.1 ± 3.0 43.5%	3.0 ± 0.8 1.5%	2.30 ± 0.08

*P<0.05, **P<0.01, ***P<0.001 ANOVA, Tukey post-hoc

In 17 neurons, (1) periodic stimulation for 40 sec produced synaptic gain, (2) spikes occurred in a subset of cardiac cycles, (3) selectively increasing secondary activity increased gain and the fraction of cardiac cycles with spikes, and (4) multiple spikes within a cardiac cycle were rare.

2.3.3 Periodic Versus Continuous Synaptic Activity

Although the previous experiments indicated that periodic stimulation is more efficient than continuous stimulation in producing gain, they were performed on separate groups of neurons using different values for f_{pre} . We therefore designed a paired experiment to compare continuous and periodic templates within the same neurons. Forty-second 1 Hz periodic and continuous templates were created with 1 primary synapse ($3x \text{ thresh-}g_{syn}$) and 4, 6, or 8 secondary synapses ($90\% \text{ thresh-}g_{syn}$). All templates were generated using a continuous or non-continuous Poisson

process. The resulting templates had nearly identical amounts of presynaptic activity to allow for the direct comparison of postganglionic activity between periodic and continuous templates.

Postsynaptic recordings revealed that periodic entrainment increased postganglionic spike output (Figure 11), and significantly increased synaptic gain (Figure 12). In both the periodic and continuous templates, the number of action potentials triggered by summation of subthreshold EPSPs significantly increased with the number of secondary synapses (Table 3), which increased the postsynaptic firing rate and gain. Neurons stimulated with the original 3 Hz template did not have a significantly different synaptic gain than the periodic and continuous 1 Hz templates encoding for 8 secondary synapses (Table 3). Despite an f_{post} that ranged from 1.50 to 6.65 Hz, synaptic gain only ranged from 1.47 to 2.49. These results are consistent with the gain hypothesis (Horn and Kullmann 2007) where the number of nicotinic synapses sets a theoretical limit for synaptic gain and changes in f_{pre} (1 Hz vs. 3 Hz) have small effects on synaptic gain (Figure 3B).

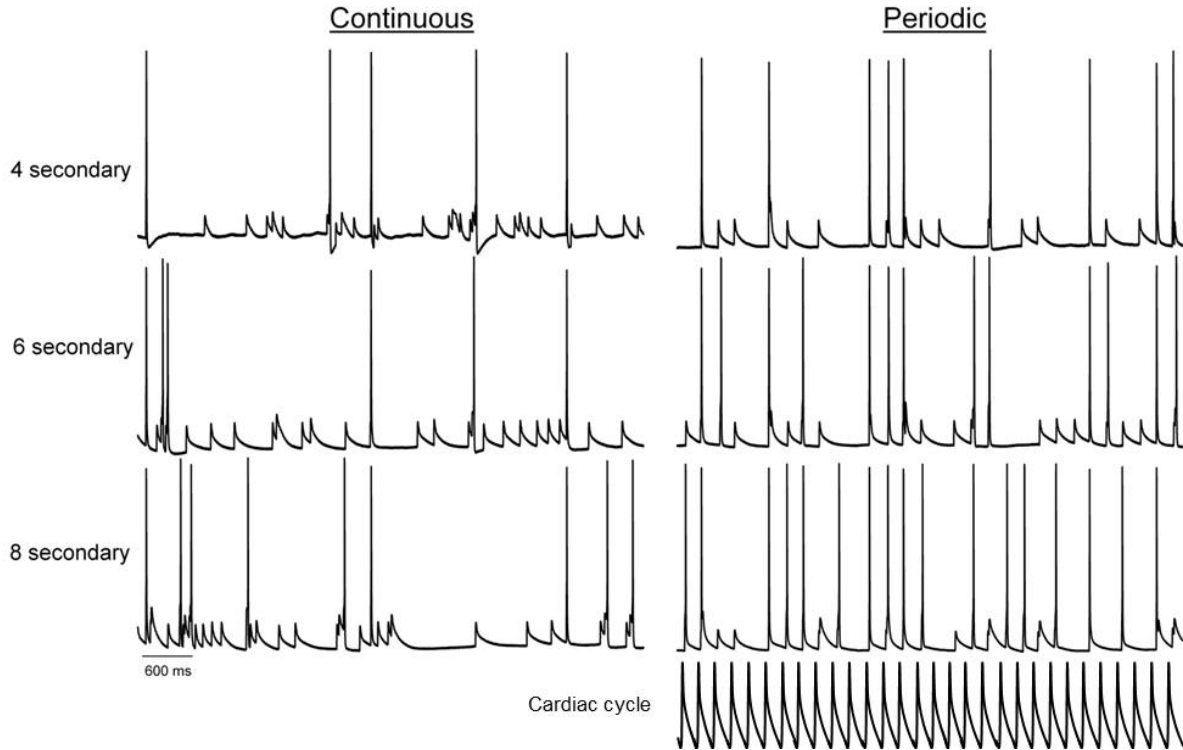


Figure 11 – Periodic entrainment increased spike output. Dynamic clamp templates encoded for 1 primary ($3x \text{ thresh-}g_{\text{syn}}$) and 4, 6, or 8 secondary ($90\% \text{ thresh-}g_{\text{syn}}$) synapses. In noisy templates, activity occurred at any timepoint, while in periodic templates, activity was confined to duty cycle windows. Templates with the same number of secondary synapses had nearly identical amounts of preganglionic activity. Periodic entrainment increased action potential spike output and activity occurred in register with a simulated cardiac cycle.

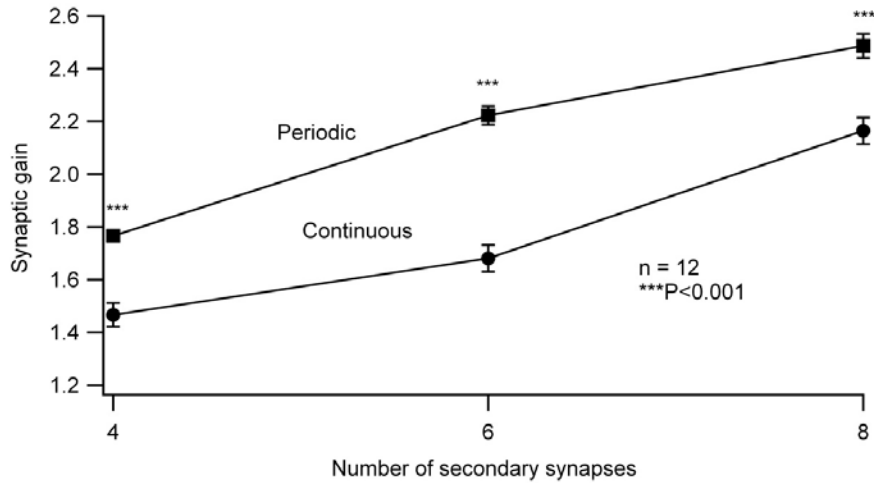


Figure 12 – Periodic entrainment significantly increased gain. The synaptic gain of periodic and noisy preganglionic activity were compared using the dynamic clamp templates employed in Figure 10. Synaptic gain increased as a function of the number of secondary synapses. Periodic entrainment of preganglionic activity significantly increased synaptic gain compared to non-periodic activity.

Table 3 – Spike count comparison of postsynaptic activity from noisy and periodic stimulation

Number of secondary synapses and average firing frequency	Spikes triggered by primary synapse	Spikes triggered by secondary synapses	Output firing frequency ($\sum 1^\circ + 2^\circ$ spikes/40 sec)	Synaptic gain ($\sum 1^\circ + 2^\circ$ spikes/ $\#1^\circ$ spikes)
Periodic: 4 @ 1 Hz (n=12)	41	30.4 ± 0.8	1.79 Hz	1.77 ± 0.02
Periodic: 6 @ 1 Hz (n=12)	41	47.8 ± 1.5	2.22 Hz	2.22 ± 0.04
Periodic: 8 @ 1 Hz (n=12)	41	59.6 ± 1.9	2.52 Hz	2.49 ± 0.05
Continuous: 9 @ 3 Hz (old template, n=30)	130	135.9 ± 10.6	6.65 Hz	2.25 ± 0.09
Continuous: 4 @ 1 Hz (n=12)	42	17.8 ± 1.8	1.50 Hz	1.47 ± 0.04
Continuous: 6 @ 1 Hz (n=12)	42	25.0 ± 2.0	1.68 Hz	1.68 ± 0.05
Continuous: 8 @ 1 Hz (n=12)	42	44.6 ± 2.0	2.17 Hz	2.16 ± 0.05

***P<0.001 ANOVA, Tukey post-hoc

Increasing the number of secondary synapses significantly increased synaptic gain. Periodic entrainment caused more action potentials to be triggered by subthreshold EPSP summation.

2.3.4 Presynaptic Activity at < 1.0 Hz is Sufficient to Generate Synaptic Gain

The previous experiments demonstrated that synaptic gain could be generated at postsynaptic firing rates in the range of 1.5 – 6.7 Hz (Table 3). However, in resting human subjects, even lower postganglionic firing rates are observed (Macefield, Wallin et al. 1994; Macefield 2011). The gain hypothesis predicts that at very low f_{pre} , all postsynaptic activity will be driven by primary synapses and synaptic gain will go to 1. (Karila and Horn 2000). This raises the question as to whether templates with lower f_{pre} would still generate gain. To answer that question, we stimulated SCG neurons with 40 -second periodic templates with an f_{pre} of 0.5 Hz (n = 10) and 0.75 Hz (n = 10), which encoded for 1 primary (3x thresh- g_{syn}) and either 4, 6, or 8 secondary synapses (90% thresh- g_{syn}). At each f_{pre} , increasing the number of secondary synapses resulted in a significant increase in synaptic gain (Figure 13; 0.5 Hz: 4: 1.52 ± 0.01 , 6: 2.07 ± 0.02 , 8: 2.81 ± 0.01 ; 0.75 Hz: 4: 1.76 ± 0.01 , 6: 2.33 ± 0.01 , 8: 2.77 ± 0.03 ; 1 Hz: 4: 1.76 ± 0.02 , 6: 2.22 ± 0.04 , 8: 2.49 ± 0.05 ; $P < 0.001$, ANOVA). Interestingly, with 8 secondary synapses, synaptic gain was significantly higher when f_{pre} was 0.5 Hz (2.81 ± 0.01) and 0.75 Hz (2.77 ± 0.03) than when f_{pre} was 1 Hz (2.49 ± 0.05 ; $P < 0.001$, ANOVA).

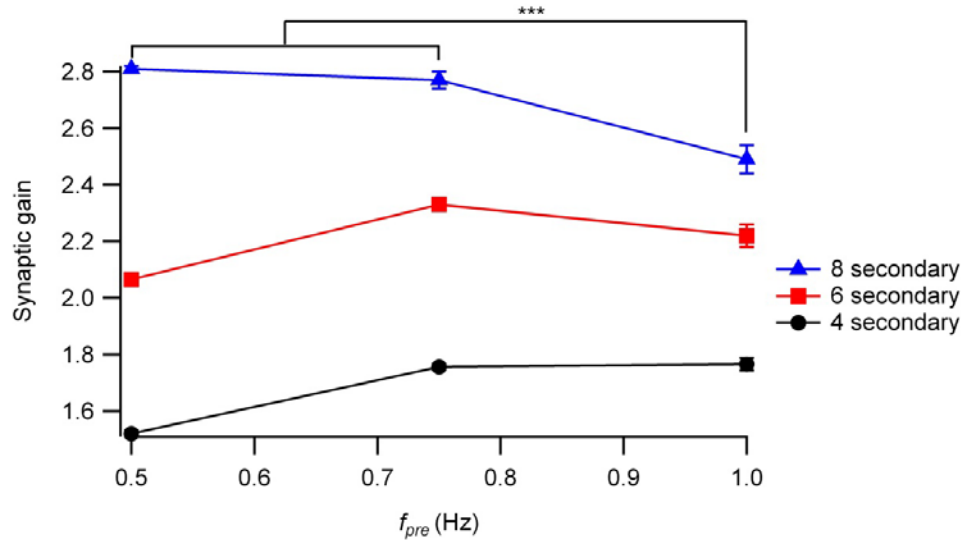


Figure 13 – Synaptic gain can increase at lower presynaptic frequencies. When preganglionic activity was periodic, synaptic gain significantly increased ($P < 0.001$, ANOVA) with the number of secondary synapses at all measured f_{pre} . With 8 secondary synapses, neurons had a significantly higher gain when f_{pre} was 0.5 Hz or 0.75 Hz. This suggests that at higher frequencies, action potential generation was inhibited and thus conforms to the synaptic gain theory.

Analysis of postganglionic activity during stimulation with 8 secondary synapses revealed why synaptic gain was higher at a lower f_{pre} . As the f_{pre} increased, pairs of subthreshold EPSPs failed to elicit action potentials because spike afterhyperpolarization, from an action potential in the previous cardiac cycle, inhibited subthreshold EPSP summation (Figure 14). At a lower f_{pre} , the propensity for subthreshold failures decreased, which resulted in a higher synaptic gain. These results demonstrate that synaptic amplification can contribute to postganglionic firing rates when presynaptic activity is 1 Hz or less.

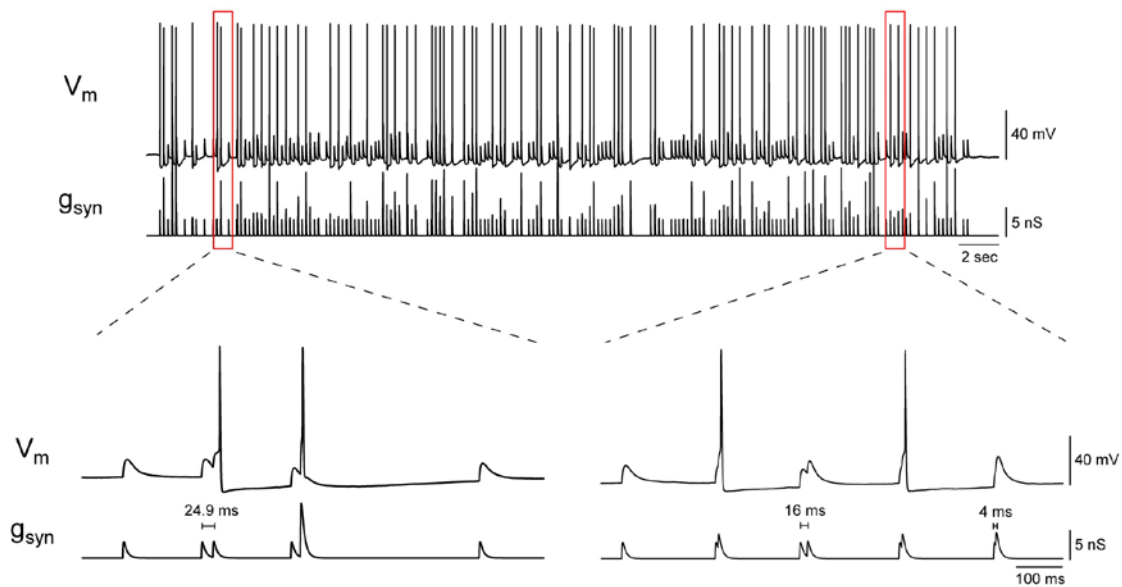


Figure 14 – Gain decreased at higher frequencies because spike afterhyperpolarization inhibited subthreshold EPSP summation. At a higher f_{pre} , there was a larger propensity that the spike afterhyperpolarization dampened subsequent subthreshold EPSP summation. This figure highlights an action potential generated from subthreshold EPSPs that are 24.9 ms apart. However, pairs of subthreshold EPSPs that are as close as 4 ms apart did not fire when preceded by an action potential.

2.3.5 Modeling Human Activity at Rest and During Disease

Human microneurographic data is typically quantitated in terms of postganglionic multi-unit spike bursts and repetitive firing of single units during bursts. Macefield (2011) attempted to model human sympathetic activity by assuming preganglionic innervation from one, two, or

three primary synapses. Each synapse was set to fire with a random distribution, characterized by a mean and standard deviation (Macefield 2011). Macefield adjusted the standard deviation to fit the spike output of human single unit data and concluded that two primary synapses, with a f_{post} of 0.22 Hz and an interspike interval distribution with a mean of 2500 ms and standard deviation of 5000 ms, can account for human sympathetic activity at rest (0.4 Hz). An unequal mean and standard deviation implies that the interspike interval distribution was non-exponential. Our goal was to determine whether similar results could be obtained using exponentially distributed synaptic intervals from continuous activity and from activity modulated by the cardiac cycle, to determine whether secondary synapses could also play a role.

We initially assumed that postganglionic activity was driven by a single primary synapse. Since modeling did not use G-clamp, we were not restricted to 40 sec simulations and instead performed 1000 sec simulations, similar to Macefield (2011). To determine the percentage of cardiac cycles with simulated action potentials, continuous activity was divided into 1 sec intervals to establish arbitrary “cardiac cycles”. For entrained simulations, we assumed a human heart rate of 60 beats per minute with activity entrained to a 200 ms duty cycle. Human muscle vasoconstrictor neurons fire at about 0.4 Hz at rest (Macefield, Wallin et al. 1994; Macefield 2011) and at 0.7 to 1.0 Hz during cardiac failure (Macefield, Rundqvist et al. 1999; Macefield 2011; Ikeda, Murai et al. 2012). Therefore, we simulated continuous and periodic primary activity at 0.25 Hz, 0.4 Hz (Figure 15A), 0.5 Hz, and 0.8 Hz (Figure 15B). Figure 15 and 16 illustrate how cardiac entrainment has no effect on f_{post} (no gain), but alters the distribution of intervals between spikes (ISI). As expected, when activity was continuous, the cumulative spike intervals were exponentially distributed (Figure 16A, Table 4). Entrainment resulted in a deviation from the exponential fit (Figure 16B, Table 4). Nevertheless, the ISI distributions for

continuous and entrained activity had similar shapes that might be difficult to distinguish in smaller data sets or in real experimental data.

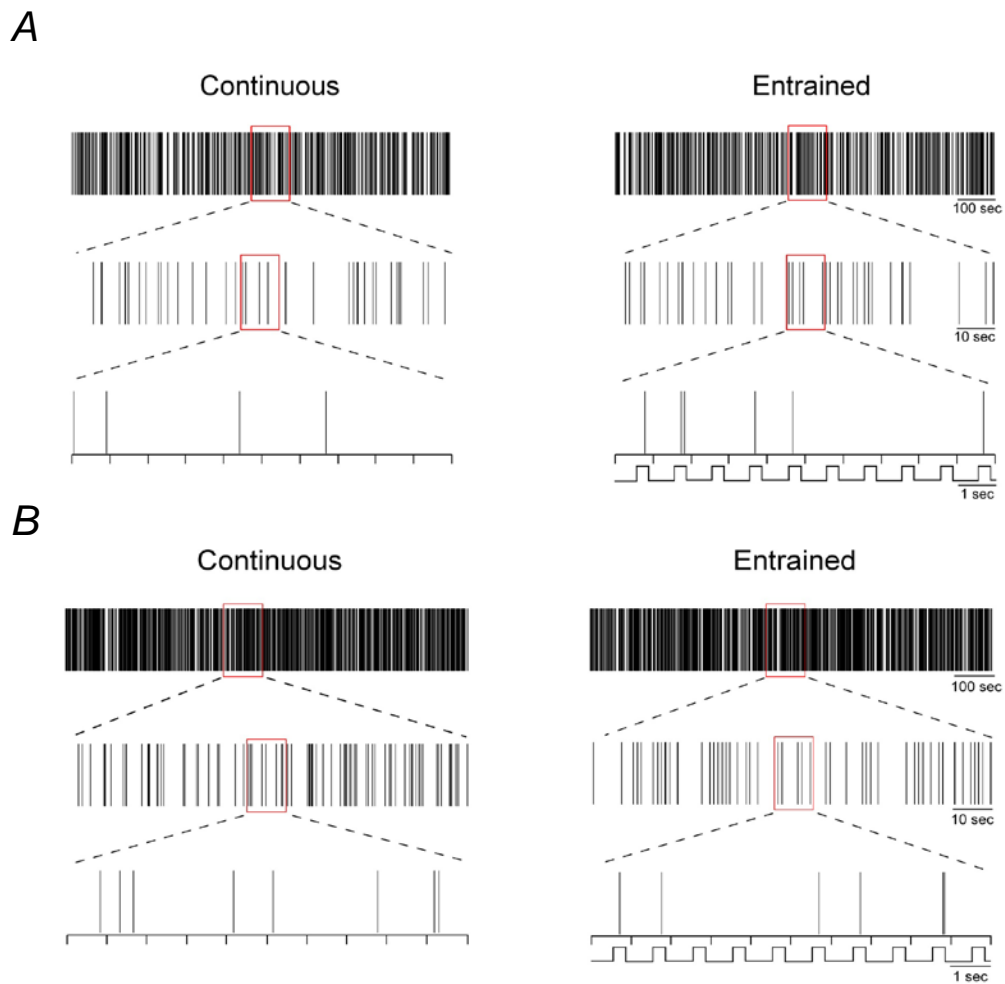


Figure 15 – Simulated postganglionic activity driven by a single primary synapse. This represents the simulated output of primary activity at 0.4 Hz (A) and 0.8 Hz (B) to model sympathetic activity at rest and during heart disease, respectively. The square wave under periodic activity models the cardiac cycle to indicate when activity is on or off.

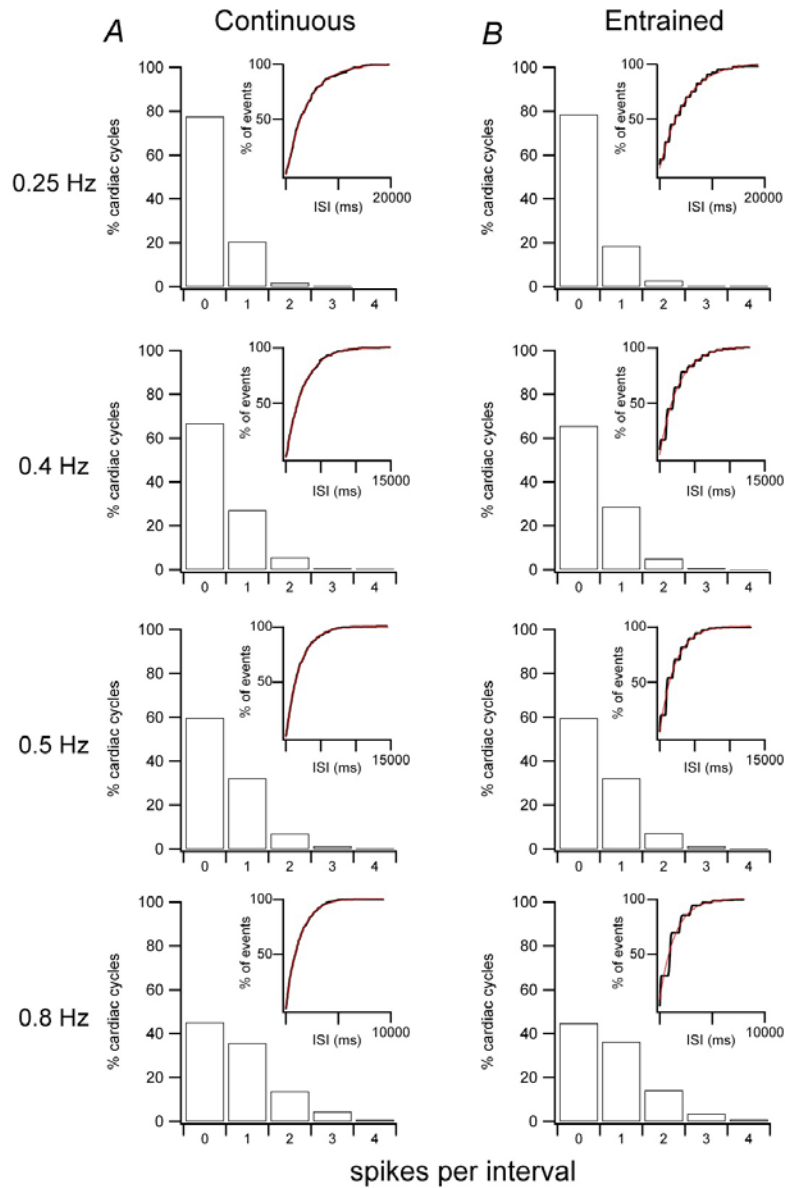


Figure 16 – Entrained primary simulations have a different exponential ISI distribution. Simulations of primary synapses had similar spikes per interval during continuous (A) and entrained (B) activity. However, the cumulative interspike interval distribution was not statistically exponential when activity was entrained.

Table 4 – Spike per interval distribution and cumulative ISI exponential analysis

Continuous with primary synapses only									
	% of spikes per interval (1000s)					H_0 : Common distribution with human		H_0 : Cumulative ISI histogram is exponential	
Frequency (Hz)	0	1	2	3	4	P-value	Conclusion	P-value	Conclusion
0.25	77.6	20.5	1.8	0.1	0			P = 0.296	Exponential
0.4	66.8	27.1	5.6	0.5	0.1	P = 0.769	Common distribution	P = 0.494	Exponential
0.5	59.7	32.1	6.9	1.2	0.1			P = 0.483	Exponential
0.8	45.1	35.7	13.8	4.5	0.9	P = 0.839	Common distribution	P = 0.331	Exponential
Entrained with primary synapses only									
	% of spikes per interval (1000s)					H_0 : Common distribution with human		H_0 : Cumulative ISI histogram is exponential	
Frequency (Hz)	0	1	2	3	4	P-value	Conclusion	P-value	Conclusion
0.25	78.3	18.7	2.8	0.2	0			P < 0.01	Non-exponential
0.4	65.6	28.7	5.1	0.6	0	P = 0.653	Common distribution	P < 0.01	Non-exponential
0.5	59.5	32.1	7.2	1.2	0			P < 0.01	Non-exponential
0.8	44.8	36.4	14.2	3.6	1.0	P = 0.875	Common distribution	P < 0.01	Non-exponential
Entrained with primary and secondary synapses									
	% of spikes per interval (1000s)					H_0 : Common distribution with human		H_0 : Cumulative ISI histogram is exponential	
Frequency (Hz)	0	1	2	3	4	P-value	Conclusion	P-value	Conclusion
0.4	66.7	27.4	4.8	1.0	0.1	P = 0.816	Common distribution	P < 0.01	Non-exponential
0.8	43.7	38.9	12.4	3.9	1.2	P = 0.962	Common distribution	P < 0.01	Non-exponential
Activity from awake human subjects									
	% of spikes per interval								
Frequency (Hz)	0	1	2	3	4	References			
0.4	66.6	21.2	6.4	1.7	0.7	Macefield <i>et al.</i> , 1994; Macefield, 2011			
0.7 – 1.0	46.8	38.8	10.0	2.8	1.6	Macefield <i>et al.</i> , 2002; Ikeda <i>et al.</i> , 2012			

The percentage of action potentials per interval from simulations was compared to the activity of awake human subjects. Chi-squared analysis of two samples was used to show that the spikes per interval of simulated activity followed a common distribution with human vasomotor activity. Chi-squared values of the exponential fit of the cumulative ISI distribution were used to calculate a P-value to determine if the intervals were exponentially distributed. When activity was continuous the ISI distribution was exponential, but entraining activity resulted in a statistically non-exponential ISI distribution.

Can simulations with secondary synapses replicate human data and generate gain? For these simulations, we implemented 6 secondary synapses into the model to test the hypothesis that activity at rest and during heart failure could be modeled with $n + 1$ convergence. By analyzing data from gain experiments of rat SCG neurons, we determined that the window of summation for secondary EPSPs (90% thresh- g_{syn}) was 82.5 ms – a pair of secondary EPSPs occurring within this window could summate to fire or spike. We also assumed that activity was entrained to a 1 Hz (60 beats/min) cardiac cycle and that all primary and secondary synapses had the same f_{pre} . The f_{pre} was adjusted until the f_{post} was equal to 0.4 Hz (Figure 17A) or 0.8 Hz (Figure 17B). Figure 17 shows how the output has a greater number of spikes (action potentials) than the input, indicating that the model is generating gain. Figure 18 shows how simulations with secondary synapses can generate similar spike per interval distributions as simulations with primary synapses alone (Figure 16, Table 4). Similarly, periodic entrainment resulted in statistically non-exponential cumulative ISI distributions (Figure 18, Table 4) though it still followed an exponential shape.

To determine if the simulated data followed a common distribution to human data, we used a chi-squared two-sample test. With P -values greater than 0.05 (Table 4), we accepted the null hypothesis that the spike outputs followed a common distribution. This suggests that exponentially distributed activity from a unitary primary synapse or activity that follows $n + 1$ convergence, can account for human sympathetic activity.

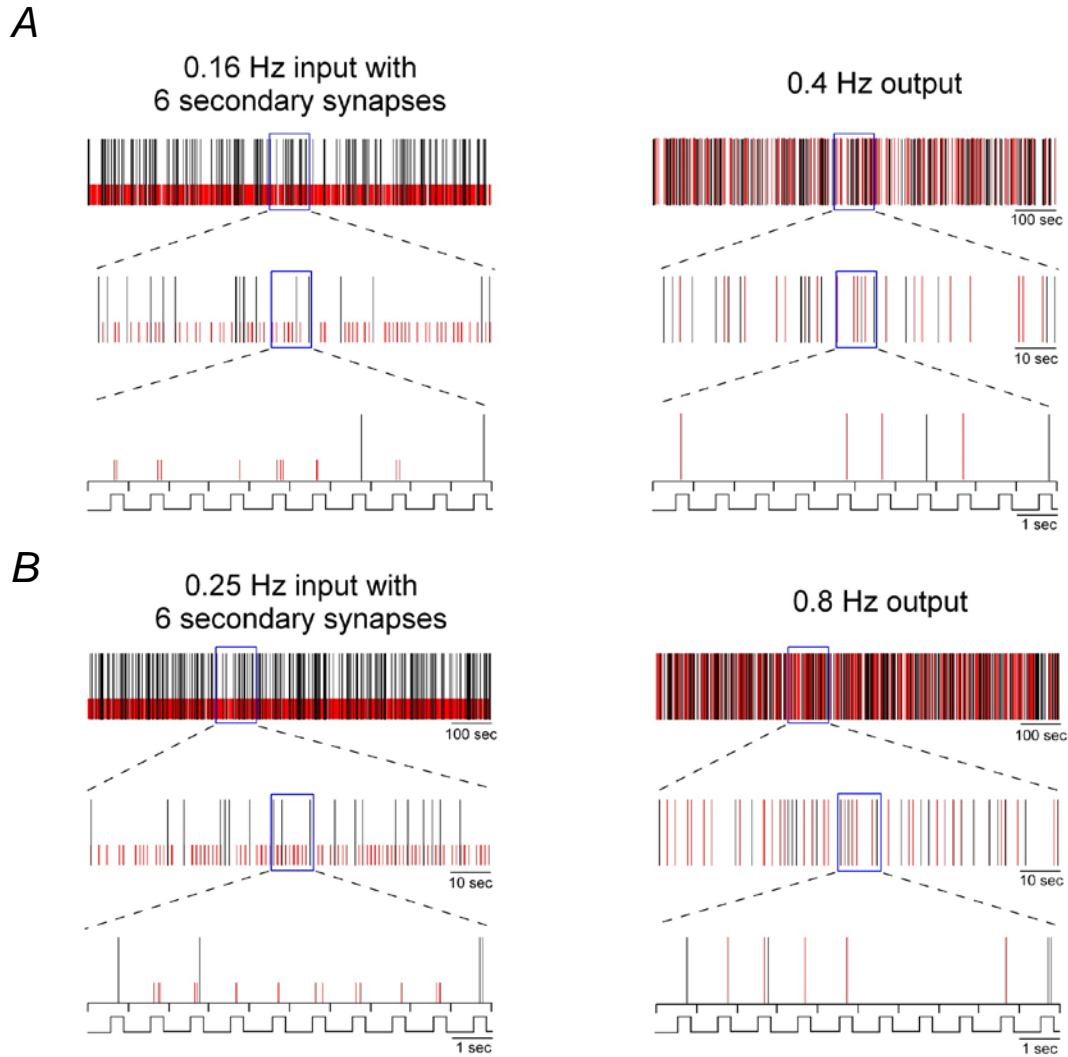


Figure 17 – Simulated postganglionic activity driven by 1 primary and 6 secondary synapses. Activity from secondary synapses (red) was modeled with primary synaptic activity (black) to generate an output frequency of 0.4 Hz (A) and 0.8 Hz (B). Action potentials from secondary synapses only occurred if pairs of events were less than 82.5 ms apart. Less preganglionic activity is required to generate a higher output because secondary synapses amplify the preganglionic signal.

Entrained with 6 secondaries

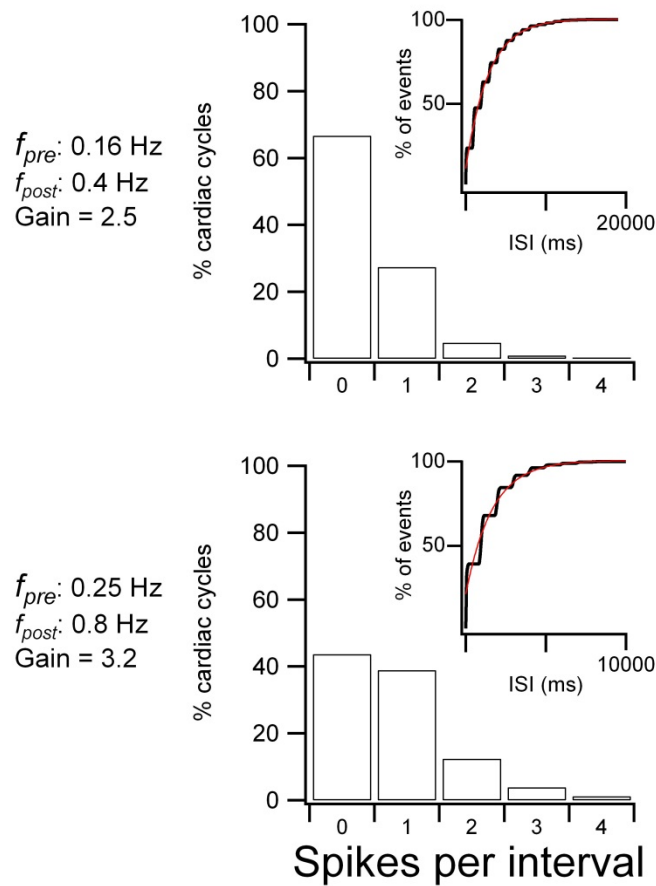


Figure 18 – Simulations incorporating secondary synapses can model sympathetic activity from human vasoconstrictor neurons. Modeling sympathetic activity with 1 primary and 6 secondary synapses generated a statistically similar spike per interval profile as observed in human vasoconstrictor neurons (Table 4). The cumulative ISI distribution of postganglionic activity did not statistically fit an exponential shape. However, the similar spike per interval distribution suggests that human vasoconstrictor activity can be modeled with $n + 1$ convergence.

2.4 DISCUSSION

With dynamic clamp, we created virtual nicotinic synapses to study how secondary synapses modulate postganglionic activity. The results show that mammalian sympathetic neurons can integrate subthreshold EPSPs to amplify and more than double preganglionic activity (Figure 8). The results also show that rhythmic activity, to simulate cardiac entrainment, can further amplify preganglionic activity (Figure 11 and 12). In addition, we show that we can model sympathetic activity from awake humans, both at rest (Figure 15A and 17A) and during heart failure (Figure 15B and 17B), and that a model of $n + I$ convergence, with rhythmic patterns of random activity (Figure 18), replicates the statistics of human vasomotor activity and generates gain.

These results support the concept that SCG neurons are integrative centers, where synaptic convergence can generate over half of the postganglionic outflow. This is the first evidence to support the gain hypothesis in rat SCG neurons. Despite arguments that primary synapses are the principal determinant of postganglionic activity (Gibbins 1995; McLachlan, Davies et al. 1997; McLachlan, Habler et al. 1998; McLachlan 2003; Macefield 2011), the present results reveal that SCG neurons have a larger integrative role and support *in vivo* intracellular evidence that weak subthreshold nicotinic synapses can drive postganglionic firing (Skok and Ivanov 1983; McLachlan, Davies et al. 1997; McLachlan, Habler et al. 1998; Bratton, Davies et al. 2010; Rimmer and Horn 2010). This amplification would have implications in regulating the activity of peripheral end organ targets.

We also show how stimulating SCG neurons with activity encoding for 8 secondary synapses at 1 Hz produces less synaptic gain than 8 secondary synapses at 0.5 Hz and 0.75 Hz (Figure 13). This result agrees with the $n + I$ convergence model, where at an infinitely low f_{pre} , all postganglionic activity is driven by primary synapses, resulting in a synaptic gain of 1. As f_{pre}

increases, synaptic gain increases to a theoretical maximum $n + 1$ level, at which point further increasing f_{pre} reduces gain (Wheeler, Kullmann et al. 2004). At 1 Hz, the activity is so frequent that summation of subthreshold EPSPs is inhibited by the afterhyperpolarization from an action potential in the previous cardiac cycle (Figure 14). This inhibition reduces the contribution of weak synapses on postganglionic activity, thus reducing synaptic gain.

One element that is unaccounted for in this model is straddling nicotinic synapses (Bratton, Davies et al. 2010; Rimmer and Horn 2010). These inputs are stronger than the typical weak synapse, but do not have the high safety factor for firing a postganglionic action potential like primary synapses (Rimmer and Horn 2010). Straddling inputs are suggested to innervate about one-third of neurons studied in the L3 lumbar sympathetic ganglia (Bratton, Davies et al. 2010) with even less evidence (6 out of 56 neurons) in the SCG (Rimmer and Horn 2010). If straddling inputs were implemented into the dynamic clamp model, it might be possible for integration of subthreshold and straddling EPSPs, or pairs of straddling EPSPs, to overcome afterhyperpolarization inhibition. Since information about straddling inputs is limited, they were left out from the current studies.

Recordings from peripheral nerves in awake human subjects have revealed characteristic firing patterns. These include a rhythmic discharge pattern that correlates to the cardiac cycle, the tendency for only one spike per cardiac cycle, an exponential distribution of interspike intervals and a low mean firing rate (Macefield 2011). A concerted effort has been made to record from different unit types (Macefield and Wallin 1996; Macefield, Rundqvist et al. 1999; Macefield and Elam 2004) in healthy subjects (Macefield, Elam et al. 2002) and in disease patients such as individuals with heart failure (Macefield, Rundqvist et al. 1999; Macefield, Elam et al. 2002; Ikeda, Murai et al. 2012), essential hypertension (Schlaich, Lambert et al. 2004), and obesity

(Lambert, Straznicky et al. 2007). Despite these efforts, the strength of synapses that drive postganglionic neurons remains unknown. Ongoing events in the SCG of anesthetized rats are thought to be driven by one or two primary synapses (McLachlan, Davies et al. 1997). Previous efforts to model muscle vasoconstrictor neurons with one or two primary synapses followed a normal distribution (Macefield 2011), however, typical synaptic activity follows a Poisson process (Berry and Meister 1998; Wheeler, Kullmann et al. 2004). Therefore, we used our model to initially replicate muscle vasoconstrictor activity with one primary synapse (Figure 15A and 16A).

Since vasomotor activity is rhythmic, we also entrained activity to a 200 ms duty cycle (Figure 15B), which had no effect on spike distribution (Figure 16B). When modeling the activity of healthy individuals (0.4 Hz) and individuals with heart failure (0.8 Hz), spike distributions were similar to those observed in awake human subjects (Table 4) (Macefield, Elam et al. 2002). However, when activity was entrained, the cumulative ISI distribution did not statistically fit an exponential distribution (Table 4). This occurs because of the nature of entrainment in our model. Outside of the duty cycle, activity is quiescent. However, physiologically this is not true and instead the probability of activity occurring at a given time point will change depending on blood pressure fluctuations during the cardiac cycle. The probability of activity occurring will be the greatest when blood pressure is at its minimal point in the cardiac cycle and this probability will decrease as blood pressure rises. This means that activity can potentially occur at any point in the cardiac cycle and in practice, it might be difficult to distinguish whether activity is continuous or periodic without using an autocorrelation. Implementing a continuous probability function into our model would blur the steps in the cumulative ISI distributions so they more closely resemble an exponential

distribution. In order to incorporate this, it would require analyzing human sympathetic activity to determine how the probability of firing changes during the cardiac cycle.

To determine the effect of secondary synapses and $n + I$ convergence, we modeled 6 secondary synapses in addition to the primary synapse (Figure 17). With the physiological assumption of a window of summation, we demonstrated that activity of healthy individuals and those with heart failure could be modeled with $n + I$ convergence (Figure 18). As a result of amplification, the input frequency of each synapse was slower than the overall output frequency. With conflicting models suggesting that unitary primary synapses (Macefield 2011) and $n + I$ convergence (Figure 18) can model human sympathetic activity, which model is correct?

McLachlan, *et al.* (1997) showed that almost 90% of rat SCG neurons receive at least one primary input, in addition to several subthreshold inputs. They argued that for the majority of neurons, the postganglionic discharge was driven primarily by suprathreshold synapses. However, these studies were conducted under hyperpolarized conditions, which would reduce the efficacy of secondary synapses while suprathreshold activity could generate action potentials unimpeded. Additionally, direct nerve stimulation of isolated SCG tissue revealed that summation of subthreshold EPSPs was sufficient to drive postganglionic action potentials (Rimmer and Horn 2010). The model proposed by Macefield (2011) suggests that the sympathetic network in animal models is more complex than that of humans, which typically is not the case. Therefore, we argue that SCG neurons are driven by primary and secondary inputs and our model incorporating $n + I$ convergence can sufficiently replicate synaptic activity in humans.

The $n + I$ convergence model also demonstrates that postganglionic activity significantly increases with modest elevation in preganglionic activity. Ganglionic amplification could prove

very beneficial for situations that require rapid changes in postganglionic activity. Studies of total postganglionic activity reveal large increases in sympathetic activity during strenuous exercise (Ichinose, Saito et al. 2008; Joyner, Charkoudian et al. 2008). Levels of postganglionic activity can change quicker and more accurately with ganglionic amplification. Therefore, we conclude that sympathetic neurons can detect coincidences of subthreshold EPSP summation, amplify preganglionic activity, and that patterns of sympathetic activity from awake humans can be accurately modeled with $n + I$ convergence. However, since spike distribution does not distinguish activity from a primary synapse or $n + I$ convergence, the debate on the nature of synaptic innervation in humans has not been resolved. Administering a submaximal dose of a nicotinic blocker would inhibit weaker synapses while having no effect on postsynaptic firing from primary synapses. A change in sympathetic activity would provide evidence of secondary synaptic innervation.

The data presented within this chapter provide evidence that mammalian SCG neurons are complex in that they are capable of integrating subthreshold EPSPs to amplify preganglionic activity and that cardiac entrainment enhances amplification. Furthermore, a novel model incorporating $n + I$ convergence is sufficient to replicate the statistics of human sympathetic activity. Further studies in animal models can provide a comprehensive overview of how presynaptic activity is modified to generate the postganglionic outflow. Therefore, results from animal models, together with human studies, will help to improve our model of human sympathetic activity.

3.0 MEMBRANE SHUNTS DEGRADE SYNAPTIC INTEGRATION

3.1 INTRODUCTION

Integration of postsynaptic activity depends upon intrinsic neuronal excitability. The ability to fire an action potential and the dynamics of repetitive firing are, in turn, determined by the types of ion channels expressed and their relative densities (Dolphin 2003; Suh, Horowitz et al. 2004; Tedford and Zamponi 2006; Suh and Hille 2008). Some neurons rapidly adapt and only fire once in response to sustained depolarization while others fire repetitively, in bursts, or behave as spontaneous pacemakers (Izhikevich 2007). This chapter examines the intrinsic excitability of rat SCG neurons and how excitability shapes synaptic integration and gain.

The intrinsic excitability of neurons is highly diverse. Cells in different brain regions exhibit different firing properties (Izhikevich 2007). Elucidating the functional significance of various neuronal firing properties is an important challenge.

Previous work on autonomic neurons suggests their firing patterns may depend upon their target of innervation. For example, paravertebral neurons of the caudal lumbar ganglia, which project to vascular targets, respond to depolarizing current pulses by firing a single action potential (phasic) while neurons in the prevertebral inferior mesenteric ganglia, which project to visceral organs, fire repetitively (tonic) (Cassell, Clark et al. 1986). Several reports indicate that most, if not all, paravertebral sympathetic neurons, including those in the SCG, exhibit phasic

firing dynamics while prevertebral sympathetic neurons display tonic firing (Weems and Szurszewski 1978; Galvan and Sedlmeir 1984; Cassell, Clark et al. 1986; Wang and McKinnon 1995). Intracellular recordings from the rat suggest that the underlying M-current is a major determinant of excitability and firing dynamics (Wang and McKinnon 1995). The M-current was weak or absent in tonic firing neurons while M-current was present in all phasic neurons. In bullfrog paravertebral ganglia 9 and 10, two major cell types were identified – B and C neurons (Dodd and Horn 1983a). Subsequent dynamic clamp studies revealed that the thresh- g_{syn} of B neurons was higher than that of C neurons (Kullmann and Horn 2010b). It was further reported that the phenotypic difference in excitability was a consequence of a differential voltage sensitivity of Na^+ channels. Collectively, this implies that neurons that perform different functions express different repertoires of ion channels and this can be a signature for cell identity.

Recent evidence from bullfrog sympathetic neurons and rat SCG neurons presents a contradictory picture pertaining to the firing dynamics and synaptic innervation of paravertebral sympathetic neurons. In bullfrog ganglia 9 and 10, both B and C neurons exhibited synaptic amplification (Kullmann and Horn 2006) and a diversity of firing patterns including both phasic and tonic firing (Kullmann and Horn 2010b). Direct nerve stimulation from rat SCG neurons revealed that pairs of subthreshold EPSPs from isolated secondary synapses are sufficient to drive postganglionic action potentials (Rimmer and Horn 2010). Furthermore, in the previous chapter we demonstrated that SCG neurons are integrative centers that generate synaptic gain. Why are reports from *in vivo* studies claiming that strong inputs are the main determinant of action potential discharge (McLachlan, Habler et al. 1998; Macefield, Rundqvist et al. 1999; Macefield, Elam et al. 2002; McLachlan 2003) whereas secondary synapses have gone

undetected? Typical *in vivo* recordings do not allow direct nerve stimulation to isolate secondary synapses, which may explain why summation was not observed in previous reports. Secondly, initial *in vivo* studies investigated the nature of SCG synapses under hyperpolarized conditions (McLachlan, Davies et al. 1997), which would have inhibited the contribution of secondary synapses to postganglionic firing. Finally, *in vivo* recordings used sharp microelectrodes, which could create membrane damage. Therefore, **we hypothesize that microelectrodes create a shunt conductance, or leak, that alters firing dynamics, reduces excitability, and diminishes the secondary synaptic contribution to action potential firing.** To test this, we used dynamic clamp to introduce a non-depolarizing shunt conductance to mimic membrane damage, and then measured changes in firing dynamics, excitability, integration, and synaptic gain.

3.2 METHODS

3.2.1 Preparation of Intact Ganglia

Microelectrode experiments were performed on adult male Sprague Dawley rats (180-250 g). Animals were killed by CO₂ inhalation following approved procedures by the Institutional Animal Care and Use Committee at the University of Pittsburgh. The SCG was removed from the animal, desheathed and pinned out, using the remaining connective tissue to flatten the SCG in a Sylgard-lined recording chamber. Throughout the procedure, the tissue was continuously immersed in extracellular Ringer's solution, which contained (in mM) 124 NaCl, 4 KCl, 25.7 NaHCO₃, 1.25 NaH₂PO₄, 2.45 CaCl₂, 1.2 MgSO₄, 11 glucose, 0.15 ascorbic acid and was equilibrated with 95/5% O₂/CO₂ gas. For whole-cell recordings, the ganglion was incubated

with 10 mg/ml Collagenase Type III (Worthington Biochemical Corp., Lakewood, NJ) in L15 medium, supplemented with 14 mM NaHCO₃ for 1 hr at 37°C in a 5% CO₂ atmosphere. The chamber was mounted on a fixed stage Zeiss WL microscope with a 40x water immersion objective and Nomarski DIC optics. The ganglion was superfused with the bicarbonate-buffered Ringer's solution at a rate of 2 ml min⁻¹ using a peristaltic pump. The preparation was maintained at 32°C with an inline heater (Warner Instruments, Hamden, CT, USA).

3.2.2 Microelectrode Recordings

Intracellular recordings were made using glass 80-120 MΩ micropipettes (Glass 1BBL with filament, 1.2 mm OD, 0.68 mm ID, World Precision Instruments, Sarasota, FL) filled with 3 M K⁺ acetate using an Axoclamp 2B amplifier (Molecular Devices, Sunnyvale, CA) with filtering set to 10 kHz. Intracellular recordings were taken using a Digidata 1440A interface with pClamp 10.3 software (Molecular Devices, Sunnyvale, CA). Current-voltage (I-V) relationships were constructed from a series of hyper- and depolarizing DC current injections, each current pulse lasting 1 second. The average steady state voltage response during the last 100 ms was used to plot current-voltage relationships, which was subsequently used to calculate input resistance.

3.2.3 SCG Primary Cell Culture

The protocol for dissection, dissociation, and culture maintenance was the same as described in [Chapter 2.2.1](#).

3.2.4 Whole-Cell Recordings

The recipes for intracellular and extracellular solutions and guidelines for the initial setup are outlined in [Chapter 2.2.2](#).

To measure neuronal excitability, neurons were stimulated with 1 second current injections ranging from -240 to 240 pA at 30 pA steps. Frequency-current relationships were constructed by measuring the time difference between the first and last action potential in a voltage response. Frequency was calculated by dividing the number of action potentials by the time difference, which was plotted against the size of the current pulse. The same voltage responses were also used to calculate input resistance (R_{input}), resting membrane potential (V_{rest}), and τ . R_{input} was calculated by constructing I-V curves. The average steady state voltage response of a 10 ms window near the end of the 1 second injection was plotted against current injection amplitude. R_{input} was calculated by fitting a linear line to the curve where it crossed 0 mV. V_{rest} was measured by taking the average voltage in a 100 ms window prior to the start of current injection. τ was measured by using a voltage response trace to a hyperpolarized current injection that did not appear to activate any hyperpolarization sensitive voltage gated channels, which was typically the voltage response to a -30 pA current injection. The exponential equation, $y = -A^{-\frac{1}{\tau} * x}$, was fit to the first 37.5 ms of the voltage response using Igor (WaveMetrics, Lake Oswego, OR), which directly calculated for τ .

Current ramp injections were also used to measure excitability. Neurons were stimulated with a current injection that increased smoothly from 0 – 400 pA over 5 seconds. The neuron was appropriately classified based on the recorded voltage response.

ZAP currents were used to determine whether a neuron was an integrator or resonator neuron. In current clamp, neurons were stimulated with a sinusoidal 20 pA current injection where the frequency of the sine wave ranged from 0 – 50 Hz over 30 seconds. The voltage response to the injection was used to classify neurons as integrators or resonators.

3.2.5 Classification of Neuronal Excitability Following Hodgkin's Criteria

Based on analysis of firing in squid axons, Hodgkin derived criteria to divide neuronal excitability into three classes (Hodgkin 1948; Izhikevich 2007). Class 1 neurons exhibit tonic firing with frequencies that vary over a broad range. Initial action potential firing occurs at a low frequency (in theory it can be infinitely low) and persists for the duration of the current pulse. The frequency of action potential firing increases as the strength of the current injection increases. Class 2 neurons exhibit tonic firing in which the frequency is relatively insensitive to changes in current injection strength. In neurons that show class 2 firing, spiking does not initially last for the duration of the current pulse. The duration of repetitive action potential firing increases with current injection strength, but the frequency of firing remains relatively constant and changes little with larger current amplitudes. Class 3 neurons exhibit phasic firing, in which only one or a few action potentials fire in response to a depolarizing current injection and neurons do not fire repetitively even with large current injections.

Class 1 and class 2 neurons can be distinguished by constructing frequency-current (F-I) curves. With class 1 neurons, a depolarizing current pulse initiates low frequency repetitive firing. Action potential firing showed little or no frequency accommodation, thus the F-I curve had a steep slope. In contrast, class 2 neurons required more current to initiate firing thus the F-I

curve is discontinuous. Additionally, action potential frequency does not change with current amplitude, therefore the slope of the relationship was shallow.

3.2.6 Dynamic Clamp Recordings

The equation describing how virtual nicotinic synapses are implemented and the procedure for determining $\text{thresh-}g_{\text{syn}}$ are found in [Chapter 2.2.5](#).

The ability of EPSPs to drive postsynaptic firing was tested by measuring the action potential response to physiological EPSP waveforms whose amplitude ranged from 90 – 650% of $\text{thresh-}g_{\text{syn}}$, which was measured under control conditions. EPSP efficacy was also tested in the presence of a shunt conductance to demonstrate how the shunt changes the response to EPSPs.

The virtual leak conductance (g_{leak}) is a voltage independent background conductance that was used to mimic a leaky membrane caused by cellular damage. The reversal potential (E_{rev}) of g_{leak} was set to V_{rest} to prevent depolarization. The effect of the shunt conductance was clearly seen when applied to a model cell consisting of a resistor and capacitor (Figure 19). Using 30 pA current injection steps ranging from -240 to 240 pA, a 2 nS shunt conductance, with $E_{\text{rev}} = 0$ mV, demonstrated how the amplitude of the voltage response to each current step was reduced with no change in the resting membrane potential. Anti-leak conductances were elicited in the exact same fashion as leak conductances except negative values were assigned to the g_{leak} amplitude.

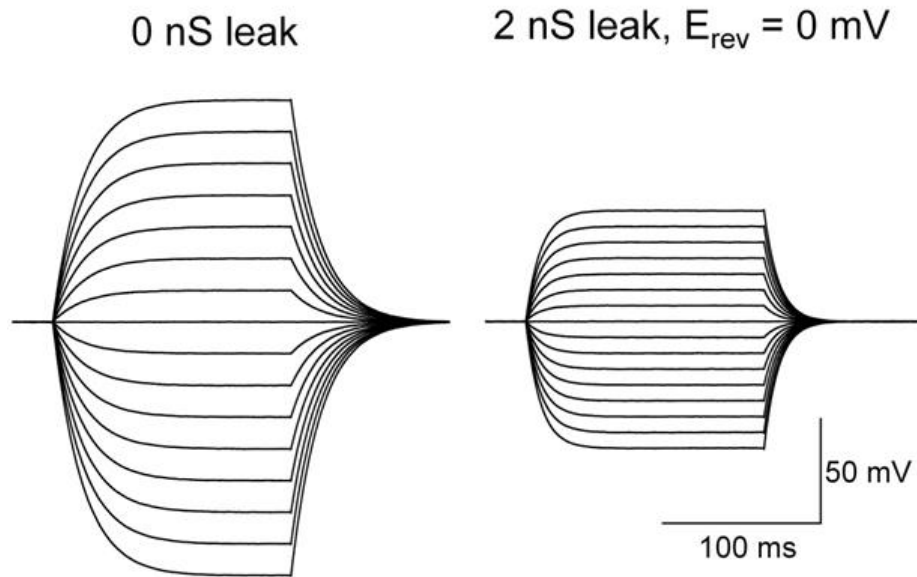


Figure 19 – The effect of a 2 nS leak on the model cell. The model cell ($R_{\text{cell}} = 500 \text{ M}\Omega$, $C_{\text{cell}} = 33 \text{ pF}$) was stimulated with 30 pA current injection steps ranging from -240 to 240 pA. When a 2 nS shunt conductance with $E_{\text{rev}} = 0$ was applied, the voltage response to each current injection was much smaller compared to a 0 nS leak. Since $E_{\text{rev}} = V_{\text{rest}}$, the membrane potential did not change.

3.2.7 Analysis and Statistics

Calculations were similar to those described in [Chapter 2.2.6](#). All statistics were prepared with GraphPad InStat 3 (La Jolla, CA) using an ANOVA and Tukey post-hoc test with $P < 0.05$ as criterion for significance. All grouped data was expressed as mean \pm S.E.M. and graphs were arranged using GraphPad Prism 4 (La Jolla, CA).

3.3 RESULTS

3.3.1 Tonic Firing is not a Tissue Culture Artifact

Initial whole-cell recordings were performed on dissociated SCG neurons ($n = 28$). We observed that 15 neurons responded to depolarizing current steps with tonic repetitive action potential firing (Figure 20). We initially thought that changes brought about by cell culturing could account for the disparity in firing from previous reports in intact ganglia. To address this possibility, Dr. Paul Kullmann, a senior researcher in our lab, performed whole-cell recordings from neurons in acutely isolated intact SCG tissue (Figure 21, top). His data showed that SCG neurons exhibit tonic firing dynamics, similar to whole-cell recordings from primary cultures (Figure 20). I then repeated earlier recordings using sharp microelectrodes to record from neurons in the acutely isolated SCG. With microelectrodes, neurons ($n = 16$) always displayed phasic firing dynamics (Figure 21). This suggests that cell culturing could not explain the tonic firing seen with whole cell recordings in dissociated SCG neurons. In other words, the recording method, not the preparation of the tissue, influences the firing dynamics one observes.

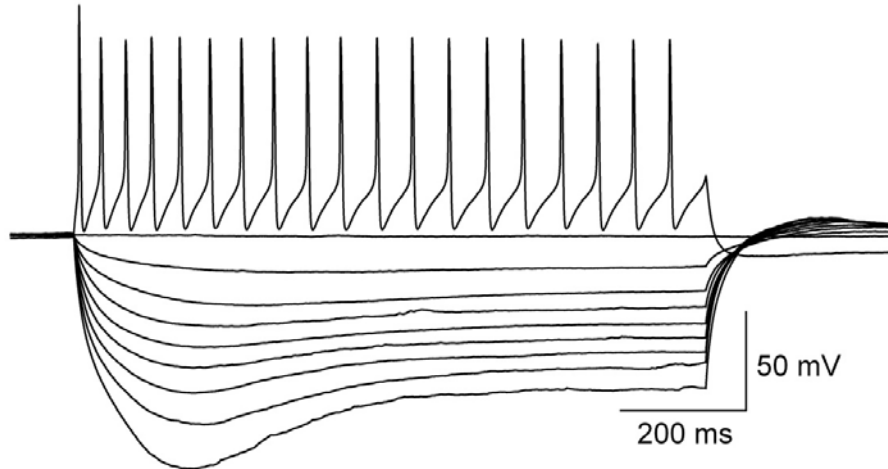


Figure 20 – A whole-cell recording from a dissociated SCG neuron displayed tonic firing dynamics.

A dissociated SCG neuron was stimulated with 30 pA current steps with maximum stimulation of 240 pA. The neuron responded with tonic, repetitive firing dynamics.

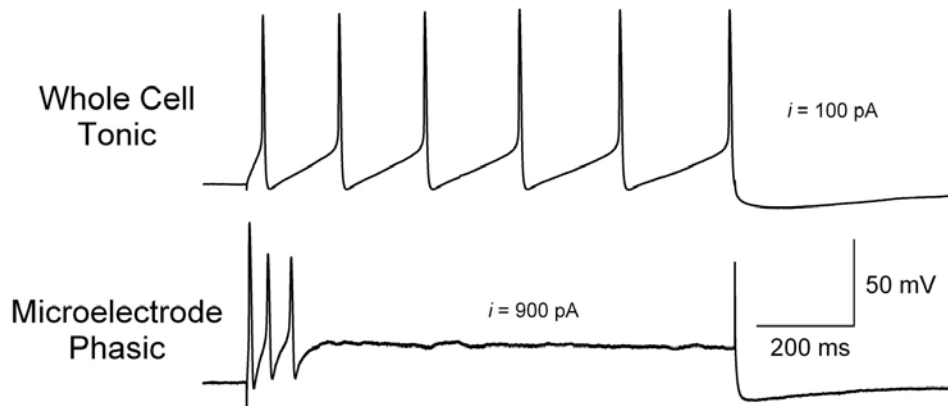


Figure 21 – Tonic firing is not an artifact of tissue culturing. Whole-cell recordings, performed by Dr.

Paul Kullmann (top), and microelectrode recordings (MGS) from neurons in the intact SCG. Neurons recorded with microelectrodes were stimulated with a 900 pA current injection and always fired in a phasic manner. In whole-cell recordings, neurons were stimulated with a 100 pA current injection and fired repetitively.

3.3.2 SCG Neurons Display Three Classes of Excitability

We hypothesize that microelectrodes alter the firing dynamics of SCG neurons by introducing a membrane shunt conductance. To test this hypothesis and mimic the leak caused by a microelectrode, we classified neurons using Hodgkin's criteria and then introduced leak conductances using dynamic clamp. I-V curves constructed with whole-cell recordings from dissociated SCG neurons and stimulated with 30 pA current steps showed that subsets of neurons fired with class 1 ($n = 5$) and class 2 ($n = 10$) tonic firing dynamics, and class 3 ($n = 13$) phasic firing dynamics (Figure 22). F-I curves were constructed to distinguish between the two classes of tonic firing (Figure 23). Class 1 neurons had a steep F-I relationship, while class 2 neurons had F-I curves that were discontinuous with a shallow slope.

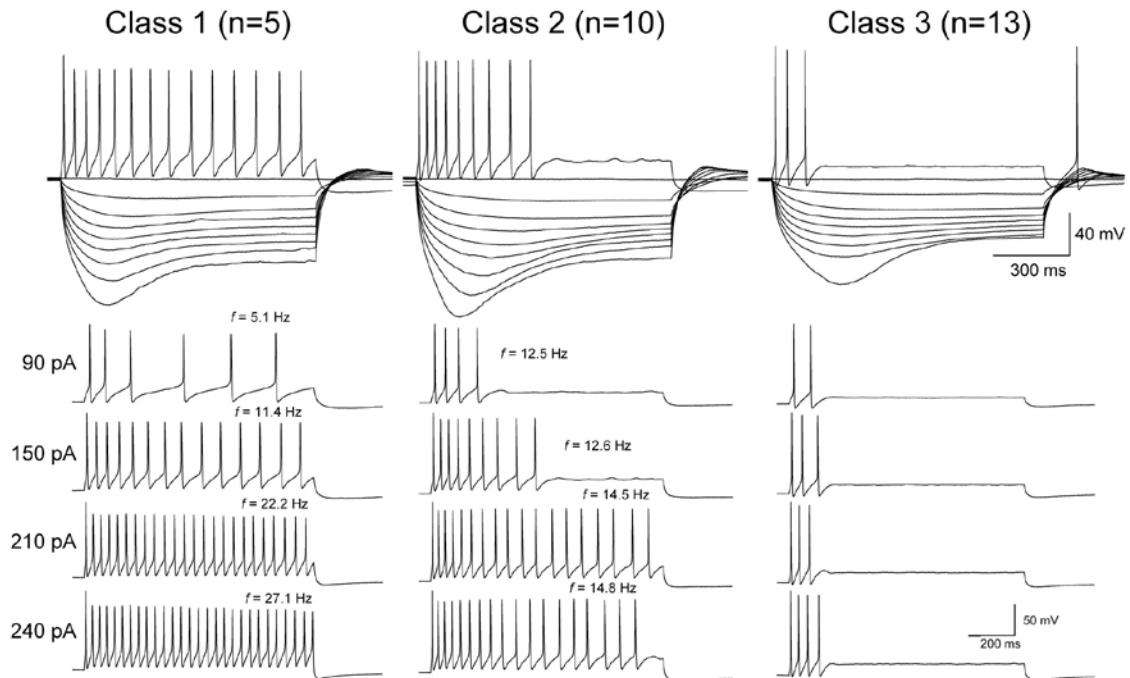


Figure 22 – SCG neurons exhibit three classes of firing dynamics. Neurons were stimulated with 30 pA current step injections ranging from -240 to 240 pA. The voltage response was used to classify neurons according to Hodgkin’s classification of neuronal excitability. Class 1 neurons fired repetitively with an action potential frequency that continuously increased with current injection strength. Class 2 neurons also fired repetitively, but the frequency of spiking remained fairly constant and was not influenced by current injection strength. Class 3 neurons fired in a phasic manner where action potential spiking adapted rapidly and stronger current injections did not induce repetitive firing. This figure shows representative examples of each firing dynamic class.

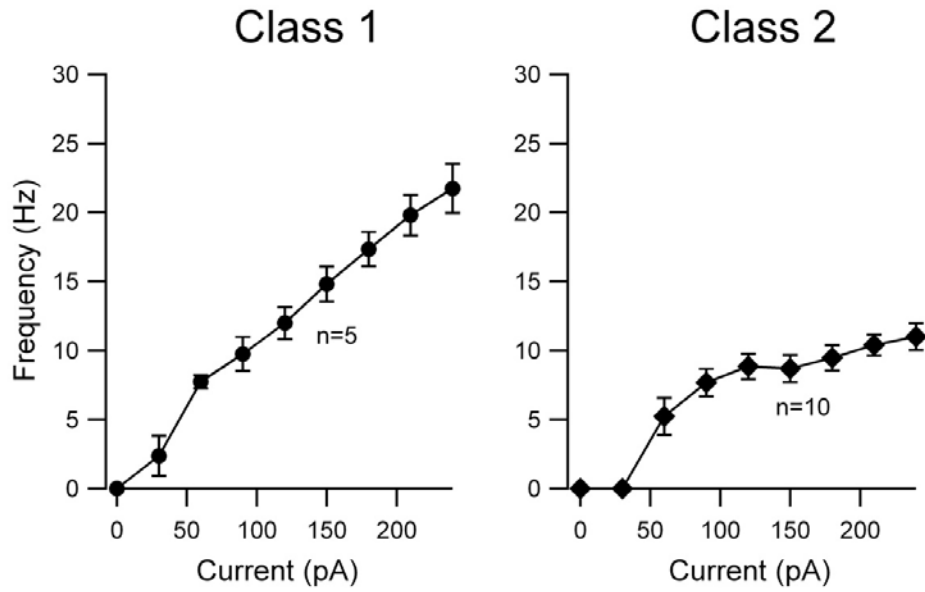


Figure 23 – Frequency-current relationships are different between class 1 and class 2 neurons. The frequency of action potential spiking was compared to the strength of the current injections. In class 1 neurons, action potential frequency started low and continuously increased as current injection strength increased. In class 2 neurons, the frequency of action potential spiking had a shallow relationship compared to current injection strength and the overall frequency was lower in class 2 neurons.

Although the average R_{input} of class 3 neurons was lower ($413.5 \pm 19.4 \text{ M}\Omega$) than class 1 ($474.86 \pm 54.3 \text{ M}\Omega$) or class 2 neurons ($496.6 \pm 26.7 \text{ M}\Omega$), the difference was not significant. V_{rest} ($-65.4 \pm 1.0 \text{ mV}$; $-71.3 \pm 1.7 \text{ mV}$; $-67.1 \pm 1.1 \text{ mV}$) and τ constant ($24.0 \pm 1.6 \text{ ms}$; $24.3 \pm 1.1 \text{ ms}$; $22.2 \pm 1.1 \text{ ms}$) did not differ between class1, class 2, and class 3 respectively. To test whether the difference in firing patterns reflected underlying membrane excitability differences relevant for synaptic integration, we used dynamic clamp to implement a virtual nicotinic synapse and measured thresh-g_{syn} . The thresh-g_{syn} of class 3 neurons ($4.60 \pm 0.36 \text{ nS}$) was

significantly higher than that of class 1 (2.52 ± 0.25 nS, $P < 0.01$, ANOVA) and class 2 (3.08 ± 0.37 nS, $P < 0.05$, ANOVA) neurons (Figure 24).

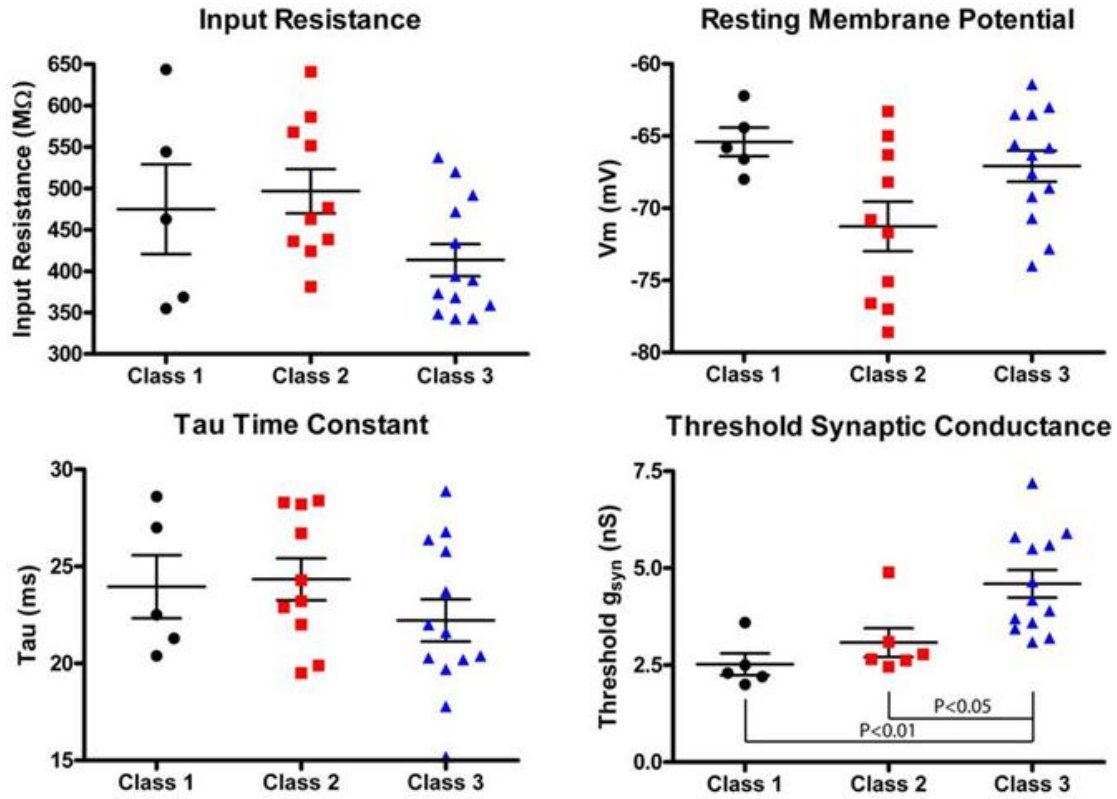


Figure 24 – Threshold synaptic conductance is higher in class 3 neurons. Various electrophysiological parameters were measured to elucidate any differences between the classes of excitability. The only statistically significant difference was that class 3 neurons had a higher thresh- g_{syn} than class 1 or class 2 neurons. Input resistance, resting membrane potential and τ were not different between any of the classes.

Ramp currents were used as an additional method of determining excitability class (Izhikevich 2007). A current ramp was injected that ranged from 0 – 400 pA over 5 seconds (Figure 25). Each class had a specific response to ramp currents. Class 1 neurons (n = 5) fired almost immediately and repetitively throughout the duration of the ramp. Class 2 neurons (n = 5) did not initially fire, but after several seconds and at a high enough current injection, these neurons fired repetitively. Class 3 neurons (n = 4) did not fire during the current ramp, even with large current injections.

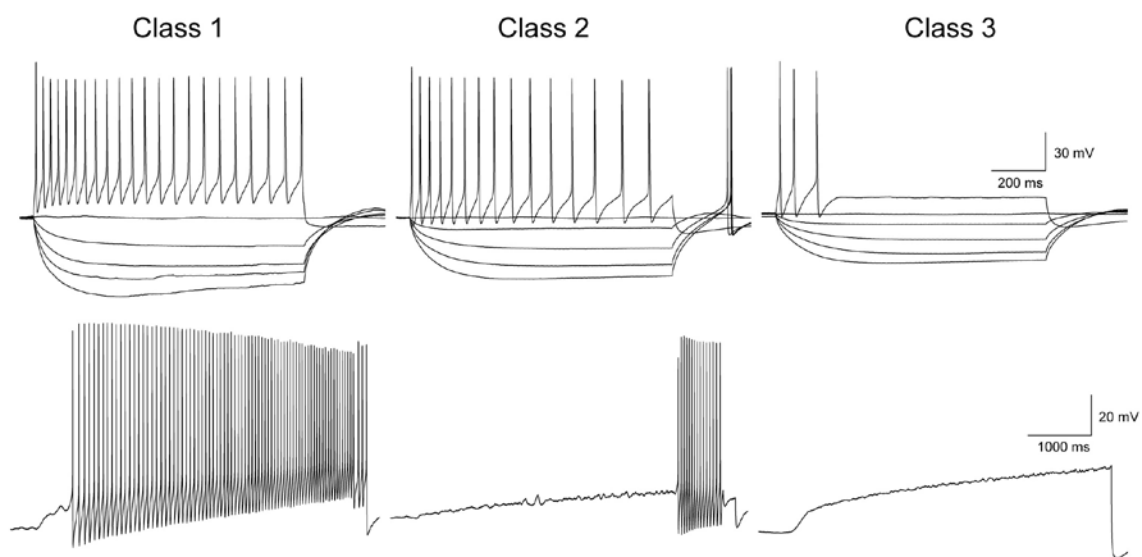


Figure 25 – Ramp currents confirm neuronal excitability classification. Ramp currents ranging from 0 – 400 pA over 5 sec were used to measure neuronal excitability. Each class had a specific response to the ramp current. Class 1 neurons fired immediately and throughout the duration of the ramp injection. Class 2 neurons did not fire immediately, but eventually fired repetitively once the current injection was high enough. Class 3 neurons did not fire an action potential in response to the ramp current.

3.3.3 SCG Neurons are Integrators

Since synaptic input to vasoconstrictor neurons is entrained to the cardiac cycle, we sought to determine whether these neurons have membrane properties attuned to this pattern and whether this would correlate with firing pattern. To test for a resonant frequency at which synaptic input would summate in a supralinear manner, we used a ZAP protocol. This experimental procedure uses a sinusoidal current injection of increasing frequency to measure neuronal impedance, a frequency extension of resistance (Kali and Zemankovics 2012) and the proclivity to subthreshold integration, which dictates whether a neuron is an integrator or resonator (Izhikevich 2007). Integrator neurons have an initial large voltage response that decreases as sine wave frequency increases, whereas resonator neurons have a peak voltage response that corresponds to an intermediate resonant frequency (Izhikevich 2007). While the rat heart rate operates at about 5 Hz, the limited phase during which synaptic input arrives (duty cycle), calls for a higher frequency. Therefore, the ZAP current injection linearly ramped from 0 – 50 Hz over 30 seconds (Figure 26). Each class (class 1: $n = 5$, class 2: $n = 5$, class 3: $n = 6$) exhibited the same voltage response, which peaked at lower frequencies and decreased as the frequency of the sine wave increased, suggesting that each class of neuron was an integrator neuron.

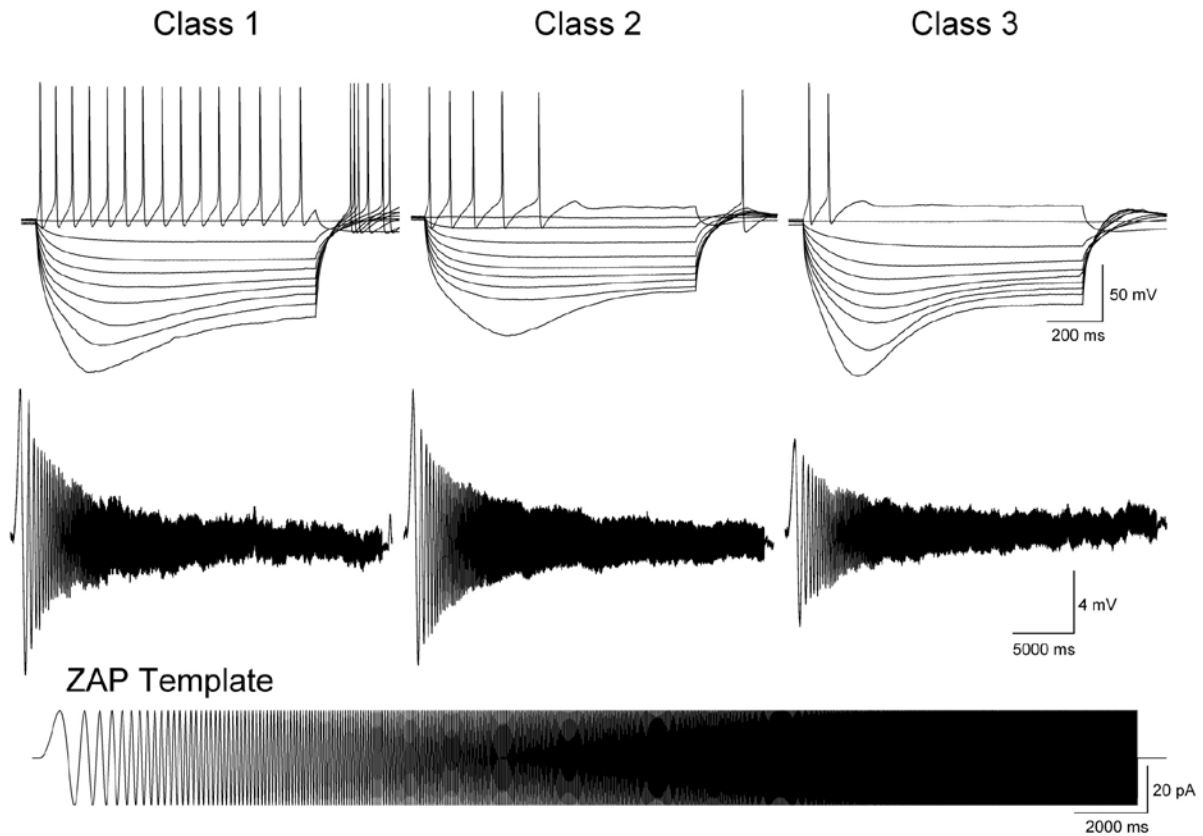


Figure 26 – ZAP currents show SCG neurons are integrator neurons. A ZAP current, a sinusoidal current injection, was used to determine whether a neuron is a resonator or an integrator neuron. The sine wave of the ZAP current had an amplitude of 20 pA and increased from 0 – 50 Hz over 30 seconds. The voltage response from each class of neuron demonstrated that these neurons are integrator neurons. Integrator neurons respond with a large initial response that decreases as the sine wave frequency increases. Resonator neurons have the largest response at an intermediate frequency.

Integration was also tested using physiological EPSP current injections (dynamic clamp) under hyperpolarized conditions to prevent action potential firing (Figure 27). A neuron was stimulated with pairs of depolarizing synaptic current pulses. Pulses 5 ms apart showed that postsynaptic potentials (V_m) were integrated on top of one another. The derivative of the response (dV/dt) showed equal amplitudes of each individual postsynaptic potential. Moving the pulses 2 ms apart caused the voltage response to merge and the derivative was approximately double the amplitude of each individual postsynaptic potential.

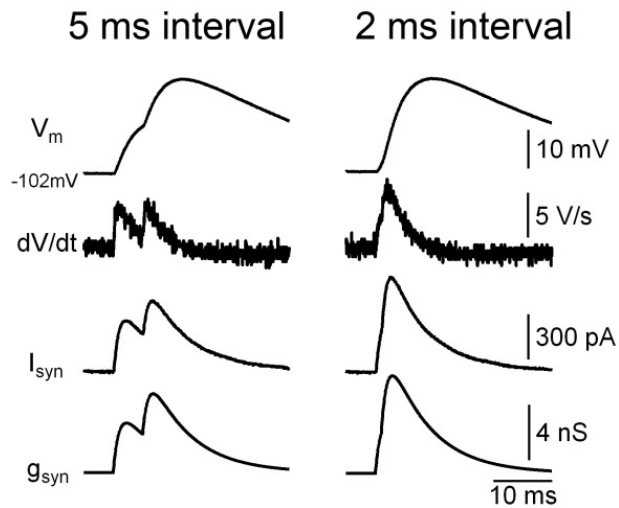


Figure 27 - Paired pulse stimulation demonstrates integration. SCG neurons were hyperpolarized to prevent action potential firing and stimulated with subthreshold paired pulses at either 5 or 2 ms apart. The voltage trace demonstrates how the two responses are able to integrate on top of each other. The derivative shows that each response has an identical amplitude. When pulses are 2 ms apart, the amplitude of the derivative shows that responses are almost completely integrated.

3.3.4 A Shunt Conductance Modulates Firing Dynamics

In addition to showing class 1 and 2 tonic firing, whole-cell recordings from SCG neurons also differed from microelectrode recordings in their response to hyperpolarizing current steps. With increasing current strength, a relaxing sag appeared in voltage responses that is indicative of h-current (I_h) activation (Izhikevich 2007). Additional recordings (not shown) using 10 μM ZD7288, an h-channel antagonist, blocked the sag response. Although we did not measure the h-current sag, it seemed less prominent in class 3 neurons and was never seen in microelectrode recordings. Therefore, we hypothesized that microelectrode damage creates a shunting leak, which obscures the presence of I_h in microelectrode recordings and alters firing dynamics. To test this hypothesis, we used dynamic clamp to add a voltage-independent leak conductance and modified its strength to simulate varying degrees of cellular damage.

The leak conductance ranged from 3 – 20 nS and neurons were stimulated with 1-second current injections ranging from -240 to 240 pA at 30 pA steps (Figure 28A). Under the control condition, hyperpolarization elicited a relaxing sag and depolarizing current steps resulted in a tonic firing pattern for class 1 or class 2 neurons. As little as a 3 nS leak obscured the I_h effect on voltage transients and transformed the firing pattern from tonic to phasic. Increasing the leak conductance amplitude eventually blocked action potential firing all together. The leak conductance linearized the current-voltage (I-V) relationship (Figure 28B) and decreased the τ constant (Figure 28C, 0 nS: 23.3 ± 0.7 ms; 3 nS: 13.5 ± 0.4 ms; 10 nS: 6.6 ± 0.3 ms; 20 nS: 3.5 ± 0.2 ms). Grouped data revealed that the leak conductance significantly decreased R_{input} (Figure 29, 0 nS: 454.1 ± 17.2 M Ω ; 3 nS: 182.7 ± 5.7 M Ω ; 10 nS: 81.5 ± 1.8 M Ω ; 20 nS: 44.8 ± 1.2 M Ω ,

$P < 0.001$, ANOVA, $n = 27$). The R_{input} from microelectrode recordings was $75.3 \pm 7.5 \text{ M}\Omega$ ($n = 16$), which was significantly different from the R_{input} with a 0 nS and 3 nS leak ($P < 0.001$, ANOVA). The non-depolarizing leak conductance had no effect on V_{rest} (Figure 30, 0 nS: $-68.3 \pm 0.9 \text{ mV}$; 3 nS: $-68.1 \pm 0.9 \text{ mV}$; 10 nS: $-68.5 \pm 0.8 \text{ mV}$; 20 nS: $-68.0 \pm 0.8 \text{ mV}$). Microelectrode recordings did have a significantly depolarized V_{rest} ($n = 16$, $-57.0 \pm 1.8 \text{ mV}$, $P < 0.001$, ANOVA). However, some microelectrode recorded neurons had a V_{rest} that fell within the range of whole-cell recorded neurons. Nonetheless, all microelectrode recordings displayed class 3 firing dynamics. This also provided a basis for estimating the amount of damage associated with *in vivo* microelectrode recordings based on firing dynamics and R_{input} . By using whole-cell recordings as a standard for calculating cellular damage, these microelectrode recordings had a leak conductance of $13.2 \pm 1.8 \text{ nS}$, which would be sufficient to alter firing dynamics and change excitability in whole-cell recordings

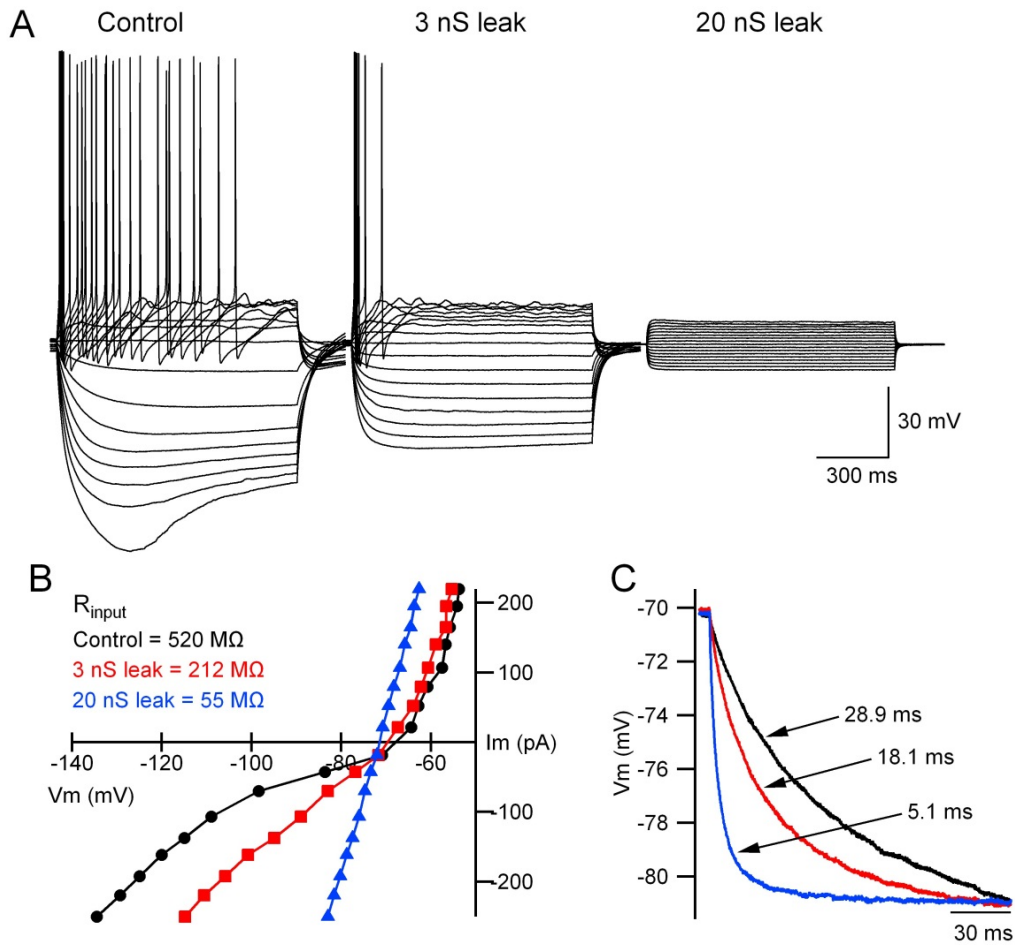


Figure 28 – Leak conductances reduced neuronal excitability, linearized IV relationships and decreased τ . Electrophysiological recordings were performed in the presence and absence of a leak conductance. (A) A repetitive firing neuron converted to phasic dynamics in the presence of a small leak. With a large leak, action potential firing was blocked altogether. (B) The leak conductance linearized the current-voltage (IV) relationship, which decreased R_{input} . (C) The leak conductance also decreased τ .

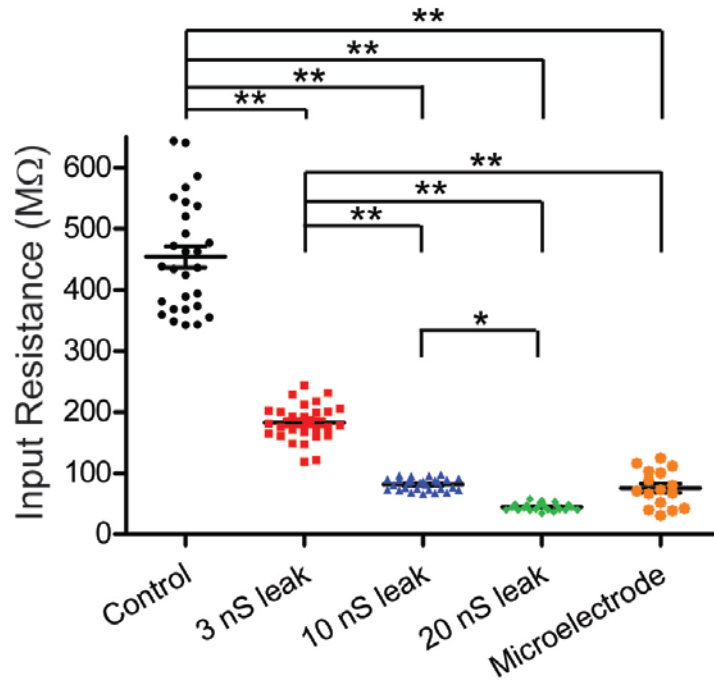


Figure 29 – A leak conductance significantly decreased input resistance. The input resistance was calculated from I-V relationships. Grouped data revealed that an increasing leak conductance significantly lowered the R_{input} . The R_{input} of microelectrode recordings was significantly different than the R_{input} of neurons with a 0 nS and 3 nS leak. * $P < 0.05$, ** $P < 0.001$.

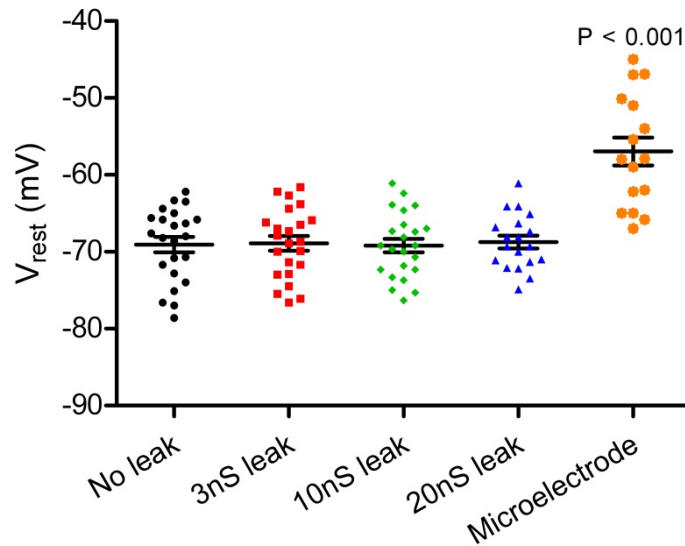


Figure 30 – Neurons from microelectrode recordings were significantly depolarized. All experiments mimicking a leak used a non-depolarizing shunt conductance by setting E_{rev} equal to V_{rest} . There was no significant difference in any of the *in vitro* recorded neurons with a simulated leak. Neurons recorded with sharp microelectrodes were significantly depolarized, but some cells still fell within the range of whole-cell neurons.

3.3.5 Anti-leak Conductances can Compensate for Leaky Membranes

Our data revealed a trend for class 3 neurons to have slightly lower input resistances than class 1 and 2 neurons (Figure 24). Might cell damage associated with whole cell recording account for such differences? To test this hypothesis, virtual anti-leak conductances were used to raise the R_{input} of class 3 cells. We found that in some cells, negative leaks could transform firing from class 3 to tonic firing, but that others remained tonic (Figure 31). Class 3 neurons were stimulated with current injections ranging from -240 to 240 pA at 30 pA current steps. Cell 1,

under control conditions, exhibited class 3 firing dynamics with an R_{input} of 332.0 M Ω . A -2 nS anti-leak conductance increased R_{input} to 492.4 M Ω , but had no effect on firing dynamics. Cell 2 exhibited class 3 phasic firing dynamics with a R_{input} of 125.9 M Ω . Application of a -2 nS anti-leak conductance increased R_{input} to 480.6 M Ω and the neuron fired repetitively.

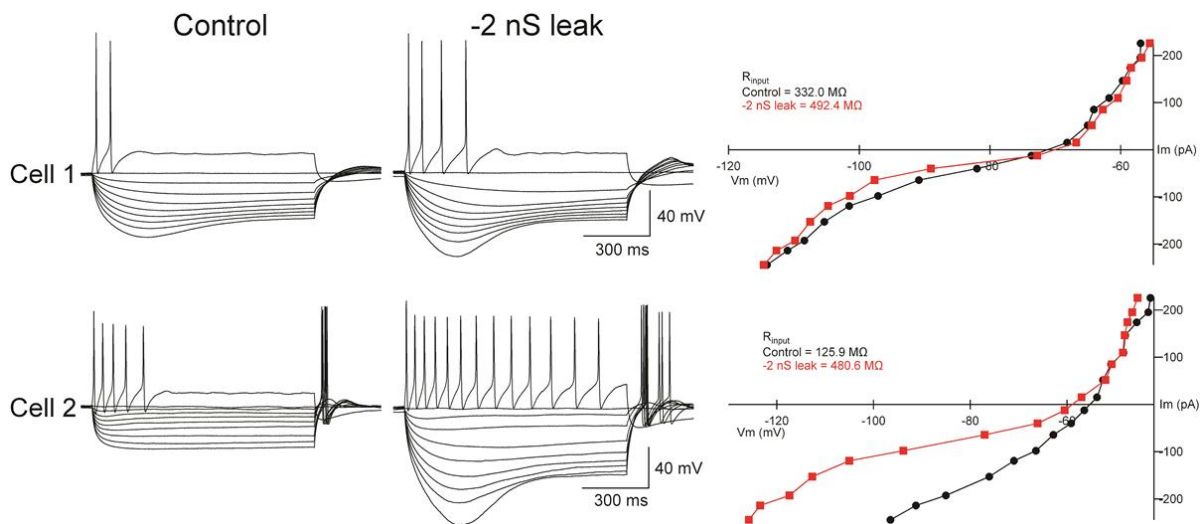


Figure 31 – Anti-leak conductances can compensate for leaky cells. An anti-leak conductance was applied to class 3 neurons to determine if they can be stimulated to fire repetitively. In both cells, a -2 nS leak increased the R_{input} . In cell 1, the neuron remained phasic, while in cell 2, the class 3 neuron converted to tonic firing. This suggests that the initial phasic firing of cell 2 was a result of membrane leakiness, which was compensated for by the anti-leak conductance.

Perhaps the failure to alter firing in some cells was due to an insufficiently small negative leak. To test this, class 3 neurons were stimulated with progressively stronger anti-leak conductances (Figure 32). The neuron would not fire repetitively even with large anti-leak conductances and current injections. The size of the maximum current injection was lowered in the presence of a -6 nS anti-leak conductance to prevent neuronal death. This confirmed that some class 3 neurons could not be pushed to fire repetitively, and were genuine class 3 cells.

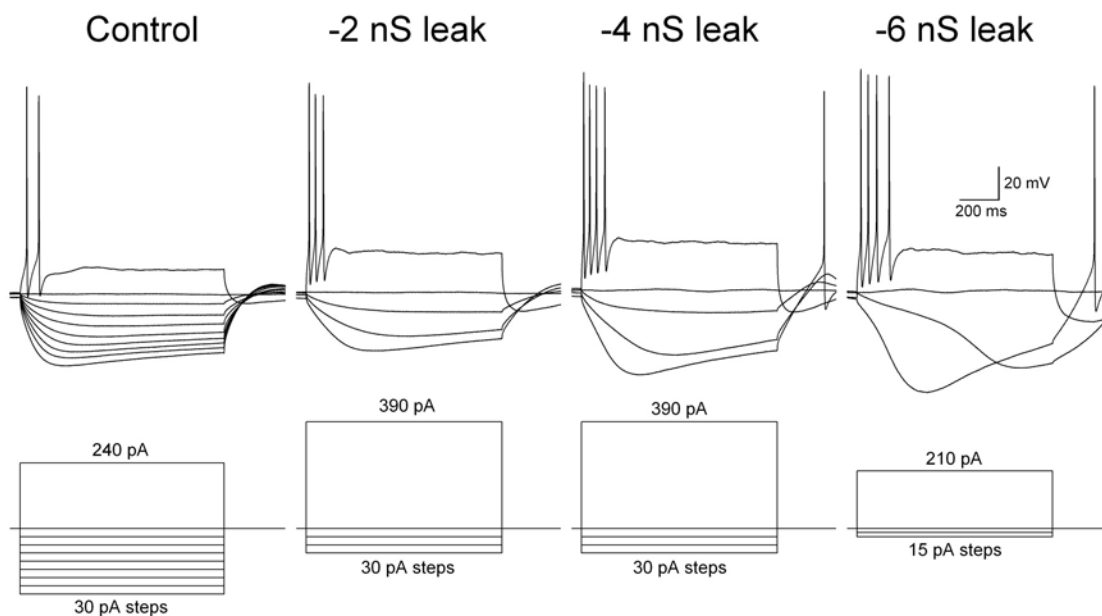


Figure 32 – Some class 3 neurons do not fire repetitively with large anti-leak conductances. Class 3 neurons were tested to determine if they are genuine phasic neurons. Anti-leak conductances, in combination with larger current injections, could not push these neurons to fire in a tonic manner. This showed that not every phasic firing neuron is a consequence of membrane leakiness.

3.3.6 Leak Conductances Reduce Synaptic Gain

After finding that small leak conductances can transform neuronal excitability, we hypothesized that they might also change synaptic gain. To test this, the efficacy of current injection waveforms was examined first by determining $\text{thresh-g}_{\text{syn}}$. Cells were stimulated with virtual conductance waveforms ranging from 90 – 650% of $\text{thresh-g}_{\text{syn}}$ and then leak conductances were introduced to measure the change in action potential discharge (Figure 33). With no leak, neurons fired at every current injection except when the strength of the waveform was 90% of $\text{thresh-g}_{\text{syn}}$. Increasing the leak conductance reduced neuronal excitability and therefore required larger current injection waveforms to initiate an action potential.

That led to the prediction that leak conductances would also decrease synaptic gain. Neurons were stimulated with a 1 Hz periodic dynamic clamp template encoding for 1 primary synapse, at three times $\text{thresh-g}_{\text{syn}}$, and 8 secondary synapses, at 90% $\text{thresh-g}_{\text{syn}}$ (Figure 34). In each condition, 41 action potentials were driven by the primary synapse, which was unaffected by the shunt conductance. Under control conditions, an average of 56 action potentials were generated by secondary synaptic summation to give an average synaptic gain of 2.44 ± 0.06 ($n = 17$). The number of action potentials driven by subthreshold EPSPs decreased with larger shunt conductances, which significantly reduced synaptic gain (3 nS: 1.95 ± 0.05 ; 10 nS: 1.29 ± 0.05 ; 20 nS: 1.00 ± 0.02 , $P < 0.001$, ANOVA). These results demonstrated how a leak conductance can occlude the contribution of weak synapses to postganglionic spike output and thereby reduce synaptic gain.

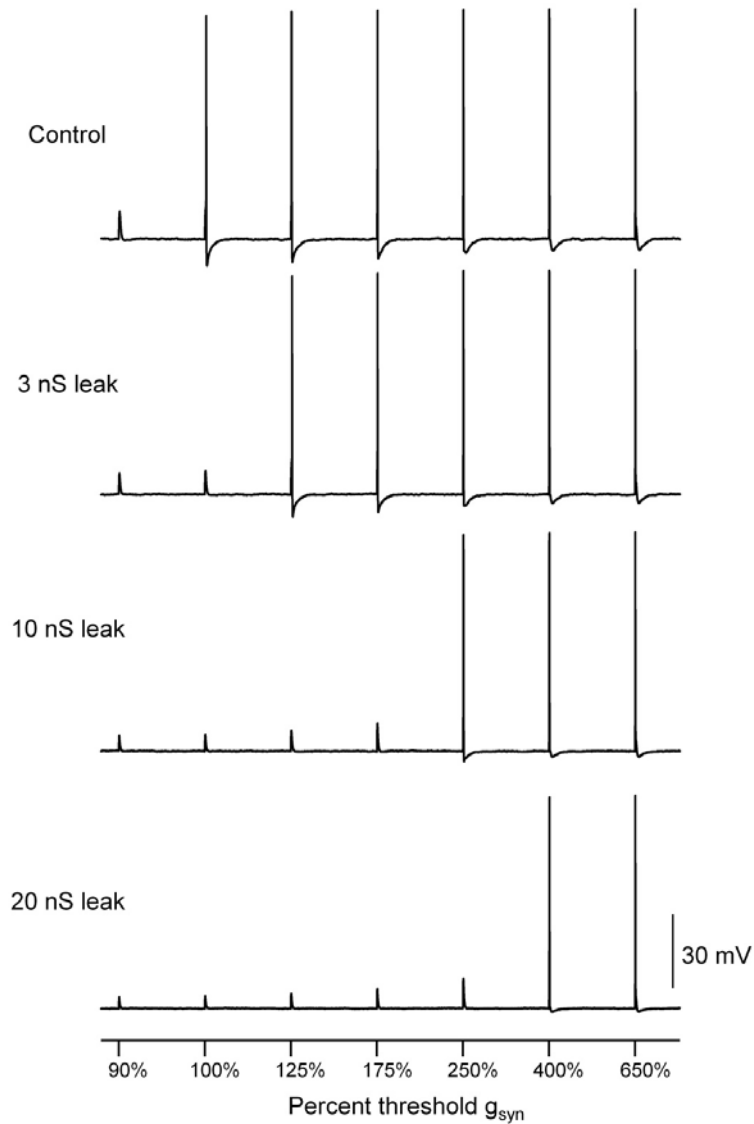


Figure 33 – A leak conductance reduced the efficacy of EPSPs. Neurons were stimulated with conductance waveforms ranging from 90% to 650% of $\text{thresh-}g_{\text{syn}}$. As the size of the leak increased, neurons required a stronger stimulus to initiate an action potential, demonstrating that a leak conductance decreased the excitability of SCG neurons.



Figure 34 – Leak conductances occluded weak nicotinic synapses. SCG neurons ($n = 17$) were stimulated with the periodic dynamic clamp template encoding for 1 primary ($3 \times \text{thresh-}g_{\text{syn}}$) and 8 secondary ($90\% \text{ thresh-}g_{\text{syn}}$) synapses. As the leak conductance increased, the secondary synaptic contribution to action potential firing decreased until it was almost completely blocked with a 20 nS leak.

3.4 DISCUSSION

In this chapter, we used Hodgkin’s classification of neuronal excitability to identify three classes of firing dynamics in SCG neurons. This result differs from previous *in vivo* reports where SCG neurons only displayed phasic firing dynamics (Weems and Szurszewski 1978; Galvan and Sedlmeir 1984; Wang and McKinnon 1995). To account for this disparity, we used dynamic

clamp to introduce shunt conductances to mimic the membrane leak caused by damage from sharp microelectrodes. We demonstrated that a small shunt conductance on the order of 3 nS can transform tonic firing into phasic firing. In addition, introduction of a virtual leak reduced the efficacy of subthreshold EPSPs thereby reducing synaptic gain. These findings indicate that the contribution of secondary synapses has been underestimated *in vivo* due to limitations imposed by microelectrode recording methods.

We first looked at the firing dynamics of SCG neurons because their properties may correlate with cell identity (Cassell, Clark et al. 1986). More than 85% of SCG neurons innervate three major targets (Gibbins 1995; Li and Horn 2006; Li and Horn 2008), all with different firing properties (Nishi and Koketsu 1960; Nja and Purves 1977; Macefield, Wallin et al. 1994; Macefield and Wallin 1996). Yet the firing dynamics of all paravertebral ganglionic neurons have been labeled as phasic (Weems and Szurszewski 1978; Galvan and Sedlmeir 1984; Wang and McKinnon 1995). Initial whole-cell recordings from neurons in culture displayed tonic firing (Figure 20), which was further supported by whole-cell recordings from intact tissue (Figure 21) suggesting that tonic firing is not an artifact of culturing. Tonic firing from cultured SCG neurons was previously observed in other studies (Jia, Bei et al. 2008; Luther and Birren 2009a). Here it was suggested that the membrane properties of intact ganglia may influence firing patterns, resulting in phasic firing (Luther and Birren 2009b). However, our results suggest that the recording method may have a greater influence on firing dynamics. Luther *et al.* (2009b) briefly mentioned that recording method may influence firing dynamics, but they did not investigate the issue further.

Before investigating how microelectrode damage changed firing, we wanted to have a method for classifying firing dynamics. Using Hodgkin's classification criteria (Hodgkin 1948;

Izhikevich 2007), we showed that SCG neurons displayed all three classes of firing dynamics (Figure 22). This is the first time that three different patterns of activity have been identified in mammalian SCG neurons. We further confirmed the three classes of dynamics with F-I relationships (Figure 23) and current ramp injections (Figure 24).

The separation of firing dynamics into three classes may provide insight into the repertoire of ion channels expressed by these neurons. In lamina I neurons, different classes of excitability result from the differential expression of underlying subthreshold currents (Prescott, De Koninck et al. 2008). Class 3 neurons do not fire action potentials in response to current ramps because these neurons express a persistent K^+ current or fast inactivating transient Na^+ current, which has enough time to inactivate during the slow current ramp (Izhikevich 2007). By using a fast current injection, such as a voltage step, the inward current overpowers the slow activating outward K^+ current or fast inactivating Na^+ current thus firing an action potential (Izhikevich 2007; Prescott, De Koninck et al. 2008).

Class 1 neurons may express an A-type K^+ conductance, which has been shown to account for the continuous F-I relationship by facilitating the rise time of the membrane voltage between action potentials (Connor and Stevens 1971; Yu, Sejnowski et al. 2011). Class 1 and class 2 behaviors have been modeled by varying the membrane density of voltage-gated K^+ and Na^+ channels (Zeberg, Blomberg et al. 2010). Models with high Na^+ and low K^+ channel density exhibited class 1 dynamics while models with higher K^+ channel density generated class 2 dynamics (Zeberg, Blomberg et al. 2010). Distinguishing the firing class of SCG neurons could help to correlate ion channel expression with cell type (St-Hilaire and Longtin 2004; Prescott, De Koninck et al. 2008). Additional voltage-clamp studies would be required to correlate firing dynamics with ion channel density.

Aside from thresh- g_{syn} , no other electrophysiological properties were different between classes (Figure 25). However, a difference in thresh- g_{syn} may also suggest the differential expression of ion channels. A previous study in paravertebral neurons showed that phasic neurons have a larger M-current (Wang and McKinnon 1995). Since M-current acts as a membrane voltage buffer to prevent or limit action potential firing, a neuron with a larger M-current would require a larger stimulus to overcome the buffer and fire an action potential. Class 3 neurons have a higher thresh- g_{syn} and therefore suggest a larger M-current. KCNQ channels, which are responsible for M-current, activate at about -60 mV. The outward K^+ efflux increases as the neuron depolarizes, thus stabilizing the membrane potential against depolarization (Brown and Passmore 2009). The relationship between firing dynamics, channel expression, and cell type is still unknown within the SCG. A recent transgenic mouse model will allow vasomotor neurons to be isolated to study firing dynamics and other gating properties in an identified cell type (see [Future Experiments](#)). However, this chapter focused on the discrepancies of firing dynamics between *in vivo* and *in vitro* recordings, in the context of how recording method influenced synaptic gain.

We wanted to understand the propensity for a neuron to integrate subthreshold signals (Izhikevich 2007). By using a ZAP current, we showed that all three classes of neurons act as integrators (Figure 26), which means they are able to summate subthreshold signals (Figure 27), and it is not required for activity to be at a resonant frequency to permit integration. A shorter distance between subthreshold EPSPs raises the probability of action potential firing (Prescott, De Koninck et al. 2008), because the voltage response to stimulation increases monotonically with increasing input frequency (Prescott and Sejnowski 2008). In contrast, increasing the frequency of stimulation in resonator neurons can delay or even terminate action potential firing

(Izhikevich 2007; Prescott, De Koninck et al. 2008). Since these neurons are integrator neurons, they support the dynamic clamp experiments, which demonstrated that SCG neurons act as variable amplifiers of presynaptic activity. Therefore, we used dynamic clamp to test the summation of subthreshold EPSPs in response to small shunt conductances.

We introduced a non-depolarizing shunt conductance to mimic membrane damage caused by sharp microelectrodes. The leak caused tonic neurons to fire in a phasic manner (Figure 28A), and linearized the I-V relationship (Figure 28B) thus reducing R_{input} (Figure 29) to values similar to *in vivo* SCG recordings (Weems and Szurszewski 1978; Galvan and Sedlmeir 1984; Wang and McKinnon 1995). The shunting effect caused by microelectrodes was originally studied in a model for frog embryonic neurons (Kobori, Harrison-Bernard et al. 2001; Ratte, Prescott et al. 2008). Shunting the input resistance from 1 G Ω to 200 M Ω lowered excitability and prevented repetitive firing (Kobori, Harrison-Bernard et al. 2001). Studies in the spinal cord of frog tadpoles investigated the effect of sharp electrodes with simultaneous recordings, where a neuron was patched prior to sharp electrode impalement (Karpuk and Hayar 2008). It was observed that microelectrode impalement significantly depolarized the resting membrane potential, similar to our observations (Figure 30). Additionally, there was about a 30% decrease in R_{input} upon impalement (Karpuk and Hayar 2008). However, shunting studies in frog spinal neurons does not allude to the effect of microelectrode damage on signaling in postganglionic neurons. By studying postganglionic neurons, we showed the consequence for reduced excitability in that the efficacy for subthreshold signaling is reduced or blocked.

We also showed that inherent membrane damage, which produces a phasic response, can be compensated with an anti-leak conductance to restore the neuron to a repetitive firing state (Figure 31, cell 2). Evidence for this was also presented in simultaneous recordings with patch

and microelectrodes in frog spinal neurons (Karpuk and Hayar 2008). By removing the sharp electrode, the R_{input} recovered to about 90% of the pre-impalement measurement (Karpuk and Hayar 2008). Together, this would suggest that compensation of the leak, whether by anti-leak conductances or sharp electrode removal, can restore membrane and firing properties to pre-leak levels. However, the anti-leak conductance does not convert every class 3 neuron to tonic firing. Like genuine phasic neurons (Gibbins 1995), even large current injections, in conjunction with anti-leak conductances, will not produce repetitive firing (Figure 32). These results demonstrate that damage, caused by sharp microelectrodes, reduces neuronal excitability. Therefore, we used dynamic clamp to investigate disparities in the strength of postganglionic synapses.

Conflicts have arisen pertaining to the nature of synaptic innervation in the SCG. Are postganglionic neurons innervated exclusively by primary synapses (McIntosh 1940; Macefield, Wallin et al. 1994; Macefield and Wallin 1996; Macefield, Rundqvist et al. 1999; Macefield, Elam et al. 2002; McLachlan 2003; Macefield and Elam 2004; Macefield 2011) or do they follow $n + 1$ convergence (Karila and Horn 2000; Wheeler, Kullmann et al. 2004; Horn and Kullmann 2007; Bratton, Davies et al. 2010; Rimmer and Horn 2010)? By stimulating neurons with EPSP waveforms of increasing amplitude, we were able to show that a leak reduces the efficacy of EPSPs (Figure 33). The leak conductance inhibits the ability of weak synaptic inputs to effectively summate and reach action potential threshold. Furthermore, the faster membrane time constant (Figure 28C), caused by a leak conductance, will speed up EPSP decay, thereby decreasing the time window during which effective summation can occur. With patterns of synaptic activity, we showed that leak conductances significantly reduced the number of action potentials generated by secondary synapses (Figure 34) demonstrating that the reduction in EPSP efficacy results in less synaptic amplification.

The results of this chapter suggest that the contribution of weak synapses on postsynaptic firing have been underestimated *in vivo*. This is a result of the use of sharp microelectrodes, which introduce leak conductances through membrane damage. This leak prevents neurons from firing repetitively and reduces the efficacy of fast nicotinic EPSPs, and thus led to reduced summation of weak nicotinic synapses and reduced synaptic gain. This chapter also reveals the potential role that metabotropic factors, which modulate small leak conductances, could have by significantly influencing firing dynamics and synaptic transmission. The potential effects of metabotropic stimulation could meaningfully alter firing dynamics or the excitability of sympathetic neurons.

3.4.1 Future Experiments

Whole-cell recordings taken from intact SCG neurons suggest that culturing does not change firing dynamics. However, it does not rule out other potential changes that could occur during the culturing process. The transgenic mouse model, B6.FVB-Tg(Npy-hrGFP)1Lowl/J (The Jackson Laboratory, Strain # 006417, Bar Harbor, ME) could be used to test if other intrinsic properties are changing during culturing. This mouse model has a fluorescently tagged NPY protein, which would label NPY⁺ vasomotor neurons. SCG tissue was previously obtained from this mouse model and NPY antibody staining of slices showed co-localization with the fluorescent tag (data not shown). Utilizing this model would allow one to record from a NPY⁺ neuron, in intact tissue, and compare the electrophysiological profile to a NPY⁺ neuron in culture. Whole-cell current clamp experiments could also be used to compare firing dynamics between *in vivo* and *in vitro* SCG neurons. In addition, voltage clamp could be used to determine

if culturing changes ion channel expression. Recording from only NPY⁺ positive neurons would ensure that the same cell type was studied in each experiment.

Additionally, correlations could be generated between strength and number of preganglionic inputs and firing dynamics and excitability. Neurons that fire in a phasic manner were thought to receive one or a few suprathreshold inputs and function as a relay (Wang and McKinnon 1995). It is possible that phasic neurons only receive suprathreshold inputs. However, it is more probable that these neurons have secondary synapses, but their reduced excitability (high thresh- g_{syn}) makes secondary synapses harder to detect. This could be evaluated by recording from NPY⁺ neurons in intact tissue using a whole-cell configuration to measure firing dynamics. Direct nerve stimulation could then be used to isolate secondary EPSPs so the number and strength of secondary synapses can be correlated to firing dynamics. Choosing only NPY⁺ neurons would ensure that vasomotor neurons are recorded in each situation.

Other SCG cell types could be labeled by using a retrograde tracing technique. Injecting tracer into salivary glands and subcutaneous tissue would back label secretomotor and pilomotor neurons respectively. Performing the same experiments as suggested on NPY⁺ neurons would provide a comprehensive profile of the major SCG cell types, describe firing dynamics from neurons *in vivo* and *in vitro*, and correlate firing dynamics to the number and strength of secondary inputs, thereby providing a better understanding of phenotypic specialization.

4.0 ANGIOTENSIN II ENHANCES SYNAPTIC GAIN

4.1 INTRODUCTION

In the previous chapters, we discussed how periodicity increased synaptic amplification and examined the role of secondary synapses in regulating amplification in the SCG. The SCG expresses several excitatory GPCRs (Table 1), whereupon activation will increase neuronal excitability and therefore synaptic amplification. Here we focus on the AngII AT₁ receptor, because AngII-induced hypertension can develop through sympathetic hyperactivity (Malpas 2010; Parati and Esler 2012). AT₁ receptor blockers are common drugs prescribed to combat hypertension by preventing AngII binding. We hypothesize that AngII acts directly on the SCG to increase excitability and synaptic gain, suggesting that the SCG may be a potential target for future therapeutic treatments of AngII-induced hypertension.

AngII is an octapeptide hormone that is part of the renin-angiotensin system (RAS) and regulates blood pressure and fluid homeostasis (Hunyady and Catt 2006). AngII is formed through a series of enzymatic steps (Figure 35). Angiotensinogen is released from the liver and is cleaved by the renal enzyme renin, released by the juxtaglomerular apparatus, to produce angiotensin I (Reid 1992). This is the rate limiting step of the RAS due to its hydrolytic activity (Savoia, Burger et al. 2011). Angiotensin converting enzyme (ACE) further cleaves angiotensin I to form AngII. The RAS is an endocrine system that plays an important role in the physiological

regulation of cardiovascular, renal, and sympathetic activity (Reid 1992; Wang, Slembrouck et al. 1996; Hunyady and Catt 2006). The RAS also plays a key role in salt and water homeostasis, the modulation of vascular tone, and can facilitate the development of hypertension and other cardiovascular disorders (Reid 1992).

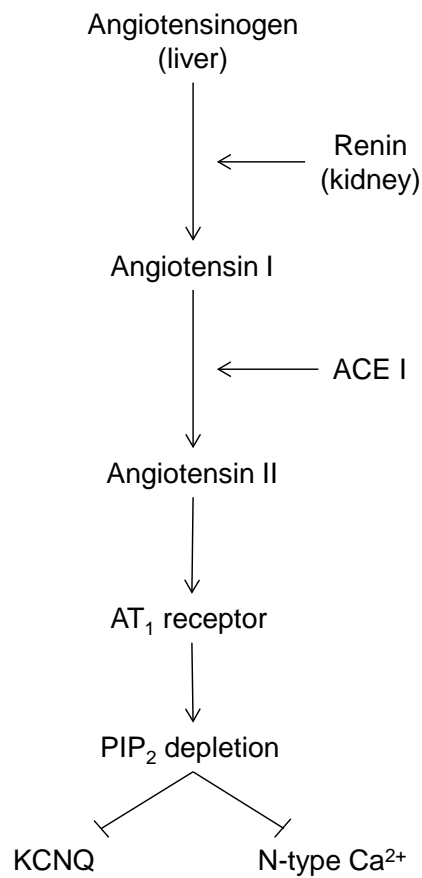


Figure 35 - The renin-angiotensin pathway. Production of AngII results in KCNQ and N-type Ca²⁺ channel inhibition.

The AT₁ receptor signals primarily through G_{q/11} proteins, but also through G_i and G_{12/13} proteins (Savoia, Burger et al. 2011). In SCG neurons, AngII inhibits KCNQ and N-type Ca²⁺ channels through phosphatidylinositol 4,5-bisphosphate (PIP₂) depletion (Shapiro, Wollmuth et al. 1994; Acosta, Mendoza et al. 2007; Zaika, Zhang et al. 2011). AngII activated phospholipase C cleaves PIP₂ to inositol triphosphate (IP₃) and diacylglycerol (DAG), which depletes PIP₂ concentration (Shapiro, Wollmuth et al. 1994). These channels require a functional PIP₂ to be active and thus global depletion leads to channel inhibition (Hernandez, Zaika et al. 2008). KCNQ and N-type Ca²⁺ channel inhibition increases sympathetic activity and therefore leads to smooth muscle contraction, which increases vascular resistance (Wynne, Chiao et al. 2009). DAG also mediates smooth muscle contraction through protein kinase C (PKC) activation. PKC directly phosphorylates myosin light chain kinase, which phosphorylates myosin light chain, and promotes smooth muscle contraction (Wynne, Chiao et al. 2009). AngII also regulates kidney activity as well as renal sodium and water reabsorption (Lavoie and Sigmund 2003).

Circulating levels of AngII are generally low (10 – 50 pM) (Hunyady and Catt 2006). However, local AngII concentration may be much higher due to tissue localized RAS. Tissue RAS occurs in any tissue that has the capacity for both the generation, and action, of AngII (Lavoie and Sigmund 2003). Tissue based RAS is independently controlled from circulating RAS (Savoia, Burger et al. 2011), but pathway components from local RAS will facilitate global AngII accumulation (Hunyady and Catt 2006). Local RAS has been found in several tissues including the brain, heart, adrenal glands, and kidney (Lavoie and Sigmund 2003), but not every factor of the RAS is synthesized locally in these tissues. For example, expression of some

constituents, specifically ACE I, will facilitate AngII formation. There is also evidence of tissue RAS in the SCG. *In situ* hybridization and antibody studies of fetal pigs showed that angiotensinogen, renin, and AngII are synthesized in SCG neurons (Wang, Slembrouck et al. 1996; Kushiku, Yamada et al. 2001). Tissue RAS as a pharmacological target also has clinical implications. The antihypertensive action of ACE inhibitors can have a greater therapeutic effect by inhibiting tissue-based ACE in addition to circulating plasma ACE. Additionally, some hypertensive patients have normal, or even low, levels of systemic RAS, but inhibitors will still be administered to control tissue RAS activity (Lavoie and Sigmund 2003).

Elevated AngII is a causative factor in about 25% of hypertensive patients (Malpas 2010). Obesity also facilitates AngII-induced hypertension because elevated levels of plasma renin activity, plasma angiotensinogen, and circulating AngII are linked to obesity (Kotsis, Stabouli et al. 2010; Ruster and Wolf 2013). In addition, adipose tissue can have a direct effect on AngII elevation because all components of the RAS are formed in adipose tissue – renin, angiotensinogen, AngII, and AngII receptors are all abundant in fat cells (Kotsis, Stabouli et al. 2010; Ruster and Wolf 2013). Since tissue RAS and circulating RAS are in constant interaction, RAS elements produced in adipose tissue can leach into the circulation, which induces vasoconstriction and increases blood pressure (Kotsis, Stabouli et al. 2010).

In addition to its vasoconstrictive actions, AngII can also transactivate growth factors, promote reactive oxygen species (ROS) formation, and activate other proinflammatory responses (Malpas 2010). AngII activates protein tyrosine kinases, serine/threonine kinases, and increases production of vasoactive hormones such as endothelin-1 and transforming growth factor (Kimura and Eguchi 2009; Savoia, Burger et al. 2011). AngII can also activate the transcription factors NF- κ B and activator protein 1 (AP-1) to orchestrate the upregulation of AT₁ receptor

expression and of other genes correlated with clinical manifestations of disease (Mitra, Gao et al. 2010).

AngII-induced ROS production occurs through the upregulation and activation of NADPH oxidase (Hunyady and Catt 2006; Sachse and Wolf 2007; Savoia, Burger et al. 2011). ROS production is an important factor of the proinflammatory actions of AngII (Hunyady and Catt 2006) and can lead to endothelial cell apoptosis (Watanabe, Barker et al. 2005), endothelial dysfunction, angiogenesis, and vascular and cardiac remodeling during hypertension (Hunyady and Catt 2006). AngII stimulates vascular endothelial growth factor release to induce proliferation and promote cell growth (Bader, Peters et al. 2001; Imanishi, Hano et al. 2004; Hunyady and Catt 2006). This recruits proinflammatory molecules to vessel walls, which, in combination with ROS production, induces vascular remodeling during hypertension (Savoia, Burger et al. 2011).

AngII induced proinflammatory upregulation is a consequence of increased vascular resistance and blood pressure. AngII enhances sympathetic tone by activating the sympathetic nervous system (Kushiku, Yamada et al. 2001; Dendorfer, Thornagel et al. 2002; Lavoie and Sigmund 2003). In the central nervous system, circulating or locally produced AngII increases sympathetic tone. In peripheral nerves, the termini of adrenergic neurons have prejunctional AT₁ receptors where AngII enhances catecholamine discharge, which accounts for the excess norepinephrine spillover observed in hypertensive individuals (Dendorfer, Thornagel et al. 2002). AngII can act directly on and stimulate SCG postganglionic neurons (Kushiku, Yamada et al. 2001) and facilitate norepinephrine release from presynaptic nerve terminals in the SCG (Reid 1992; Dendorfer, Thornagel et al. 2002). Since we have shown that postganglionic neurons can generate more than half of its postganglionic output, the SCG becomes an important target for

the study of AngII-induced changes in sympathetic activity and is a potential target for blood pressure regulation. **We hypothesize that stimulation of postganglionic neurons with AngII increases excitability, thereby increasing postganglionic amplification.** To test this hypothesis, we looked for evidence of local RAS elements and used dynamic clamp to assess AngII mediated effects on synaptic amplification.

4.2 METHODS

4.2.1 mRNA Extraction and RT-PCR

Procedures for dissecting the SCG were as those outlined in [Chapter 3.2.4](#). Once removed, the SCG was isolated from the surrounding tissue and desheathed. mRNA was extracted with the Rneasy Micro Kit (Qiagen, Hilden, Germany) and quantified with UV spectroscopy. cDNA was synthesized using the RT² First Strand Kit (Qiagen, Hilden, Germany). Each 25 μ l RT-PCR reaction contained a final concentration of 50 μ M dNTP, 80 pM forward and reverse primers (Table 5), 1x PCR buffer, 1.25 U Taq polymerase and 250 ng cDNA. The PCR reaction was performed using 30 cycles of 30 sec at 94°C, 45 sec at 60°C, and 90 sec at 72°C with a final 7 min extension at 72°C. PCR products were isolated on a 2% agarose gel containing ethidium bromide. Bands on gels were visualized with a Kodak EDAS 290 camera positioned above a UV box and photographed using the Carestream MI SE software (Kodak, Rochester, NY).

Positive bands were removed from the gel with a scalpel and the DNA was extracted using the Min Elute Gel Extraction Kit (Qiagen, Hilden, Germany). The extracted products were sequenced using the Genomics and Proteomics Core Laboratories of the University of

Pittsburgh, following their protocol for sample preparation. Sequences were analyzed with ChromasPro (Technelysium, South Brisbane, Australia) and products were verified using manual sequence comparison and BLAST queries (NCBI).

Table 5 – Primer pairs for RT-PCR analysis

Gene Name	Forward Primer	Reverse Primer
Angiotensinogen	5'-TTCAGGCCAAGACCTCCC-3'	5'-CCAGCCGGGAGGTGCAGT-3'
Renin	5'-CGGTGGTCCTCACCAACT-3'	5'-GCCCATGCCCAGACCCCC-3'
ACE I	5'-CCTGATCAACCAGGAGTTTGCAGAG-3'	5'-GCCAGCCTTCCCAGGCAAACAGCAC-3'
ACE II	5'-TTAAGCCACCTTACGAGCCT-3'	5'-TCCCAGTGACGATCAGGATA-3'
MAS	5'-TTGTGGGCACGCAGTAAGAAG-3'	5'-GATACAGTGTTGCCATTGCC-3'
AT _{1A} R	5'-CGTCATCCATGACTGTAAAATTTC-3'	5'-GGGCATTACATTGCCAGTGTG-3'
AT _{1B} R	5'-CATTATCCGTGACTGTGAAATTG-3'	5'-GCTGCTTAGCCCAAATGGTCC-3'
Actin	5'-TGTCACCAACTGGGACGATA-3'	5'-AGGAAGGAAGGCTGGAAGAG-3'
NPY	5'-TACTCCGCTCTGCGACACTA-3'	5'-GGGTCTTCAAGCCTTGTCT-3'

4.2.2 SCG Primary Cell Culture

The protocol for SCG dissection and dissociation is outlined in [Chapter 2.2.1](#).

4.2.3 Whole-cell Current Clamp Recording

The recipes for solutions and procedures to perform whole-cell recordings are found in [Chapter 2.2.2](#).

AngII experiments were conducted by adding 50 nM AngII (Sigma-Aldrich, St. Louis, MO) to the external Ringer's solution and bath applying it to the dissociated neurons in the recording chamber.

4.2.4 Dynamic Clamp

The equation to implement virtual nicotinic synapses and procedures to develop templates of synaptic activity are described in [Chapter 2.2.5](#).

4.3 RESULTS

4.3.1 SCG Neurons Contain a Subset of RAS Elements

Initial experiments were designed to determine if any elements of the RAS machinery were expressed in the adult rat SCG. Whole SCG tissue was isolated from adult rats and mRNA was extracted, reverse transcribed, and PCR tested for tissue specific RAS elements. ACE I, the MAS receptor, and both AT₁ receptors were identified in the SCG (Figure 36). The MAS receptor binds angiotensin 1-7, which is a product of AngII cleavage by ACE II, and elicits actions that

oppose AngII (Savoia, Burger et al. 2011). Since the MAS receptor was present, but ACE II was not, we assumed that angiotensin 1-7 is not produced in the SCG. Actin and NPY were used as positive controls. Visualized bands were excised and the DNA product was extracted and used for sequencing to confirm the identity of each band.

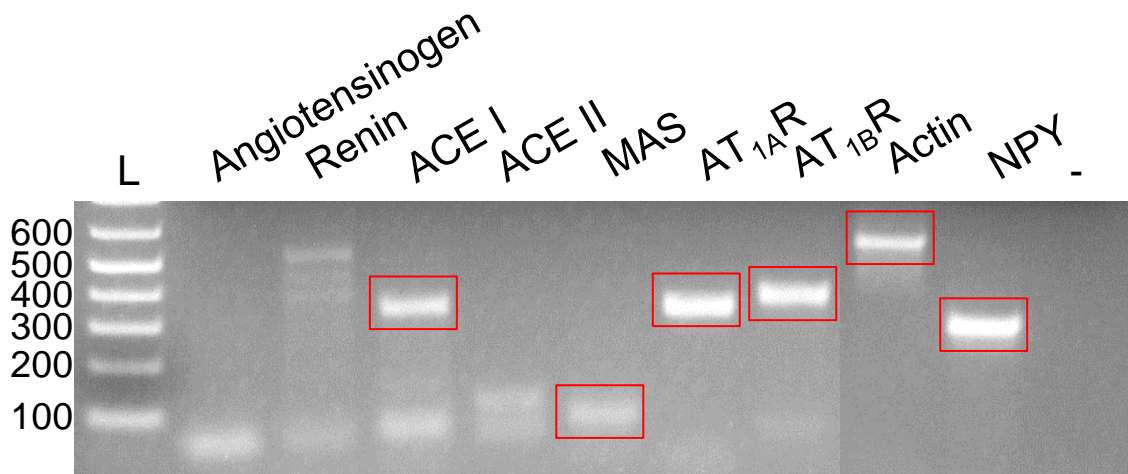


Figure 36 – RT-PCR of RAS elements in SCG neurons. Various RAS elements were probed using RT-PCR in SCG neurons. ACE I, the MAS receptor, and both AT₁ receptors were identified. Products were extracted to confirm with DNA sequencing.

4.3.2 AngII Increased Excitability and Synaptic Gain

Since AngII acts directly on SCG neurons to inhibit KCNQ and N-type Ca^{2+} channels (Shapiro, Wollmuth et al. 1994), we wanted to determine if this inhibition was sufficient to increase excitability and modulate synaptic gain. Dissociated neurons ($n = 6$) from 2 – 5 day old cultures were recorded under whole-cell configuration at room temperature using dynamic clamp to measure $\text{thresh-g}_{\text{syn}}$ and monitor AngII-induced changes in excitability. To measure excitability, I-V curves were constructed by injecting cells with 30 pA current steps ranging from -240 to 240 pA. Bath application of 50 nM AngII increased the spike output of the voltage response to the depolarizing current injections (Figure 37A) and shifted the I-V curve to the right due to depolarization (Figure 37B). In each of the 6 neurons, the action potential output increased with AngII, regardless of the firing dynamics before AngII application. About 1 min post AngII wash in, $\text{thresh-g}_{\text{syn}}$ rapidly decreased, and V_{rest} depolarized (Figure 38). AngII blocks KCNQ M-type K^+ channels, which act as a depolarization buffer. As a neuron depolarizes, M-current will act as a buffer to prevent depolarization. Reducing M-current will increase excitability. The increased spike output and rapid decrease in $\text{thresh-g}_{\text{syn}}$ suggest an AngII-mediated increase in neuronal excitability.

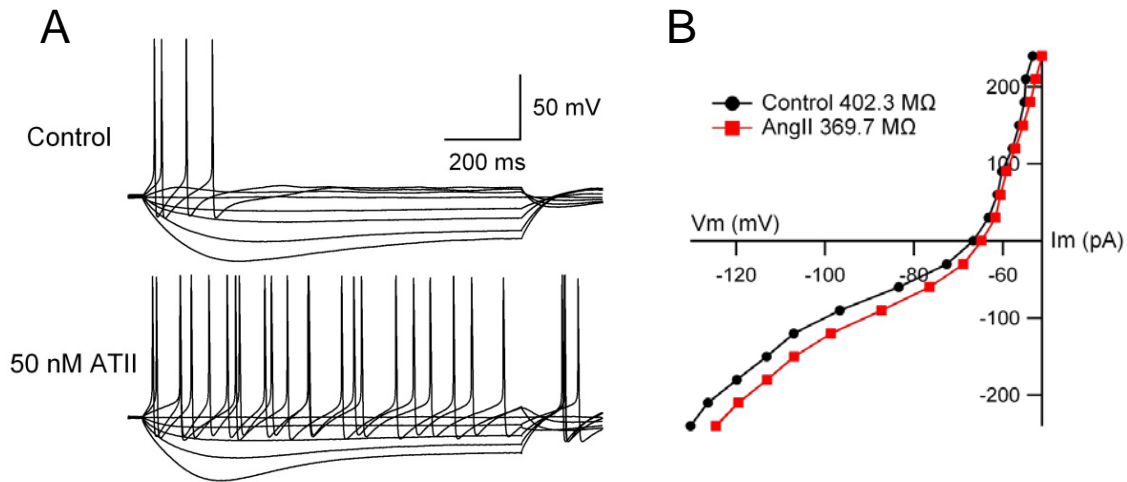


Figure 37 – AngII increased action potential output. Neurons were stimulated with 30 pA current steps ranging from -240 to 240 pA. (A) The bath applied AngII increased the action potential response to the depolarizing current pulses, demonstrating an AngII-mediated increase in excitability. (B) The I-V curve shifted to the right due to membrane depolarization.

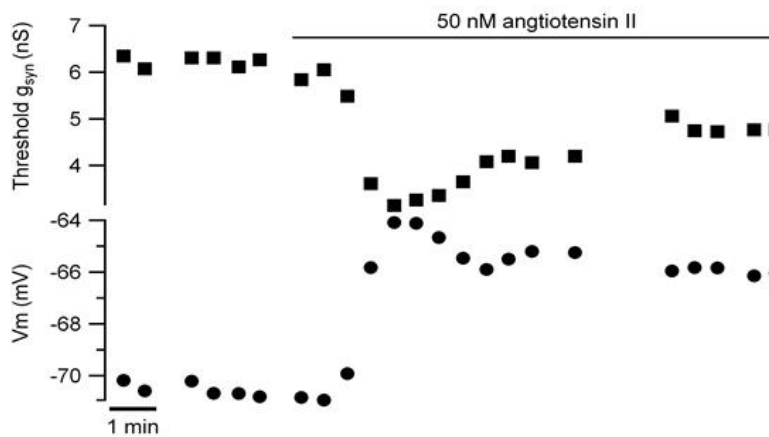


Figure 38 – AngII decreased thresh- g_{syn} and depolarized V_{rest} . Thresh- g_{syn} and V_{rest} were monitored during AngII application. About 1 minute post AngII, there was a rapid decrease in thresh- g_{syn} and a depolarization of V_{rest} . The decrease in thresh- g_{syn} demonstrates how AngII increases neuronal excitability.

We then designed experiments using dynamic clamp to test the effect of AngII on synaptic amplification and gain. A 1 Hz periodic dynamic clamp template that encoded for 1 primary synapse ($3\times \text{thresh-g}_{\text{syn}}$) and 6 secondary synapses ($60\% \text{ thresh-g}_{\text{syn}}$) was used to stimulate neurons and measure gain. Pre-AngII, there was a modest amount of amplification and neurons exhibited a synaptic gain of 1.50 ± 0.07 ($n = 6$). Bath application of 50 nM AngII significantly increased subthreshold EPSP summation, which increased synaptic gain to 2.17 ± 0.08 (Figure 39, $P < 0.001$, paired t-test). Group data revealed there was no significant change in R_{input} ($P > 0.05$, paired t-test), but there was a significant decrease in τ in the presence of AngII (control: 25.85 ± 1.42 ms; AngII: 24.08 ± 1.29 ms, $P < 0.05$, paired t-test). AngII caused significant membrane depolarization (-72.4 ± 1.6 mV to -68.7 ± 2.3 mV, $P < 0.01$, paired t-test) and a large decrease in $\text{thresh-g}_{\text{syn}}$ (6.19 ± 0.78 nS to 2.17 ± 0.08 nS, $P < 0.001$, paired t-test), which resulted in the significant increase in synaptic gain (Figure 40).

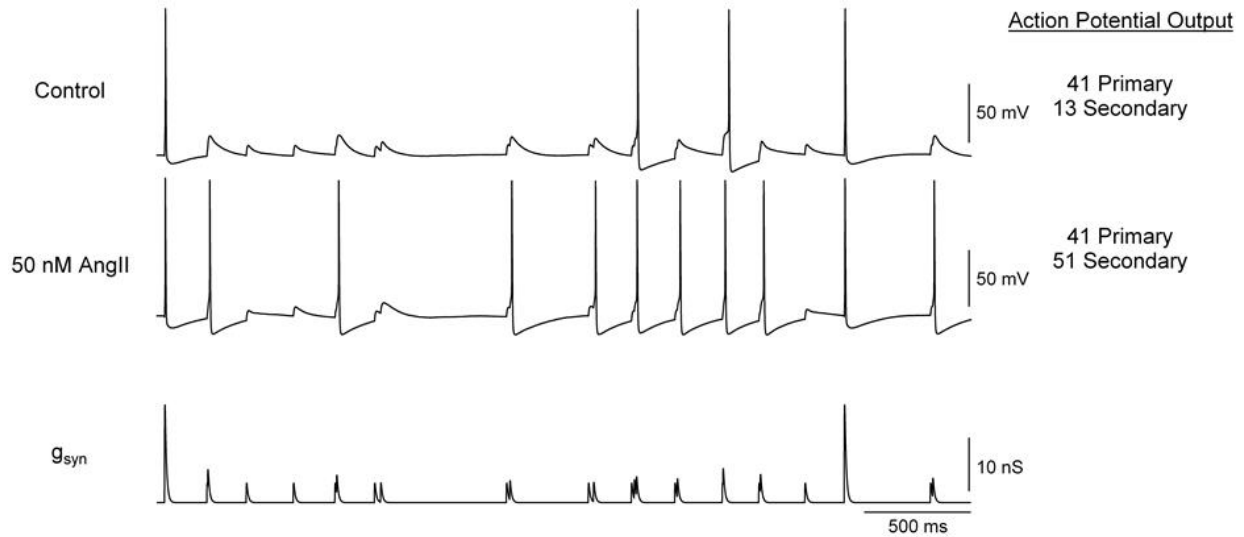


Figure 39 – AngII increased sympathetic output and synaptic gain. Neurons were stimulated with a 1 Hz periodic dynamic clamp template encoding for 1 primary ($3 \times \text{thresh-}g_{\text{syn}}$) and 6 secondary ($60\% \text{ thresh-}g_{\text{syn}}$) synapses. Bath application of AngII significantly increased the number of action potentials generated by secondary synapses. This shows that the AngII-induced increase in excitability will make it easier for subthreshold EPSPs to summate and fire action potentials thus increasing synaptic gain.

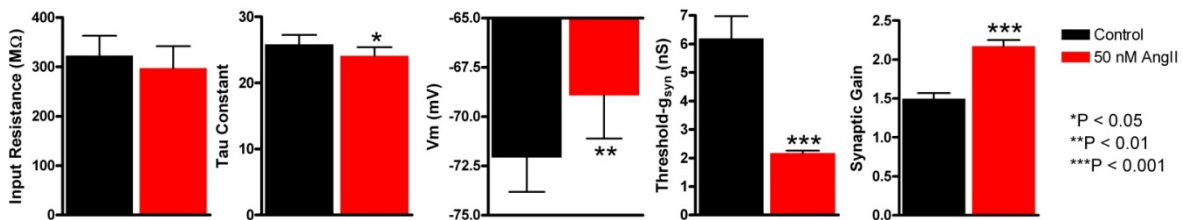


Figure 40 – AngII effects on electrophysiological properties. Various electrophysiological characteristics of SCG neurons ($n = 6$) were measured in the absence and presence of bath applied AngII. AngII did not change R_{input} , but did significantly reduce τ . There was also a significant AngII induced depolarization and $\text{thresh-}g_{\text{syn}}$ significantly decreased with AngII, which led to a large increase in synaptic gain.

4.4 DISCUSSION

The goal of this chapter was to evaluate the effect of AngII on ganglionic amplification in SCG neurons and determine if any elements of the RAS machinery were present in SCG tissue. It was previously shown that SCG neurons express AT₁ receptors and that AngII can act directly on postganglionic neurons (Kushiku, Yamada et al. 2001). Additionally, the mechanism of AngII mediated KCNQ and N-type Ca²⁺ channel inhibition has been evaluated in sympathetic neurons (Shapiro, Wollmuth et al. 1994; Zaika, Zhang et al. 2011). We provide evidence of elements of a local RAS in adult rat SCG neurons and analyze the activity of AngII in terms of ganglionic amplification, to emphasize a potential role of the SCG in AngII induced hypertension.

RT-PCR analysis showed that ACE I, the MAS receptor, and the AT_{1A} and AT_{1B} receptors are expressed in SCG tissue. These results do not agree with the immunohistological studies on fetal pig SCG neurons where angiotensinogen and renin were identified (Wang, Slembrouck et al. 1996). Though many signaling pathways and mechanisms are preserved across mammalian species, different speciation could account for the differential expression of angiotensinogen and renin. Additionally, experiments in pig neurons were performed during the fetal stage (Wang, Slembrouck et al. 1996) while the current RT-PCR experiments were performed on SCG tissue from adult animals. Birth and development may also account for differential expression of these RAS elements. This differential expression was observed with the AngII receptor subtype. The AT₂ receptor is the primary AngII receptor in fetal rats. This

quickly changes after birth when the AT₁ receptor becomes the dominant isoform (Savoia, Burger et al. 2011). The same could be true for angiotensinogen and renin. Additional evidence for age related changes have been identified in the liver, where angiotensinogen expression decreases as the animal ages (van Esch, Gembardt et al. 2010).

To test for the differential expression of angiotensinogen and renin, one could perform RT-PCR experiments on fetal rats or perform *in situ* hybridization experiments on fetal rat and pup SCG cultures. This would compare mRNA expression of RAS elements to determine if expression changes after birth. It could also be determined whether chronic AngII affects the expression levels of tissue RAS elements. There is evidence that chronic AngII mediates the upregulation of AT₁ receptors in CATH.a neurons (Mitra, Gao et al. 2010) and renal angiotensinogen (Kobori, Harrison-Bernard et al. 2001), but chronic AngII effects have never been explored in SCG neurons. Osmotic minipumps could administer long term AngII to create an AngII hypertensive rat model (Rajagopalan, Kurz et al. 1996). Quantitative RT-PCR (qPCR) in the SCG would allow one to compare expression levels of RAS elements in sham and AngII hypertensive models to determine the differential expression of any RAS elements.

The results from this chapter suggest that some elements of the RAS machinery are not made in SCG neurons. Does this mean that AngII concentration could never be high enough to modulate excitability and synaptic gain in SCG neurons? Circulating levels of AngII range from 10 to 50 pM, depending on the subject's diet and hypertensive state (Hunyady and Catt 2006). The half-life of circulating AngII ranges from 15 – 30 seconds (van Kats, de Lannoy et al. 1997; van Esch, Gembardt et al. 2010). This concentration is probably insufficient to elicit any measurable effects on excitability or synaptic gain. Without a fully functional RAS, SCG neurons cannot produce AngII from angiotensinogen. However, the activity of ACE I may be

sufficient to produce AngII-induced effects in the SCG. Circulating levels of angiotensin I range from 9.3 pM to 1.5 nM (Hunyady and Catt 2006). ACE I would convert angiotensin I to AngII directly in the SCG. Once AngII binds the AT₁ receptor, the half-life of AngII increases 20 – 30 fold to about 15 min (van Kats, de Lannoy et al. 1997). This allows tissue AngII levels to exceed the circulating AngII concentration (van Esch, Gemhardt et al. 2010). Accumulated tissue AngII, in combination with circulating angiotensin I and tissue ACE I, could generate enough AngII to elicit a physiological effect in the SCG.

Regulation of blood pressure and AngII-induced hypertension is typically thought to be a consequence of AngII mediated effects on sodium and water reabsorption in the kidney (Berne 1986; Wesson 2001; Hall 2011b; Stolarz-Skrzypek, Bednarski et al. 2013). The results of this chapter suggest that the SCG cannot be overlooked as a potential AngII-sensitive regulator of blood pressure. With postganglionic convergence and direct AngII activity, SCG neurons have the potential to significantly regulate postganglionic activity, vascular tone, and blood pressure.

5.0 CONCLUSION

The goal of this thesis was to use temporal patterns of synaptic activity to assess the ability of mammalian sympathetic neurons in the SCG to behave as variable amplifiers of presynaptic activity. With dynamic clamp, we created virtual nicotinic synapses, which were used to demonstrate how rhythmic entrainment of preganglionic activity can enhance synaptic gain. Furthermore, we showed that a model incorporating secondary synapses could replicate the timing and statistics of human sympathetic data. We also examined the intrinsic excitability of SCG neurons by introducing a leak conductance and determined that the input of secondary synapses has been underestimated *in vivo* due to membrane damage caused by microelectrodes. Finally, we showed how AngII acts directly on SCG neurons to increase excitability and gain, marking the SCG as a potential target for future therapeutic studies.

The results from this work show that SCG neurons are not simply relays of activity, but instead can act as integrative centers that can more than double presynaptic activity. SCG neurons have three classes of firing dynamics, which opposes previous claims that all paravertebral sympathetic neurons are phasic (Weems and Szurszewski 1978; Galvan and Sedlmeir 1984; Cassell, Clark et al. 1986; Wang and McKinnon 1995). These inconsistencies arise because of membrane damage caused by sharp microelectrodes used during *in vivo* recordings. Tonic firing is not an artifact of cell culture because whole-cell recordings from intact ganglia showed similar firing dynamic as *in vitro* recordings. Mimicking cellular damage

with a leak conductance resulted in the loss of tonic firing dynamics. Likewise, virtual leak conductances occluded weak nicotinic synapses and reduced synaptic gain, thus explaining how the contribution of secondary synapses was underestimated *in vivo*.

We also laid the foundation for a model that can replicate the bursting pattern of human sympathetic recordings by incorporating secondary synapses. The model not only reproduced the statistics of human data, but also was able to generate gain. This suggests that the regulation of synaptic amplification by secondary synapses may play a significant role in human ganglionic transmission.

Finally, we showed how AngII increased neuronal excitability, resulting in an increase in synaptic gain. RT-PCR analysis revealed that the SCG expresses ACE I, the MAS, AT_{1A}, and AT_{1B} receptors. Despite lacking the full RAS machinery, ACE I may be sufficient to elevate AngII concentration to a physiological level. The membrane effects of AngII also suggest that other metabotropic factors, which may modulate small leak conductances, could significantly influence firing dynamics and synaptic gain. This makes SCG neurons a potential therapeutic target for blood pressure regulation in AngII-induced hypertension.

It is conceivable that cell type correlates with a class of excitability and ion channel and GPCR density. Elucidating these patterns would provide information about phenotypic specialization. Further refinement of the human data model is required to eliminate the steps in the cumulative ISI exponential distribution. Calculating the timing of events based on the probability of firing during a specific time point of the cardiac cycle may help to smooth the stepping created by quiescent time intervals.

The results presented herein help to broaden our view of the role of the SCG. Previously it was thought that the SCG acts as a waypoint for presynaptic activity where it is sorted and sent

to the proper end organs. However, these studies show that much more is occurring in the ganglia than originally believed. Importantly, this has implications for barosensitive neurons and the regulation of blood pressure. The central sympathetic control of blood pressure begins in the brain, where the hypothalamus, nucleus solitary tract, and rostral ventrolateral medulla can modulate blood pressure (Guyenet 2006). However, once that information exits the spinal cord, it goes through sympathetic ganglia to get to the heart, arterioles or kidneys. Since the SCG can generate synaptic gain, it becomes an important target for the control and regulation of blood pressure. The kidneys are typically thought to be the major modulator in blood pressure control, but the work described in this thesis suggests that ganglia may also play a significant role in blood pressure regulation.

Although data presented in the previous chapters argues against conclusions drawn in previous examinations of SCG firing dynamics and signal transduction, we cannot disregard those studies. Neurobiology in general and the concepts regarding ganglionic function in particular, would not be as developed had it not been for the previous work by Langley, Feldberg, Dale, Eccles, and Skok. The work presented here illuminates how the recording quality of electrophysiological studies can alter results. Even minor perturbations can significantly change neuronal behavior. The field of neurobiology is rooted in history, but we, as neuroscientists, must be willing to modify our ideas and paradigms to advance the field and to better understand the mechanisms that regulate the sympathetic nervous system.

APPENDIX A

LIST OF ABBREVIATIONS

Abbreviation	Full Terminology
ACE	Angiotensin Converting Enzyme
ACh	Acetylcholine
AngII	Angiotensin II
AT ₁ receptor	Angiotensin II receptor type 1
AT ₂ receptor	Angiotensin II receptor type 2
DAG	Diacylglycerol
EPSP	Excitatory postsynaptic potential
E_{rev}	Reversal potential
F-I	Frequency-current
f_{post}	Postsynaptic frequency
f_{pre}	Presynaptic frequency
g_{leak}	Virtual leak conductance
GPCR	G-protein coupled receptor
ID	Inner diameter
IP ₃	Inositol triphosphate
ISI	Interspike interval
I-V	Current-voltage
LHRH	Luteinizing hormone releasing hormone
MEM	Minimal essential media
nAChR	Nicotinic acetylcholine receptor
NPY	Neuropeptide Y
OD	Outer diameter
PIP ₂	Phosphatidylinositol 4,5-bisphosphate
PKC	Protein kinase C
RAS	Renin-angiotensin system
R _{input}	Input resistance
ROS	Reactive oxygen species
RT-PCR	Reverse transcription polymerase chain reaction

S.E.M.	Standard error of the mean
SCG	Superior cervical ganglion
Threshold- g_{syn} or Thresh- g_{syn}	Threshold synaptic conductance
V_{rest} or V_m	Resting membrane potential
ZAP	Sinusoidal current injection

BIBLIOGRAPHY

- Acosta, E., V. Mendoza, E. Castro and H. Cruzblanca (2007). "Modulation of a delayed-rectifier K⁺ current by angiotensin II in rat sympathetic neurons." Journal of neurophysiology **98**(1): 79-85.
- Adrian, E. D., D. W. Bronk and G. Phillips (1932). "Discharges in mammalian sympathetic nerves." The Journal of physiology **74**(2): 115-133.
- Alexander, S. P., A. Mathie and J. A. Peters (2011). "Guide to Receptors and Channels (GRAC), 5th edition." British journal of pharmacology **164 Suppl 1**: S1-324.
- Anderson, W. P., R. G. Evans and S. C. Malpas (1995). "Pressure natriuresis and long-term blood pressure control." Journal of cardiovascular pharmacology **26 Suppl 2**: S17-23.
- Bader, M., J. Peters, O. Baltatu, D. N. Muller, F. C. Luft and D. Ganten (2001). "Tissue renin-angiotensin systems: new insights from experimental animal models in hypertension research." Journal of molecular medicine **79**(2-3): 76-102.
- Baluk, P. (1995). Structure of Autonomic Ganglia. Autonomic Ganglia. E. M. McLachlan. Luxembourg, Harwood Academic Publishers: 13 - 71.
- Beaudet, M. M., R. L. Parsons, K. M. Braas and V. May (2000). "Mechanisms mediating pituitary adenylate cyclase-activating polypeptide depolarization of rat sympathetic neurons." The Journal of neuroscience : the official journal of the Society for Neuroscience **20**(19): 7353-7361.
- Berne, R. M. L., M. N. (1986). Cardiovascular Physiology, The C.V. Mosby Company.
- Berry, M. J., 2nd and M. Meister (1998). "Refractoriness and neural precision." The Journal of neuroscience : the official journal of the Society for Neuroscience **18**(6): 2200-2211.
- Blackman, J. G., B. L. Ginsborg and C. Ray (1963). "Synaptic transmission in the sympathetic ganglion of the frog." The Journal of physiology **167**: 355-373.
- Boulpaep, E. L. (2012). Integrated control of the cardiovascular system. Medical physiology. W. F. Boron and E. L. Boulpaep. Philadelphia, Saunders Elsevier: 593 - 609.

- Bratton, B., P. Davies, W. Janig and R. McAllen (2010). "Ganglionic transmission in a vasomotor pathway studied in vivo." The Journal of physiology **588**(Pt 9): 1647-1659.
- Brown, D. A. and G. M. Passmore (2009). "Neural KCNQ (Kv7) channels." British journal of pharmacology **156**(8): 1185-1195.
- Cassell, J. F., A. L. Clark and E. M. McLachlan (1986). "Characteristics of phasic and tonic sympathetic ganglion cells of the guinea-pig." The Journal of physiology **372**: 457-483.
- Connor, J. A. and C. F. Stevens (1971). "Prediction of repetitive firing behaviour from voltage clamp data on an isolated neurone soma." The Journal of physiology **213**(1): 31-53.
- Davenport, H. W. (1991). "Early history of the concept of chemical transmission of the nerve impulse." The Physiologist **34**(4): 129, 178-190.
- Del Castillo, J. and B. Katz (1954). "Quantal components of the end-plate potential." The Journal of physiology **124**(3): 560-573.
- Dendorfer, A., A. Thornagel, W. Raasch, O. Grisk, K. Tempel and P. Dominiak (2002). "Angiotensin II induces catecholamine release by direct ganglionic excitation." Hypertension **40**(3): 348-354.
- Derkach, V. A., A. A. Selyanko and V. I. Skok (1983). "Acetylcholine-induced current fluctuations and fast excitatory post-synaptic currents in rabbit sympathetic neurones." The Journal of physiology **336**: 511-526.
- Dodd, J. and J. P. Horn (1983a). "A reclassification of B and C neurones in the ninth and tenth paravertebral sympathetic ganglia of the bullfrog." The Journal of physiology **334**: 255-269.
- Dodd, J. and J. P. Horn (1983b). "Muscarinic inhibition of sympathetic C neurones in the bullfrog." The Journal of physiology **334**: 271-291.
- Dolphin, A. C. (2003). "G protein modulation of voltage-gated calcium channels." Pharmacological reviews **55**(4): 607-627.
- Dorval, A. D., D. J. Christini and J. A. White (2001). "Real-Time linux dynamic clamp: a fast and flexible way to construct virtual ion channels in living cells." Annals of biomedical engineering **29**(10): 897-907.
- Dorval, A. D. and J. A. White (2006). "Synaptic input statistics tune the variability and reproducibility of neuronal responses." Chaos **16**(2): 026105.
- Eccles, J. C. (1935a). "The action potential of the superior cervical ganglion." The Journal of physiology **85**(2): 179-206.
- Eccles, J. C. (1935b). "Facilitation and inhibition in the superior cervical ganglion." The Journal of physiology **85**(2): 207-238.

- Eccles, J. C. (1964). The Physiology of Synapses. Berlin, Springer Verlag.
- Eccles, R. M. (1955). "Intracellular potentials recorded from a mammalian sympathetic ganglion." The Journal of physiology **130**(3): 572-584.
- Eccles, R. M. and B. Libet (1961). "Origin and blockade of the synaptic responses of curarized sympathetic ganglia." The Journal of physiology **157**: 484-503.
- Edelbauer, H., S. G. Lechner, M. Mayer, T. Scholze and S. Boehm (2005). "Presynaptic inhibition of transmitter release from rat sympathetic neurons by bradykinin." Journal of neurochemistry **93**(5): 1110-1121.
- Elenkov, I. J., R. L. Wilder, G. P. Chrousos and E. S. Vizi (2000). "The sympathetic nerve--an integrative interface between two supersystems: the brain and the immune system." Pharmacological reviews **52**(4): 595-638.
- Esler, M. D., H. Krum, P. A. Sobotka, M. P. Schlaich, R. E. Schmieder and M. Bohm (2010). "Renal sympathetic denervation in patients with treatment-resistant hypertension (The Symplicity HTN-2 Trial): a randomised controlled trial." Lancet **376**(9756): 1903-1909.
- Fargali, S., M. Sadahiro, C. Jiang, A. L. Frick, T. Indall, V. Cogliani, J. Welagen, W. J. Lin and S. R. Salton (2012). "Role of neurotrophins in the development and function of neural circuits that regulate energy homeostasis." Journal of molecular neuroscience : MN **48**(3): 654-659.
- Fatt, P. and B. Katz (1951). "An analysis of the end-plate potential recorded with an intracellular electrode." The Journal of physiology **115**(3): 320-370.
- Feldberg, W. and J. H. Gaddum (1934). "The chemical transmitter at synapses in a sympathetic ganglion." The Journal of physiology **81**(3): 305-319.
- Fernandez-Fernandez, J. M., F. C. Abogadie, G. Milligan, P. Delmas and D. A. Brown (2001). "Multiple pertussis toxin-sensitive G-proteins can couple receptors to GIRK channels in rat sympathetic neurons when expressed heterologously, but only native G(i)-proteins do so in situ." The European journal of neuroscience **14**(2): 283-292.
- Galvan, M. and P. R. Adams (1982). "Control of calcium current in rat sympathetic neurons by norepinephrine." Brain research **244**(1): 135-144.
- Galvan, M. and C. Sedlmeir (1984). "Outward currents in voltage-clamped rat sympathetic neurones." The Journal of physiology **356**: 115-133.
- Gao, L. and I. H. Zucker (2011). "AT2 receptor signaling and sympathetic regulation." Current opinion in pharmacology **11**(2): 124-130.
- Georgiopoulou, V. V., A. P. Kalogeropoulos and J. Butler (2012). "Heart failure in hypertension: prevention and treatment." Drugs **72**(10): 1373-1398.

- Gewirtz, J. R. and J. D. Bisognano (2011). "Catheter-based renal sympathetic denervation: a targeted approach to resistant hypertension." Cardiology journal **18**(1): 97-102.
- Gibbins, I. (1995). Chemical Neuroanatomy of Sympathetic Ganglia. Autonomic Ganglia. E. M. McLachlan. Luxembourg, Harwood Academic Publishers: 73 - 121.
- Gibbins, I. L. (1991). "Vasomotor, pilomotor and secretomotor neurons distinguished by size and neuropeptide content in superior cervical ganglia of mice." Journal of the autonomic nervous system **34**(2-3): 171-183.
- Gibbins, I. L., E. H. Teo, P. Jobling and J. L. Morris (2003). "Synaptic density, convergence, and dendritic complexity of prevertebral sympathetic neurons." The Journal of comparative neurology **455**(3): 285-298.
- Gold, M. S., S. Dastmalchi and J. D. Levine (1997). "Alpha 2-adrenergic receptor subtypes in rat dorsal root and superior cervical ganglion neurons." Pain **69**(1-2): 179-190.
- Gotti, C. and F. Clementi (2004). "Neuronal nicotinic receptors: from structure to pathology." Progress in neurobiology **74**(6): 363-396.
- Guyenet, P. G. (2006). "The sympathetic control of blood pressure." Nature reviews. Neuroscience **7**(5): 335-346.
- Hall, J. E. (2011b). Role of the kidneys in long-term control of arterial pressure and in hypertension: the integrated system for arterial pressure regulation. Guyton and Hall textbook of medical physiology. R. Grulow. Philadelphia, Saunders Elsevier: 213 - 228.
- Henon, B. K. and D. A. McAfee (1983). "The ionic basis of adenosine receptor actions on post-ganglionic neurones in the rat." The Journal of physiology **336**: 607-620.
- Hernandez, C. C., O. Zaika, G. P. Tolstykh and M. S. Shapiro (2008). "Regulation of neural KCNQ channels: signalling pathways, structural motifs and functional implications." The Journal of physiology **586**(7): 1811-1821.
- Hille, B. (2001). Ion channels of excitable membranes. Sunderland, Sinauer Associates, Inc.
- Hirst, G. D. and E. M. McLachlan (1986). "Development of dendritic calcium currents in ganglion cells of the rat lower lumbar sympathetic chain." The Journal of physiology **377**: 349-368.
- Hodgkin, A. L. (1948). "The local electric changes associated with repetitive action in a non-medullated axon." The Journal of physiology **107**(2): 165-181.
- Honma, S. (1970). "Functional differentiation in sB and sC neurons of toad sympathetic ganglia." The Japanese journal of physiology **20**(3): 281-295.
- Horn, J. P. and P. H. Kullmann (2007). "Dynamic Clamp Analysis of Synaptic Integration in Sympathetic Ganglia." Neirofiziologia = Neurophysiology **39**(6): 423-429.

- Horn, J. P. and D. A. McAfee (1979). "Norepinephrine inhibits calcium-dependent potentials in rat sympathetic neurons." Science **204**(4398): 1233-1235.
- Horn, J. P. and W. D. Stofer (1988). "Double labeling of the paravertebral sympathetic C system in the bullfrog with antisera to LHRH and NPY." Journal of the autonomic nervous system **23**(1): 17-24.
- Horn, J. P. and W. D. Stofer (1989). "Preganglionic and sensory origins of calcitonin gene-related peptide-like and substance P-like immunoreactivities in bullfrog sympathetic ganglia." The Journal of neuroscience : the official journal of the Society for Neuroscience **9**(7): 2543-2561.
- Horn, J. P. and L. W. Swanson (2013). The Autonomic Motor System and the Hypothalamus. Principles of Neural Science. E. R. Kandel, J. H. Schwartz, T. M. Jessell, S. A. Siegelbaum and A. J. Hudspeth. New York, McGraw-Hill Company: 1057 - 1077.
- Hunyady, L. and K. J. Catt (2006). "Pleiotropic AT1 receptor signaling pathways mediating physiological and pathogenic actions of angiotensin II." Molecular endocrinology **20**(5): 953-970.
- Ichinose, M., M. Saito, N. Fujii, T. Ogawa, K. Hayashi, N. Kondo and T. Nishiyasu (2008). "Modulation of the control of muscle sympathetic nerve activity during incremental leg cycling." The Journal of physiology **586**(Pt 11): 2753-2766.
- Ikeda, T., H. Murai, S. Kaneko, S. Usui, D. Kobayashi, M. Nakano, K. Ikeda, S. Takashima, T. Kato, M. Okajima, H. Furusho and M. Takamura (2012). "Augmented single-unit muscle sympathetic nerve activity in heart failure with chronic atrial fibrillation." The Journal of physiology **590**(Pt 3): 509-518.
- Imanishi, T., T. Hano and I. Nishio (2004). "Angiotensin II potentiates vascular endothelial growth factor-induced proliferation and network formation of endothelial progenitor cells." Hypertension research : official journal of the Japanese Society of Hypertension **27**(2): 101-108.
- Ivanoff, A. Y. and P. A. Smith (1995). "In vivo activity of B- and C-neurons in the paravertebral sympathetic ganglia of the bullfrog." The Journal of physiology **485** (Pt 3): 797-815.
- Ivanov, A. (1991). "Pattern of ongoing activity in rat superior cervical ganglion neurons projecting to a specific target." Journal of the autonomic nervous system **32**(1): 77-79.
- Ivanov, A. and D. Purves (1989). "Ongoing electrical activity of superior cervical ganglion cells in mammals of different size." The Journal of comparative neurology **284**(3): 398-404.
- Izhikevich, E. (2007). Dynamical Systems in Neuroscience: The Geometry of Excitability and Bursting. Cambridge, MIT Press.

- Jan, L. Y. and Y. N. Jan (1982). "Peptidergic transmission in sympathetic ganglia of the frog." The Journal of physiology **327**: 219-246.
- Jan, Y. N., L. Y. Jan and S. W. Kuffler (1979). "A peptide as a possible transmitter in sympathetic ganglia of the frog." Proceedings of the National Academy of Sciences of the United States of America **76**(3): 1501-1505.
- Jan, Y. N., L. Y. Jan and S. W. Kuffler (1980). "Further evidence for peptidergic transmission in sympathetic ganglia." Proceedings of the National Academy of Sciences of the United States of America **77**(8): 5008-5012.
- Janig, W. (1988). "Pre- and postganglionic vasoconstrictor neurons: differentiation, types, and discharge properties." Annual review of physiology **50**: 525-539.
- Janig, W. (2006). The Integrative Action of the Autonomic Nervous System. Cambridge, Cambridge University Press.
- Janig, W. and H. J. Habler (2003). "Neurophysiological analysis of target-related sympathetic pathways--from animal to human: similarities and differences." Acta physiologica Scandinavica **177**(3): 255-274.
- Janig, W. and E. M. McLachlan (1992). "Characteristics of function-specific pathways in the sympathetic nervous system." Trends in neurosciences **15**(12): 475-481.
- Jia, Z., J. Bei, L. Rodat-Despoix, B. Liu, Q. Jia, P. Delmas and H. Zhang (2008). "NGF inhibits M/KCNQ currents and selectively alters neuronal excitability in subsets of sympathetic neurons depending on their M/KCNQ current background." The Journal of general physiology **131**(6): 575-587.
- Jones, S., D. A. Brown, G. Milligan, E. Willer, N. J. Buckley and M. P. Caulfield (1995). "Bradykinin excites rat sympathetic neurons by inhibition of M current through a mechanism involving B2 receptors and G alpha q/11." Neuron **14**(2): 399-405.
- Joyner, M. J., N. Charkoudian and B. G. Wallin (2008). "A sympathetic view of the sympathetic nervous system and human blood pressure regulation." Experimental physiology **93**(6): 715-724.
- Joyner, M. J., N. Charkoudian and B. G. Wallin (2010). "Sympathetic nervous system and blood pressure in humans: individualized patterns of regulation and their implications." Hypertension **56**(1): 10-16.
- Kafka, M. S., J. P. Horn, N. B. Thoa and D. A. McAfee (1980). "Alpha-adrenergic receptors in the rat superior cervical ganglion." Annals of the New York Academy of Sciences **358**: 342-345.
- Kali, S. and R. Zemankovics (2012). "The effect of dendritic voltage-gated conductances on the neuronal impedance: a quantitative model." Journal of computational neuroscience **33**(2): 257-284.

- Kang, J., C. Summers and P. Posner (1993). "Angiotensin II type 2 receptor-modulated changes in potassium currents in cultured neurons." The American journal of physiology **265**(3 Pt 1): C607-616.
- Karila, P. and J. P. Horn (2000). "Secondary nicotinic synapses on sympathetic B neurons and their putative role in ganglionic amplification of activity." The Journal of neuroscience : the official journal of the Society for Neuroscience **20**(3): 908-918.
- Karpuk, N. and A. Hayar (2008). "Activation of postsynaptic GABAB receptors modulates the bursting pattern and synaptic activity of olfactory bulb juxtglomerular neurons." Journal of neurophysiology **99**(1): 308-319.
- Katz, B. (1966). Nerve, Muscle and Synapse, McGraw-Hill, Inc.
- Katz, B. (2003). "Neural transmitter release: from quantal secretion to exocytosis and beyond." Journal of neurocytology **32**(5-8): 437-446.
- Kimura, K. and S. Eguchi (2009). "Angiotensin II type-1 receptor regulates RhoA and Rho-kinase/ROCK activation via multiple mechanisms. Focus on "Angiotensin II induces RhoA activation through SHP2-dependent dephosphorylation of the RhoGAP p190A in vascular smooth muscle cells"." American journal of physiology. Cell physiology **297**(5): C1059-1061.
- Kobori, H., L. M. Harrison-Bernard and L. G. Navar (2001). "Enhancement of angiotensinogen expression in angiotensin II-dependent hypertension." Hypertension **37**(5): 1329-1335.
- Kobori, H., L. M. Harrison-Bernard and L. G. Navar (2001). "Expression of angiotensinogen mRNA and protein in angiotensin II-dependent hypertension." Journal of the American Society of Nephrology : JASN **12**(3): 431-439.
- Kotsis, V., S. Stabouli, S. Papakatsika, Z. Rizos and G. Parati (2010). "Mechanisms of obesity-induced hypertension." Hypertension research : official journal of the Japanese Society of Hypertension **33**(5): 386-393.
- Kuba, K. and K. Koketsu (1976a). "Analysis of the slow excitatory postsynaptic potential in bullfrog sympathetic ganglion cells." The Japanese journal of physiology **26**(6): 651-669.
- Kuba, K. and K. Koketsu (1976b). "The muscarinic effects of acetylcholine on the action potential of bullfrog sympathetic ganglion cells." The Japanese journal of physiology **26**(6): 703-716.
- Kullmann, P. H. and J. P. Horn (2006). "Excitatory muscarinic modulation strengthens virtual nicotinic synapses on sympathetic neurons and thereby enhances synaptic gain." Journal of neurophysiology **96**(6): 3104-3113.
- Kullmann, P. H. and J. P. Horn (2010b). "Vasomotor sympathetic neurons are more excitable than secretomotor sympathetic neurons in bullfrog paravertebral ganglia." Autonomic neuroscience : basic & clinical **155**(1-2): 19-24.

- Kullmann, P. H., D. W. Wheeler, J. Beacom and J. P. Horn (2004). "Implementation of a fast 16-Bit dynamic clamp using LabVIEW-RT." J Neurophysiol **91**(1): 542-554.
- Kushiku, K., H. Yamada, K. Shibata, R. Tokunaga, T. Katsuragi and T. Furukawa (2001). "Upregulation of immunoreactive angiotensin II release and angiotensinogen mRNA expression by high-frequency preganglionic stimulation at the canine cardiac sympathetic ganglia." Circulation research **88**(1): 110-116.
- Lambert, E., N. Straznicky, M. Schlaich, M. Esler, T. Dawood, E. Hotchkin and G. Lambert (2007). "Differing pattern of sympathoexcitation in normal-weight and obesity-related hypertension." Hypertension **50**(5): 862-868.
- Langley, J. N. (1921). The Autonomic Nervous System, Cambridge: W. Heffer.
- Langley, J. N. and W. L. Dickinson (1890). "Pituri and Nicotin." The Journal of physiology **11**(4-5): 265-306.
- Lavoie, J. L. and C. D. Sigmund (2003). "Minireview: overview of the renin-angiotensin system--an endocrine and paracrine system." Endocrinology **144**(6): 2179-2183.
- Li, C. and J. P. Horn (2006). "Physiological classification of sympathetic neurons in the rat superior cervical ganglion." Journal of neurophysiology **95**(1): 187-195.
- Li, C. and J. P. Horn (2008). "Differential Inhibition of Ca²⁺ channels by alpha₂-adrenoceptors in three functional subclasses of rat sympathetic neurons." Journal of neurophysiology **100**(6): 3055-3063.
- Libet, B., S. Chichibu and T. Tosaka (1968). "Slow synaptic responses and excitability in sympathetic ganglia of the bullfrog." Journal of neurophysiology **31**(3): 383-395.
- Lichtman, J. W., D. Purves and J. W. Yip (1979). "On the purpose of selective innervation of guinea-pig superior cervical ganglion cells." The Journal of physiology **292**: 69-84.
- Lim, K., S. L. Burke and G. A. Head (2013). "Obesity-Related Hypertension and the Role of Insulin and Leptin in High-Fat-Fed Rabbits." Hypertension.
- Liu, Z., J. Zhang and D. K. Berg (2007). "Role of endogenous nicotinic signaling in guiding neuronal development." Biochemical pharmacology **74**(8): 1112-1119.
- Luther, J. A. and S. J. Birren (2009a). "p75 and TrkA signaling regulates sympathetic neuronal firing patterns via differential modulation of voltage-gated currents." The Journal of neuroscience : the official journal of the Society for Neuroscience **29**(17): 5411-5424.
- Luther, J. A. and S. J. Birren (2009b). "Neurotrophins and target interactions in the development and regulation of sympathetic neuron electrical and synaptic properties." Autonomic neuroscience : basic & clinical **151**(1): 46-60.

- Macefield, V. G. (2009). "Developments in autonomic research: a review of the latest literature." Clinical autonomic research : official journal of the Clinical Autonomic Research Society **19**(4): 193-196.
- Macefield, V. G. (2011). "On the number of preganglionic neurons driving human postganglionic sympathetic neurons: a comparison of modeling and empirical data." Frontiers in neuroscience **5**: 132.
- Macefield, V. G. and M. Elam (2003). "Why do human postganglionic neurones primarily only fire once during a sympathetic burst?" Acta physiologica Scandinavica **177**(3): 247-253.
- Macefield, V. G. and M. Elam (2004). "Comparison of the firing patterns of human postganglionic sympathetic neurones and spinal alpha motoneurones during brief bursts." Experimental physiology **89**(1): 82-88.
- Macefield, V. G., M. Elam and B. G. Wallin (2002). "Firing properties of single postganglionic sympathetic neurones recorded in awake human subjects." Autonomic neuroscience : basic & clinical **95**(1-2): 146-159.
- Macefield, V. G., B. Rundqvist, Y. B. Sverrisdottir, B. G. Wallin and M. Elam (1999). "Firing properties of single muscle vasoconstrictor neurons in the sympathoexcitation associated with congestive heart failure." Circulation **100**(16): 1708-1713.
- Macefield, V. G. and B. G. Wallin (1996). "The discharge behaviour of single sympathetic neurones supplying human sweat glands." Journal of the autonomic nervous system **61**(3): 277-286.
- Macefield, V. G., B. G. Wallin and A. B. Vallbo (1994). "The discharge behaviour of single vasoconstrictor motoneurones in human muscle nerves." The Journal of physiology **481** (Pt 3): 799-809.
- Malpas, S. C. (2010). "Sympathetic nervous system overactivity and its role in the development of cardiovascular disease." Physiological reviews **90**(2): 513-557.
- Mao, D., R. P. Yasuda, H. Fan, B. B. Wolfe and K. J. Kellar (2006). "Heterogeneity of nicotinic cholinergic receptors in rat superior cervical and nodose Ganglia." Molecular pharmacology **70**(5): 1693-1699.
- May, V., M. M. Beaudet, R. L. Parsons and K. M. Braas (2000). "PACAP modulates rat sympathetic neuron depolarization through IP3." Annals of the New York Academy of Sciences **921**: 186-194.
- McAllen, R. M. and S. C. Malpas (1997). "Sympathetic burst activity: characteristics and significance." Clinical and experimental pharmacology & physiology **24**(11): 791-799.
- McGehee, D. S. and L. W. Role (1995). "Physiological diversity of nicotinic acetylcholine receptors expressed by vertebrate neurons." Annual review of physiology **57**: 521-546.

- McIntosh, R. A. (1940). "The Autonomic Nervous System." Canadian journal of comparative medicine and veterinary science **4**(8): 221-227.
- McLachlan, E. M. (2003). "Transmission of signals through sympathetic ganglia--modulation, integration or simply distribution?" Acta physiologica Scandinavica **177**(3): 227-235.
- McLachlan, E. M., P. J. Davies, H. J. Habler and J. Jamieson (1997). "On-going and reflex synaptic events in rat superior cervical ganglion cells." The Journal of physiology **501** (Pt 1): 165-181.
- McLachlan, E. M., H. J. Habler, J. Jamieson and P. J. Davies (1998). "Analysis of the periodicity of synaptic events in neurones in the superior cervical ganglion of anaesthetized rats." The Journal of physiology **511** (Pt 2): 461-478.
- Mitra, A. K., L. Gao and I. H. Zucker (2010). "Angiotensin II-induced upregulation of AT(1) receptor expression: sequential activation of NF-kappaB and Elk-1 in neurons." American journal of physiology. Cell physiology **299**(3): C561-569.
- Nishi, S. and K. Koketsu (1960). "Electrical properties and activities of single sympathetic neurons in frogs." Journal of cellular and comparative physiology **55**: 15-30.
- Nishi, S., H. Soeda and K. Koketsu (1965). "Studies on sympathetic B and C neurons and patterns of preganglionic innervation." Journal of cellular physiology **66**(1): 19-32.
- Nja, A. and D. Purves (1977). "Specific innervation of guinea-pig superior cervical ganglion cells by preganglionic fibres arising from different levels of the spinal cord." The Journal of physiology **264**(2): 565-583.
- Papke, R. L., J. Boulter, J. Patrick and S. Heinemann (1989). "Single-channel currents of rat neuronal nicotinic acetylcholine receptors expressed in *Xenopus* oocytes." Neuron **3**(5): 589-596.
- Parati, G. and M. Esler (2012). "The human sympathetic nervous system: its relevance in hypertension and heart failure." European heart journal **33**(9): 1058-1066.
- Piwkowska, Z., A. Destexhe and T. Bal (2009). Associating living cells and computational models: an introduction to dynamic clamp principles and its applications. Dynamic-Clamp: From Principles to Applications. A. Destexhe and B. T. New York, Springer Science: 1 - 30.
- Prescott, S. A., Y. De Koninck and T. J. Sejnowski (2008). "Biophysical basis for three distinct dynamical mechanisms of action potential initiation." PLoS computational biology **4**(10): e1000198.
- Prescott, S. A. and T. J. Sejnowski (2008). "Spike-rate coding and spike-time coding are affected oppositely by different adaptation mechanisms." The Journal of neuroscience : the official journal of the Society for Neuroscience **28**(50): 13649-13661.

- Purves, D. and R. I. Hume (1981). "The relation of postsynaptic geometry to the number of presynaptic axons that innervate autonomic ganglion cells." The Journal of neuroscience : the official journal of the Society for Neuroscience **1**(5): 441-452.
- Purves, D., E. Rubin, W. D. Snider and J. Lichtman (1986). "Relation of animal size to convergence, divergence, and neuronal number in peripheral sympathetic pathways." The Journal of neuroscience : the official journal of the Society for Neuroscience **6**(1): 158-163.
- Rajagopalan, S., S. Kurz, T. Munzel, M. Tarpey, B. A. Freeman, K. K. Griendling and D. G. Harrison (1996). "Angiotensin II-mediated hypertension in the rat increases vascular superoxide production via membrane NADH/NADPH oxidase activation. Contribution to alterations of vasomotor tone." The Journal of clinical investigation **97**(8): 1916-1923.
- Rando, T. A., C. W. Bowers and R. E. Zigmond (1981). "Localization of neurons in the rat spinal cord which project to the superior cervical ganglion." The Journal of comparative neurology **196**(1): 73-83.
- Ratte, S., S. A. Prescott, J. Collinge and J. G. Jefferys (2008). "Hippocampal bursts caused by changes in NMDA receptor-dependent excitation in a mouse model of variant CJD." Neurobiology of disease **32**(1): 96-104.
- Reid, I. A. (1992). "Interactions between ANG II, sympathetic nervous system, and baroreceptor reflexes in regulation of blood pressure." The American journal of physiology **262**(6 Pt 1): E763-778.
- Rimmer, K. and J. P. Horn (2010). "Weak and straddling secondary nicotinic synapses can drive firing in rat sympathetic neurons and thereby contribute to ganglionic amplification." Frontiers in neurology **1**: 130.
- Role, L. W. (1992). "Diversity in primary structure and function of neuronal nicotinic acetylcholine receptor channels." Current opinion in neurobiology **2**(3): 254-262.
- Rust, G., J. M. Burgunder, T. E. Lauterburg and A. B. Cachelin (1994). "Expression of neuronal nicotinic acetylcholine receptor subunit genes in the rat autonomic nervous system." The European journal of neuroscience **6**(3): 478-485.
- Ruster, C. and G. Wolf (2013). "The role of the Renin-Angiotensin-aldosterone system in obesity-related renal diseases." Seminars in nephrology **33**(1): 44-53.
- Sacchi, O., M. L. Rossi, R. Canella and R. Fesce (2006). "Synaptic and somatic effects of axotomy in the intact, innervated rat sympathetic neuron." J Neurophysiol **95**(5): 2832-2844.
- Sachse, A. and G. Wolf (2007). "Angiotensin II-induced reactive oxygen species and the kidney." Journal of the American Society of Nephrology : JASN **18**(9): 2439-2446.

- Sargent, P. B. (1993). "The diversity of neuronal nicotinic acetylcholine receptors." Annual review of neuroscience **16**: 403-443.
- Savoia, C., D. Burger, N. Nishigaki, A. Montezano and R. M. Touyz (2011). "Angiotensin II and the vascular phenotype in hypertension." Expert reviews in molecular medicine **13**: e11.
- Schlaich, M. P., E. Lambert, D. M. Kaye, Z. Krozowski, D. J. Campbell, G. Lambert, J. Hastings, A. Aggarwal and M. D. Esler (2004). "Sympathetic augmentation in hypertension: role of nerve firing, norepinephrine reuptake, and Angiotensin neuromodulation." Hypertension **43**(2): 169-175.
- Schobesberger, H., D. W. Wheeler and J. P. Horn (2000). "A model for pleiotropic muscarinic potentiation of fast synaptic transmission." Journal of neurophysiology **83**(4): 1912-1923.
- Schoepfer, R., W. G. Conroy, P. Whiting, M. Gore and J. Lindstrom (1990). "Brain alpha-bungarotoxin binding protein cDNAs and MAbs reveal subtypes of this branch of the ligand-gated ion channel gene superfamily." Neuron **5**(1): 35-48.
- Shapiro, M. S., L. P. Wollmuth and B. Hille (1994). "Angiotensin II inhibits calcium and M current channels in rat sympathetic neurons via G proteins." Neuron **12**(6): 1319-1329.
- Skok, V. I. and A. Y. Ivanov (1983). "What is the ongoing activity of sympathetic neurons?" Journal of the autonomic nervous system **7**(3-4): 263-270.
- St-Hilaire, M. and A. Longtin (2004). "Comparison of coding capabilities of Type I and Type II neurons." Journal of computational neuroscience **16**(3): 299-313.
- Stolarz-Skrzypek, K., A. Bednarski, D. Czarnecka, K. Kawecka-Jaszcz and J. A. Staessen (2013). "Sodium and potassium and the pathogenesis of hypertension." Current hypertension reports **15**(2): 122-130.
- Suh, B. C. and B. Hille (2008). "PIP2 is a necessary cofactor for ion channel function: how and why?" Annual review of biophysics **37**: 175-195.
- Suh, B. C., L. F. Horowitz, W. Hirdes, K. Mackie and B. Hille (2004). "Regulation of KCNQ2/KCNQ3 current by G protein cycling: the kinetics of receptor-mediated signaling by Gq." The Journal of general physiology **123**(6): 663-683.
- Takeuchi, A. and N. Takeuchi (1960). "On the permeability of end-plate membrane during the action of transmitter." The Journal of physiology **154**: 52-67.
- Tedford, H. W. and G. W. Zamponi (2006). "Direct G protein modulation of Cav2 calcium channels." Pharmacological reviews **58**(4): 837-862.
- Tompkins, J. D., Y. T. Lawrence and R. L. Parsons (2009). "Enhancement of I_h, but not inhibition of I_M, is a key mechanism underlying the PACAP-induced increase in excitability of guinea pig intrinsic cardiac neurons." American journal of physiology. Regulatory, integrative and comparative physiology **297**(1): R52-59.

- van Esch, J. H., F. Gembardt, A. Sterner-Kock, S. Heringer-Walther, T. H. Le, D. Lassner, T. Stijnen, T. M. Coffman, H. P. Schultheiss, A. H. Danser and T. Walther (2010). "Cardiac phenotype and angiotensin II levels in AT1a, AT1b, and AT2 receptor single, double, and triple knockouts." Cardiovascular research **86**(3): 401-409.
- van Kats, J. P., L. M. de Lannoy, A. H. Jan Danser, J. R. van Meegen, P. D. Verdouw and M. A. Schalekamp (1997). "Angiotensin II type 1 (AT1) receptor-mediated accumulation of angiotensin II in tissues and its intracellular half-life in vivo." Hypertension **30**(1 Pt 1): 42-49.
- Wahlestedt, C., R. Hakanson, C. A. Vaz and Z. Zukowska-Grojec (1990). "Norepinephrine and neuropeptide Y: vasoconstrictor cooperation in vivo and in vitro." The American journal of physiology **258**(3 Pt 2): R736-742.
- Wang, F. B., M. C. Holst and T. L. Powley (1995). "The ratio of pre- to postganglionic neurons and related issues in the autonomic nervous system." Brain research. Brain research reviews **21**(1): 93-115.
- Wang, H. S. and D. McKinnon (1995). "Potassium currents in rat prevertebral and paravertebral sympathetic neurones: control of firing properties." The Journal of physiology **485** (Pt 2): 319-335.
- Wang, J. M., D. Slembrouck and W. D. Potter (1996). "Expression of angiotensinogen mRNA and localization of angiotensin II and renin in peripheral adrenergic neurons in primary culture." Biochemical and biophysical research communications **229**(3): 876-881.
- Watanabe, T., T. A. Barker and B. C. Berk (2005). "Angiotensin II and the endothelium: diverse signals and effects." Hypertension **45**(2): 163-169.
- Weems, W. A. and J. H. Szurszewski (1978). "An intracellular analysis of some intrinsic factors controlling neural output from inferior mesenteric ganglion of guinea pigs." Journal of neurophysiology **41**(2): 305-321.
- Weitsen, H. A. and F. F. Weight (1977). "Synaptic innervation of sympathetic ganglion cells in the bullfrog." Brain research **128**(2): 197-211.
- Wesson, D. E. (2001). "Hypertension and the kidney." Current hypertension reports **3**(6): 511-516.
- Wheeler, D. W., P. H. Kullmann and J. P. Horn (2004). "Estimating use-dependent synaptic gain in autonomic ganglia by computational simulation and dynamic-clamp analysis." Journal of neurophysiology **92**(5): 2659-2671.
- Womack, M. D., R. Morris, T. C. Gent and R. Barrett-Jolley (2007). "Substance P targets sympathetic control neurons in the paraventricular nucleus." Circulation research **100**(11): 1650-1658.

- Wynne, B. M., C. W. Chiao and R. C. Webb (2009). "Vascular Smooth Muscle Cell Signaling Mechanisms for Contraction to Angiotensin II and Endothelin-1." Journal of the American Society of Hypertension : JASH **3**(2): 84-95.
- Yu, T., T. J. Sejnowski and G. Cauwenberghs (2011). "Biophysical Neural Spiking, Bursting, and Excitability Dynamics in Reconfigurable Analog VLSI." IEEE transactions on biomedical circuits and systems **5**(5): 420-429.
- Zaika, O., J. Zhang and M. S. Shapiro (2011). "Combined phosphoinositide and Ca²⁺ signals mediating receptor specificity toward neuronal Ca²⁺ channels." The Journal of biological chemistry **286**(1): 830-841.
- Zeberg, H., C. Blomberg and P. Arhem (2010). "Ion channel density regulates switches between regular and fast spiking in soma but not in axons." PLoS computational biology **6**(4): e1000753.
- Zhu, Y. and S. R. Ikeda (1993). "Adenosine modulates voltage-gated Ca²⁺ channels in adult rat sympathetic neurons." Journal of neurophysiology **70**(2): 610-620.